NUREG/CR-3363
TS-831-I
Vol. 1

Measurement of Axially Varying Nonequilibrium in Post-Critical-Heat-Flux Boiling in a Vertical Tube

Main Report and Appendices A - D

Prepared by D. G. Evans, S. W. Webb, J. C. Chen

Lehigh University

Prepared for
U.S. Nuclear Regulatory
Commission

GPO Printed copy price $6.00

NUREG/CR-3363
TS-831-I
Vol. 1
R2

Measurement of Axially Varying Nonequilibrium in Post-Critical-Heat-Flux Boiling in a Vertical Tube

Main Report and Appendices A - D

Manuscript Completed: May 1983
Date Published: June 1983

Prepared by
D. G. Evans, S. W. Webb, J. C. Chen

Institute of Thermo-Fluid Engineering and Science
Lehigh University
Bethlehem, PA 18015

Prepared for
Division of Accident Evaluation
Office of Nuclear Regulatory Research
U.S. Nuclear Regulatory Commission
Washington, D.C. 20555
NRC FIN B6794

TABLE OF CONTENTS

VOLUME 1

LIST OF TABLES

LIST OF FIGURES

LIST OF FIGURES -- Cont'd

LIST OF FIGURES -- Cont'd

LIST OF FIGURES -- Cont'd

LIST OF FIGURES -- Cont'd

ACKNOWLEDGEMENT

This research was sponsored by the U.S. Nuclear Regulatory Commission under Contract No. NRC-04-81-183.

The authors acknowledge with gratitude the continued interest, encouragement, and technical participation provided by Dr. Yih-Yun Hsu and Mr. Michael Young, program managers at USNRC, throughout the course of this work. The technical discussions with Dr. Ralph Nelson and Dr. Rex Shumway of EG&G Idaho Inc., and with Mr. Kenneth Williams of Los Alamos National Laboratory were also very helpful to the research effort.

ABSTRACT

In convective film boiling, under both blowdown and reflood conditions of nuclear safety concern, one often finds that wall heat flux, wall temperature, fluid equilibrium quality, and the local heat transfer coefficient all vary with axial position. Since the two-phase flow may exist in a nonequilibrium state, one needs to also know the axial variations of fluid actual quality and vapor superheat.

To supplement the very limited steady-state data available, experiments have been run with quench fronts propagating up into a tubular test section. During this slow "reflood" process, it was possible to obtain measurements of wall heat flux, wall temperature, and nonequilibrium vapor temperature as functions of distance beyond the quench front. Since the time required for the quench front to propagate a few millimeters corresponded to many fluid residence-times, transient convective heat transfer theory indicates that the thermal data thus obtained are quasi-steady state. Comparisons of wall superheats and vapor superheats at axial distances greater than one meter beyond the critical heat flux (CHF) point with data obtained from previously reported fixed quench front experiments at similar inlet conditions confirm this conclusion.

An unexpected finding was a "transition" region immediately downstream from CHF where the two-phase fluid remained close to

the equilibrium thermodynamic state. It was hypothesized that the liquid requires a finite axial distance to engage with the faster flowing vapor, and in this engagement region the volumetric presence of liquid is greater than heretofore understood. The greater liquid volume fraction would decrease the tendency for vapor superheating in this near-CHF region. At greater distances, the vapor superheat increases rapidly with axial distance indicating a surprisingly ineffective vapor to liquid heat transfer process.

Thus, the significant experimental findings indicate a zone near the CHF location where the vaporization source intensity (Γ) is relatively high, followed by a far zone where the source intensity drops off to a relatively low magnitude (approaching zero). If these findings are confirmed by future experiments, phenomenological modeling of the nonequilibrium heat transfer process in convective film boiling must account for these two regions of different behavior.

1. INTRODUCTION

Convective film boiling beyond critical-heat-flux (CHF) is encountered in a number of applications such as cryogenic systems, metallurgical processing, steam generators, and nuclear reactor loss of coolant accidents. In a number of these situations, post CHF boiling occurs with very high void fractions wherein dispersed two-phase flow occurs in the heated channels. In this regime, termed convective film boiling, the two-phase mixture may exist in a nonequilibrium thermodynamic state with superheated vapor entraining drops or globules of saturated liquid, as illustrated in figure 1-1. In this situation, the local actual-flow-quality (X_a) is not equal to the classical equilibrium quality (X_e) but is related to it by the following equation

$$\frac{X_a}{X_e} = \frac{i_{fg}}{i_v(P,T_v)-i_{ls}} \tag{1}$$

Analysis of this two-phase heat transfer problem requires solution of the vapor continuity and energy equations, which in one-dimensional differential form can be written as,

$$GdX_a = \Gamma\, dZ \tag{2}$$

$$q''_w P_H dZ = GAi_{fg} dX_e \tag{3}$$

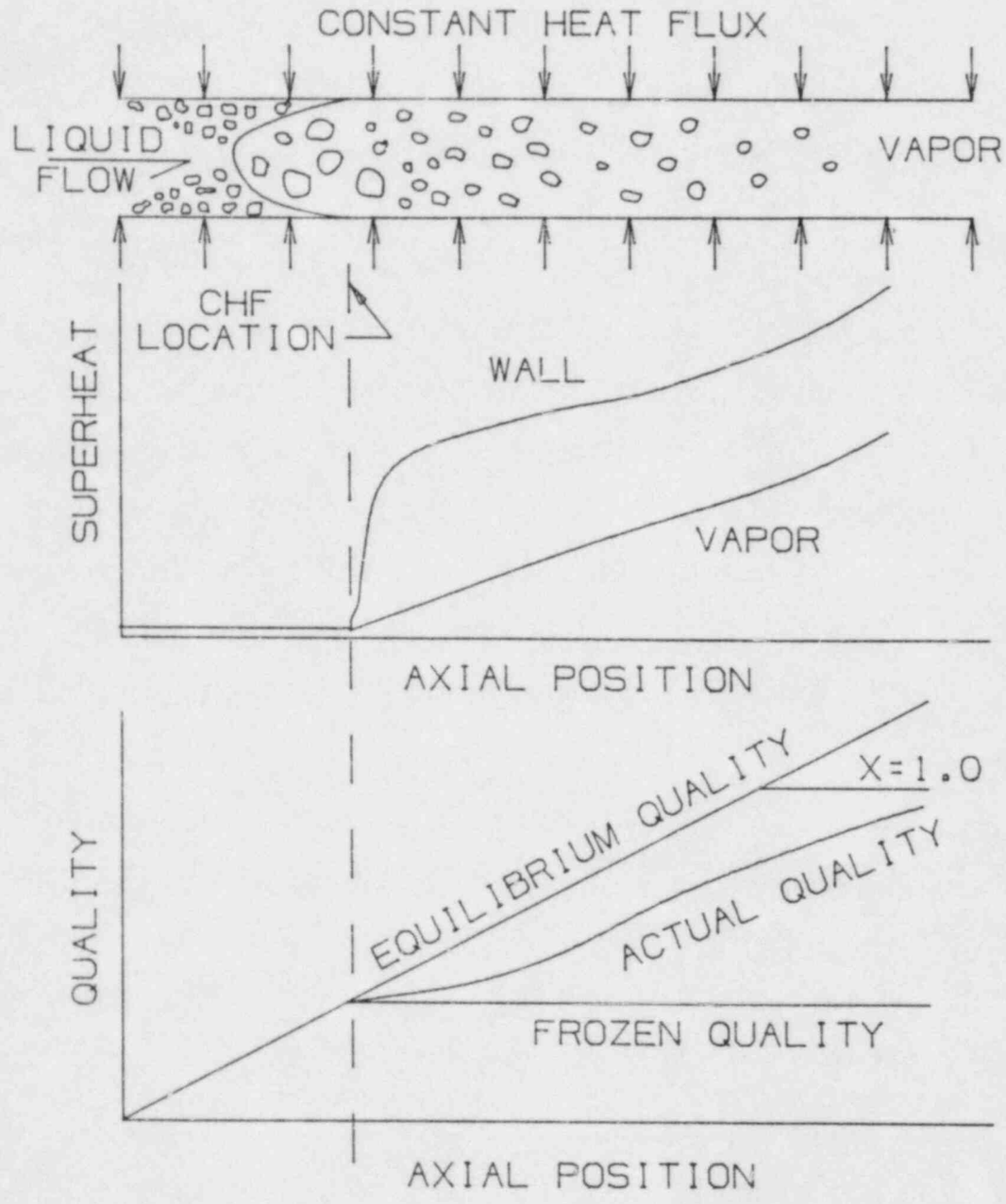

Figure 1-1. Typical conditions in convective film boiling.

In these equations, gamma (Γ) is defined as the vapor volumetric source term representing mass of liquid evaporated per unit time per unit mixture volume.

At the present time, the state of knowledge is lacking in the constitutive relations required to estimate the magnitude of the vapor source term, Γ. As noted by many researchers [1.1, 1.2], the evaporative source intensity results from the simultaneous competitive heat transfer between the hot wall surfaces to the vapor and liquid phases and between the liquid and superheated vapor phases (figure 1-2). A few preliminary models for estimating Γ have been proposed, including those of Saha [1.3] and of Webb and Chen [1.4]. The assessments of the available gamma models, and the development of improved models, are hampered by a lack of experimental data regarding the degree of thermodynamic nonequilibrium in convective film boiling.

In an effort to quantify the vapor source term Γ, a number of convective film boiling experiments have been conducted over the past twenty years. However, due to the extreme difficulty of measuring superheated vapor temperature in the presence of dispersed liquid, only a few attempts to quantify the degree of thermodynamic nonequilibrium have been reported. Mueller [1.5] and Polomik [1.6] obtained some limited data at high vapor qualities for internal flow in a tube. Hochreiter [1.7]

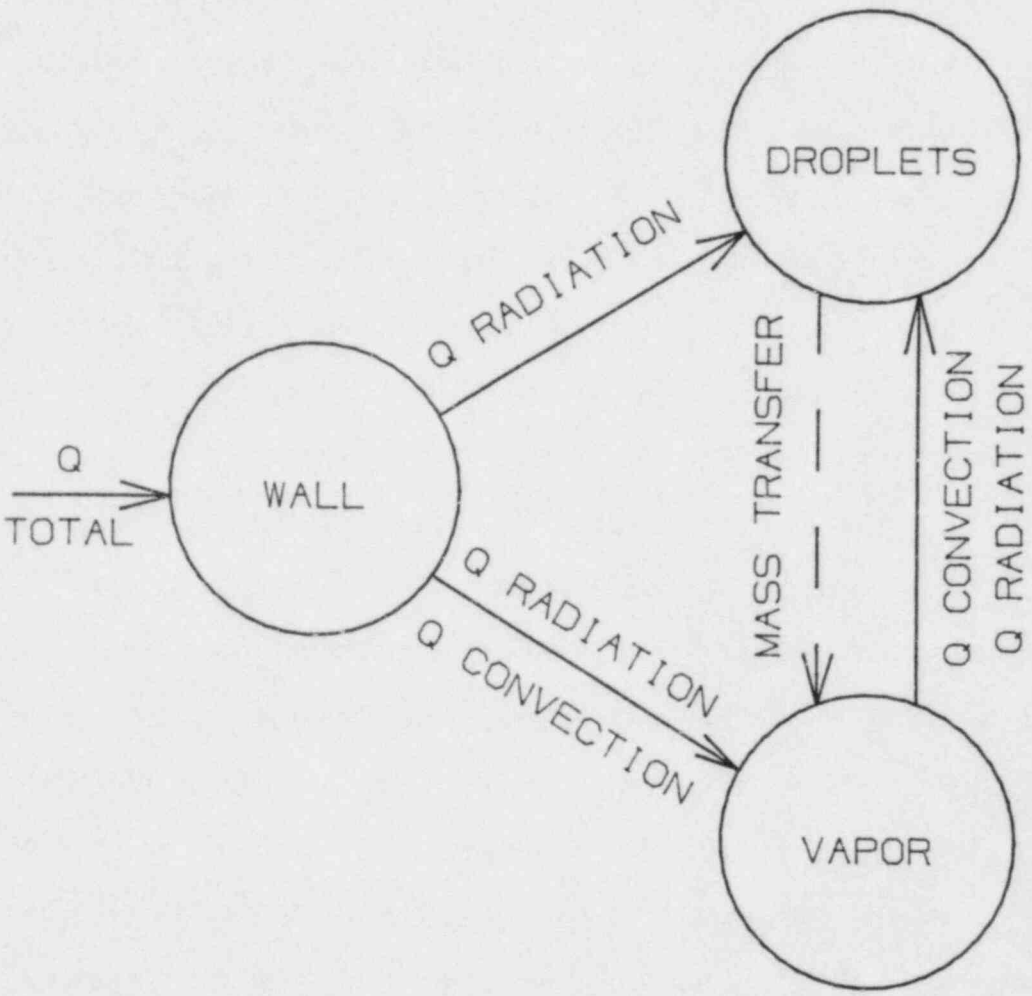

Figure 1-2. Heat transfer mechanisms in post-CHF dispersed-flow boiling.

obtained some indication of vapor superheats in rod bundles, limited primarily to high vapor quality conditions [1.8]. In previous work at Lehigh, Nijhawan et al. [1.9, 1.10] successfully used an aspirated thermocouple probe to obtain measurements of vapor superheats at one axial location for convective film boiling in a tube. Gottula et al. [1.11] is extending Nijhawan's technique to obtain simultaneous measurements of vapor superheats at three axial locations for convective film boiling in a tube. Recently, Annunziato et al. [1.12] reported actual flow qualities in convective film boiling by measuring the bulk temperature with exposed thermocouples in low mass flux, atmospheric pressure experiments. To date, the available data base for nonequilibrium flow film boiling is rather sparse, especially with regard to information on the axial variation of nonequilibrium vapor temperatures and flow qualities. Such data are needed for the development of constitutive models for the vapor source term, Γ.

2. SCOPE OF PRESENT EXPERIMENTAL INVESTIGATION

Measurement of the axial variation of vapor superheat would ideally be obtained under steady-state conditions downstream from a fixed critical-heat-flux (CHF) location. This requires the placement of multiple vapor probes along the axial direction of the heated channel, and also requires that the location of the CHF point be held constant with time. Nijhawan [2.1, 2.2] and Gottula et al. [2.3] both used the hot patch technique to fix the CHF location in order to permit steady state post-CHF conditions as shown in figure 2-1.

During the present research effort, experimental difficulties associated with fixing the location of CHF and concerns with probe intrusive effects limited this approach to the same narrow range of inlet flow conditions reported by Gottula, et al. [2.3]. Within these constraints, a limited quantity of fixed CHF data were obtained using the hot patch technique to fix the CHF location at the inlet to the test section. The high thermal conductivity of the copper hot patch (see fig. 3-3), maintained at typical post CHF temperatures, sustained continuous critical heat fluxes at the inlet of the hot patch, thereby maintaining convective film boiling conditions downstream of the copper block. This technique was limited to low mass fluxes and medium to high flow qualities. In

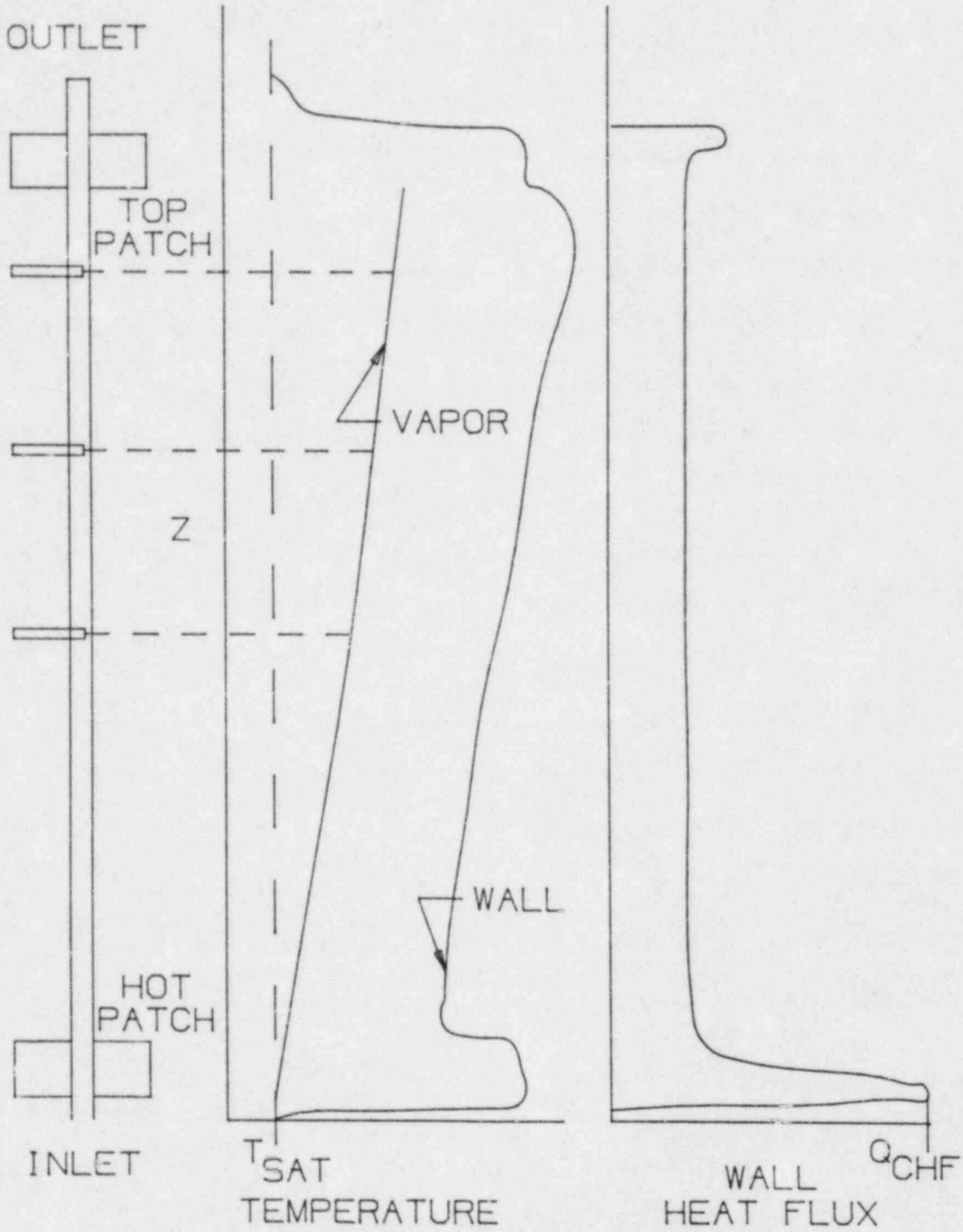

Figure 2-1. Vapor temperature profile obtained with multiple vapor probes.

addition, at low and medium flow qualities the vapor probe preferrentially quenched the test section wall at the probe and immediately downstream of the probe (figure 2-2). With a quenched wall region at the first vapor probe, measurements by succeeding vapor probes located further downstream were impossible to interpret. During low quality experiments, a descending quench front would propagate from the quench region to the wall upstream of the vapor probe, further corrupting the vapor measurements. As a result, only a limited amount of fixed CHF data at low mass fluxes and high flow qualities was obtained during these experiments.

In order to expand the data base, the present investigation took a different experimental approach to obtain information on vapor superheats as a function of axial distance from the CHF location. In this approach, starting with the test section in a flow film-boiling state, the CHF location was permitted to slowly propagate as a quench front along the test section (figure 2-3). By restricting the quench front propagation to low velocities, such that the displacement of the CHF location was negligible during a fluid residence-period in the test section, the thermal hydraulic conditions downstream of the CHF location were quasi-steady state. Theoretical analysis of transient convective heat transfer

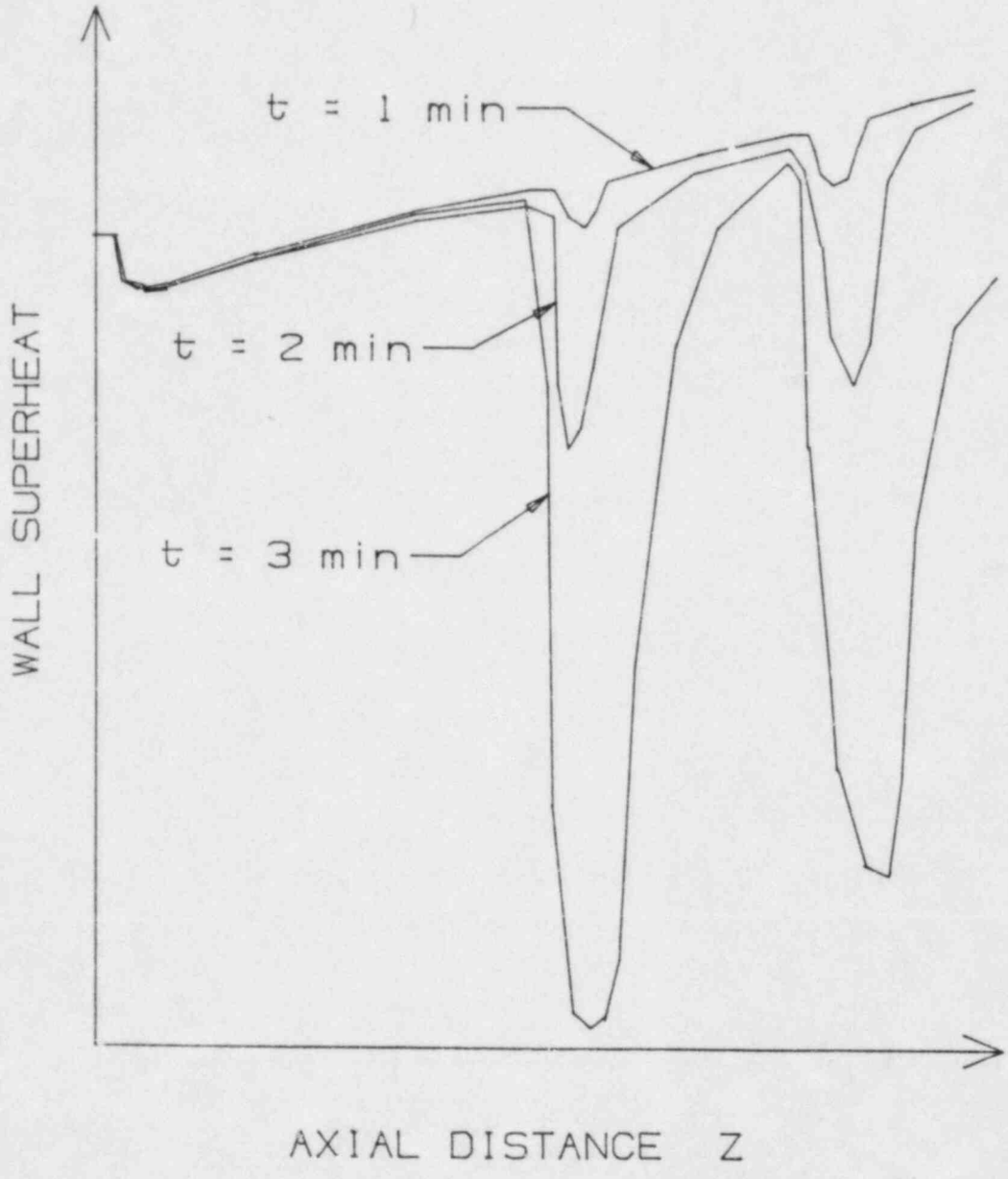

Figure 2-2. Vapor probe wake effect with two vapor probes installed.

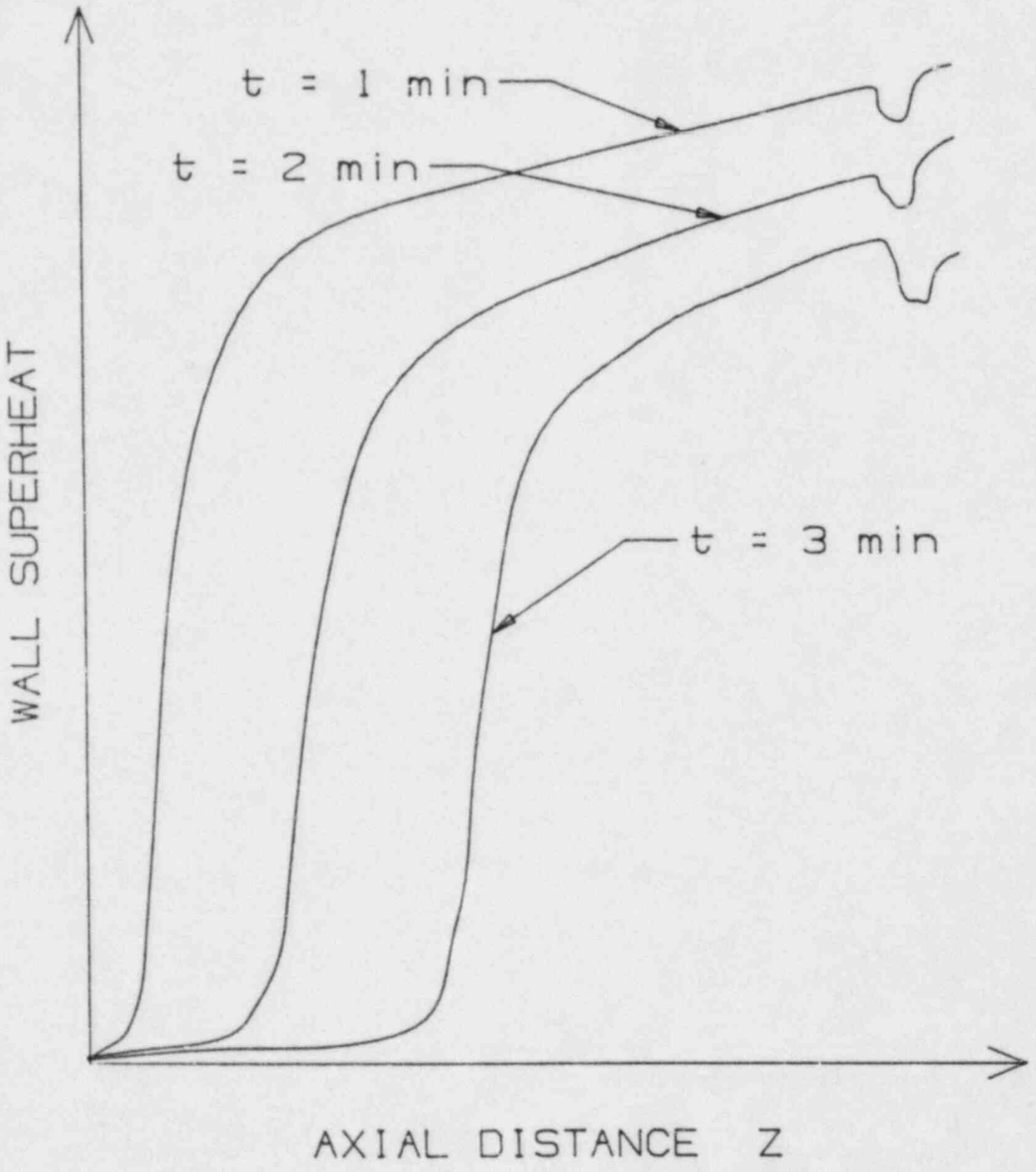

Figure 2-3. Wall temperature profiles during moving quench front experiment.

[2.4, 2.5] have clearly shown that heat transfer coefficients downstream from an inlet perturbation essentially attain steady state conditions within one to two fluid residence-periods. Therefore, by providing for a minimum of five to ten fluid residence periods in the time that it takes the CHF location to propagate a small acceptable distance (of the order of 1 cm), it was possible to obtain quasi-steady state heat transfer measurements downstream of the CHF location. In this manner, as the quench front approached the single vapor probe station, measurements of wall and vapor superheats could be obtained as a function of axial distance from the CHF point.

The moving quench front technique provided data over a wider range of inlet conditions than possible with fixed quench front experiments, although the probe intrusive effects continued to prevent vapor measurements at some inlet conditions. In addition, data were difficult to obtain at some inlet conditions due to the occurrence of severe flow pattern oscillations. Further expansion of the data base was prevented by facility limitations rather than experimental technique.

3. THE EXPERIMENTAL FACILITY

3.1 System Overview

The vapor superheat measurements obtained during these experiments utilized an improved version of the vapor probe developed by Nijhawan, et al. [3.1]. The vapor probe was inserted into an Inconel tubular test section maintained at typical post-CHF conditions. A two-phase heat transfer loop featuring a vertical single tube internal flow boiler, of the same geometry as the test section, was used to provide a steady flow of saturated steam and water to the test section. The vapor superheat measurements were continuously recorded on a stripchart recorder along with a differential pressure measurement over the 50 cm preceeding the vapor probe. Test section wall temperatures, pressures, and power levels were recorded every 5.2 seconds by the data acquisition system, which provided real time monitoring of the experiment.

3.2 The Two-Phase Heat Transfer Loop

The experiments were carried out in a forced-convection two-phase flow loop (figure 3-1), capable of tests with steam and water at pressures up to 5 atmospheres. A high capacity centrifugal pump was used to generate a constant mass flow-rate by operating the pump at high pressure head and maximum

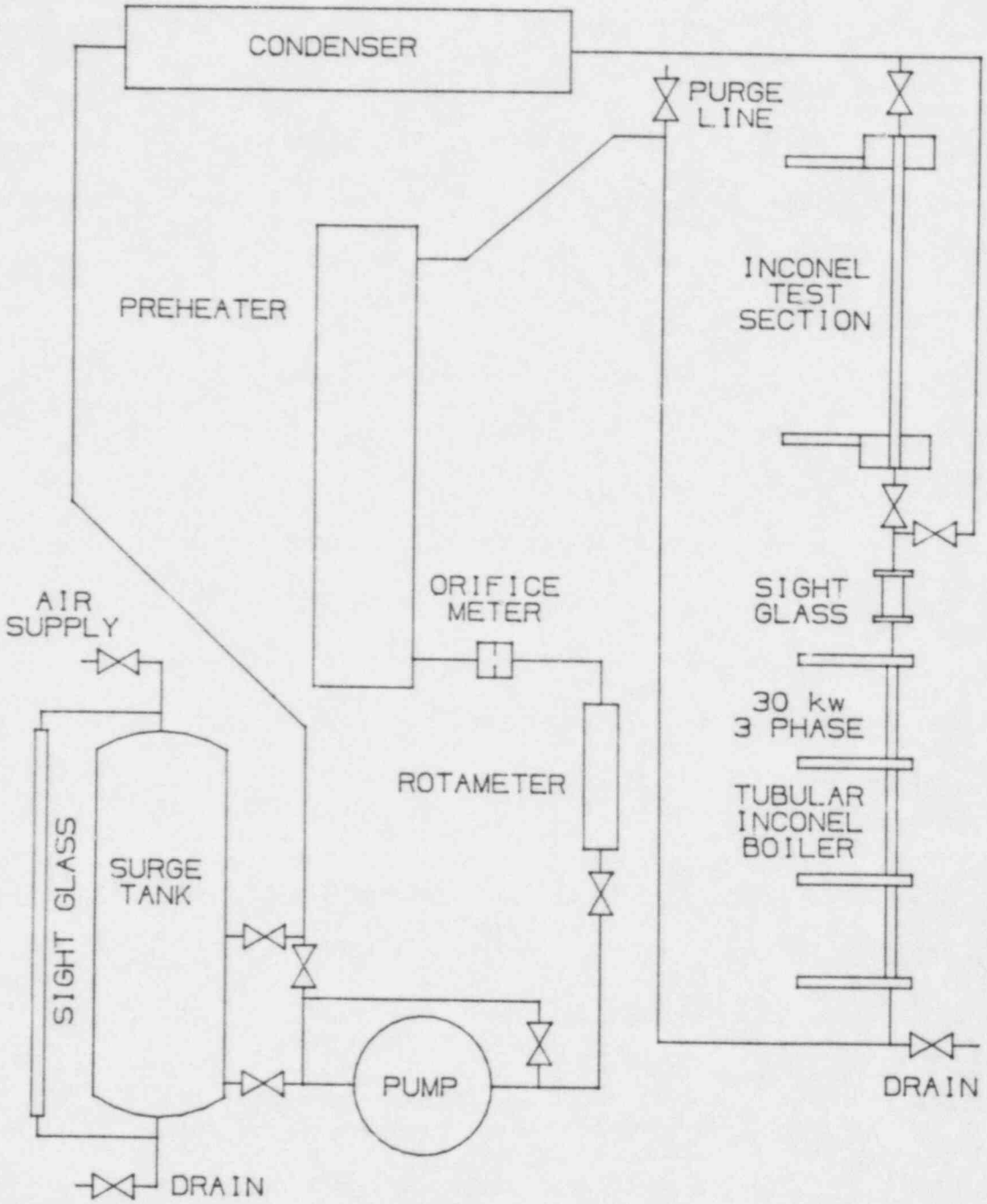

Figure 3-1. Lehigh two-phase heat transfer loop.

speed to minimize the effect of variations in the loop pressure on the mass flowrate. A surge tank placed between the outlet of the condenser and the pump inlet insured that the pump inlet was maintained at a constant pressure. The mass flow rate was regulated and measured by a valve and a rotameter. By maintaining a large pressure rise across the pump and a large pressure drop across the flow regulating valve, variations in test section pressure did not significantly alter the mass flowrate at the outlet of the rotameter. Due to difficulties with the orifice type flow meter located downstream of the rotameter, the mass flux was measured with the rotameter. A preheater was used downstream of the orifice flow meter to bring the fluid temperature to within approximately ten degrees of the saturation temperature.

A vertical upflow boiler constructed of the same Inconel tube as the test section was used to generate the desired inlet quality. Up to 13 kw of power was added to the flow in the 1.54 cm internal diameter tube over a length of 107 cm. A low voltage 3 phase AC variable reactance power supply provided direct heat generation in the wall. At the entrance to the boiler the fluid temperature was measured for use in the heat balance calculations to establish boiler exit quality. Electrical power for each phase of the power supply was measured

by a high speed analog to digital converter in the PDP 11 computer. The non-sinusoidal waveform of the variable reactance power supply neccessitated a numerical integration of the analog to digital output. The AC power supply featured separate controls for each of the three phases, permitting the operators to input more power to the fluid in one phase than the others. While the energy input to the flow over each of the three phases was calculated separately, only the total power was recorded in the data files. The results of a heat loss calibration experiment for the boiler insulation provided closure of the flow energy balance equation, yielding the outlet flow quality. Inlet sub-cooling varied from 25 C to 10 C, depending on mass flowrate, and outlet flow quality varied from 0 to 70 percent. The upper quality limit decreased with increasing mass flowrate due to limitations on boiler power input.

A sight glass positioned at the outlet of the boiler permitted observations of the flow pattern. This proved invaluable during both the trouble shooting phase of the investigation and during the production runs. In particular, the sight glass provided visual confirmation when the test data indicated flow pattern oscillations. During the initial phases of the investigation, the sight glass greatly

facilitated the diagnosis of several problems related to the introduction of flow to the test section at the beginning of an experiment. At the outlet of the sight glass, the flow could be directed through a bypass tube to the condenser or into the test section. Ball valves in the bypass and at the test section inlet permitted test section isolation and flow control (fig. 3-2). Standardized pipe was selected to minimize the variation in flow area from the boiler outlet to the test section inlet. The hardware was selected to avoid unswept regions where liquid could accumulate.

Both the bypass and test section outlet exited to the condenser which returned the working fluid to the surge tank to provide a closed system. This type of system provides a uniform system pressure, and conservation of the demineralized water. The loop pressure was controlled by adjusting an air pressure regulator on the surge tank. By allowing a slow discharge of air from the surge tank, the system pressure was maintained at a constant level regardless of system fluid inventory.

3.3 Test Section

The post-CHF test section (illustrated in figure 3-3) featured a 1.35 m heated length Inconel-600 tube with an

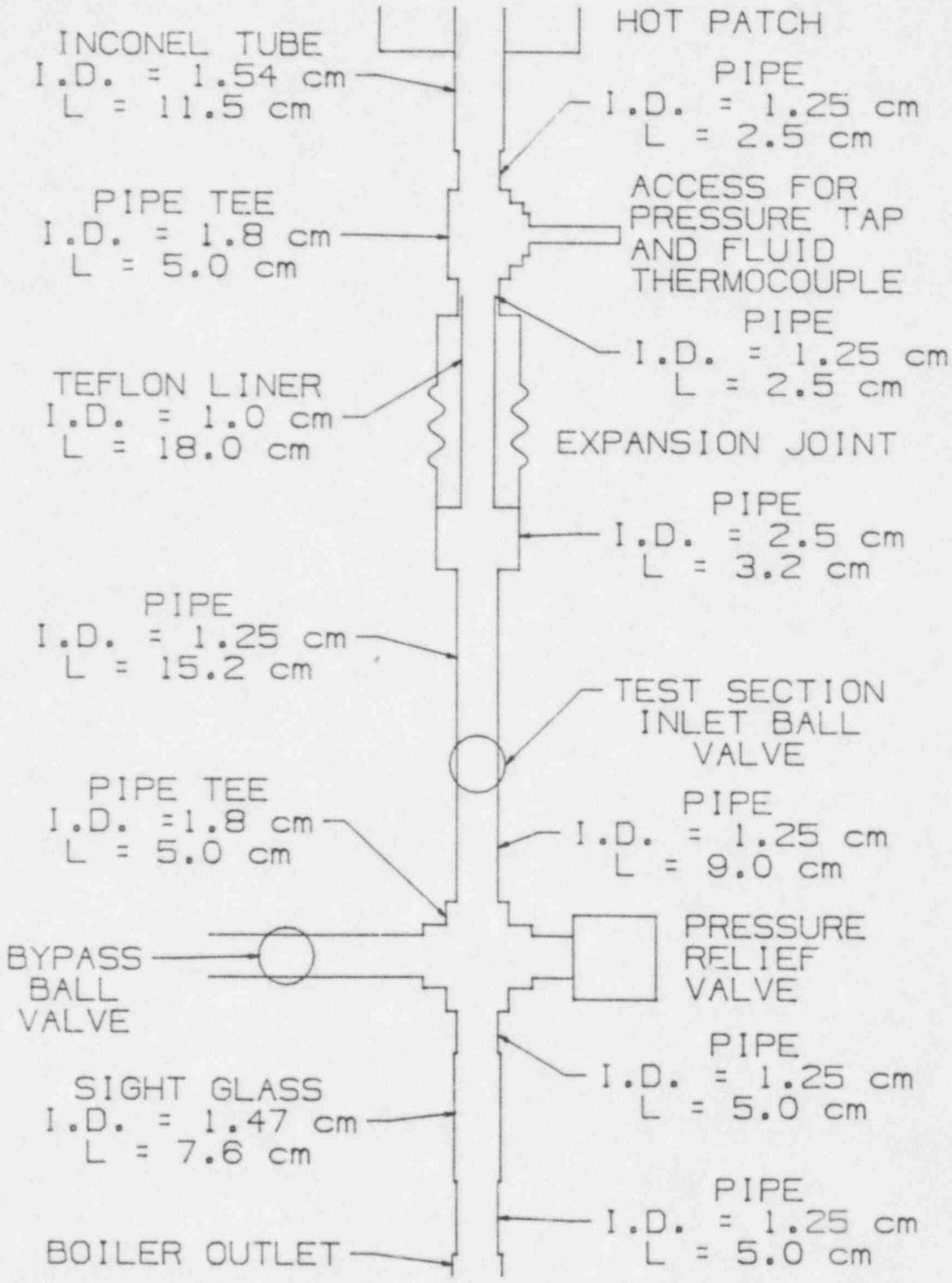

Figure 3-2. Pipe from boiler outlet to test section inlet.

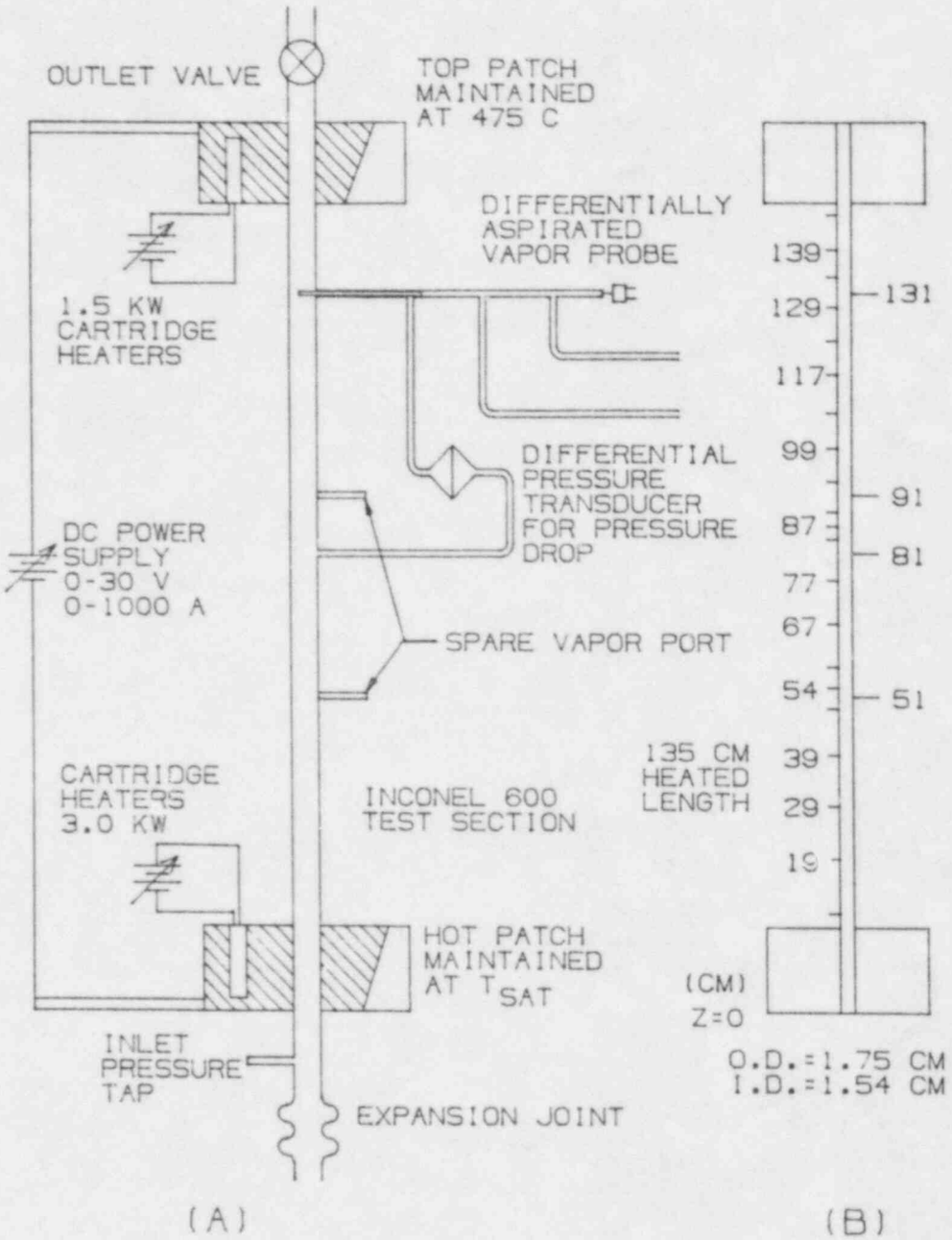

Figure 3-3. Post-CHF test section.

A) Test section components
B) Thermocouple locations

internal diameter of 1.54 cm and a wall thickness of 1.02 mm. A total of six small diameter Inconel tubes were welded to the test section at various axial locations. Three of the tubes, with an internal diameter of 3.2 mm and wall thickness of 0.8 mm, provided access for vapor probes. These "vapor ports" were located at 51.3 cm, 91.3 cm, and 131.3 cm above the bottom of the copper hot patch. All data presented in this report refer to the distance term "Z", which is referenced from the bottom of the hot patch. The other three tubes, with an internal diameter of 1.6 mm and wall thickness of 0.8 mm, were all located at a Z of 81.2 cm. These tubes were originally intended to provide support for a spacer, and were welded in a plane perpendicular to the axis of the test section. The tubes are evenly spaced at 120 degree intervals around the circumference of the test section. All six tubes were welded perpendicular to the surface of the test section with a tungsten inert gas welding technique (TIG).

The use of small diameter tubes with a minimum of fill metal at the weld was necessary to minimize the effect of the tubes on both the electrical heat flux generation and heat losses. This was particularly important in view of the multiple probe experiment. Previous work at Lehigh featured only one vapor probe inserted through a large diameter vapor port with

a large quantity of weld filler metal. The resulting disturbance of the wall temperature profile was undesirable for multiple probe experiments. In addition, the new vapor probes were much smaller than the vapor probes used previously (2.4 mm vs. 6.4 mm O.D.), which enabled the use of a smaller diameter vapor port with thin walls.

This was the first attempt at Lehigh to weld thin walled Inconel tube, and the task proved to be quite difficult. Most welds suffered from small cracks which weeped during hydrostatic pressure tests. Attempts to repair the cracks usually led to the formation of additional cracks near the repair. Eventually, a successful technique was developed, although by then two test sections had been fabricated, each with several leaks. It was determined that attempts to repair the leaks by welding might further damage the test sections, so high temperature braze was used to patch the leaks. This placed a temperature limit of 650 C on the test section in the regions of the braze patches. Discussions with vendors after this lengthy process suggested that more filler metal of a different composition would lead to a higher rate of success during the fabrication of future test sections.

Fixed CHF steady state experiments utilize the hot patch technique developed by Groeneveld et al. [3.2] to prevent a

quench front from propagating into the test section. Previous work at Lehigh demonstrated the need for a "top patch" to prevent the formation of a descending quench front at the test section outlet. Two large copper blocks containing cartridge heaters were brazed to the test section to serve as the hot patch and top patch. The hot patch, with a diameter of 15 cm and an axial length of 7.5 cm, contained 3 kw of cartridge heaters controlled with a variable transformer. Eight K-type ungrounded-junction thermocouples were placed in the hot patch for temperature measurement (fig. 3-4). The top patch contained 1.5 kw of cartridge heaters controlled with a variable transformer and four K-type ungrounded-junction thermocouples. Both the hot patch and the top patch were used as the power leads for the test section D. C. power supply. This power supply was capable of operation at 0-30v at 0-1000 amps, resulting in a maximum possible test section wall heat flux of 400 kw/m2.

The test section and hot patches were insulated with multiple layers of fibrous ceramic (Fiberfrax) insulative blankets. At a wall temperature of 550 C, test section heat loss was 210 watts, which represented a $3kw/m^2$ reduction in test section wall heat flux. This is approximately the same level as the heat losses experienced by researchers using

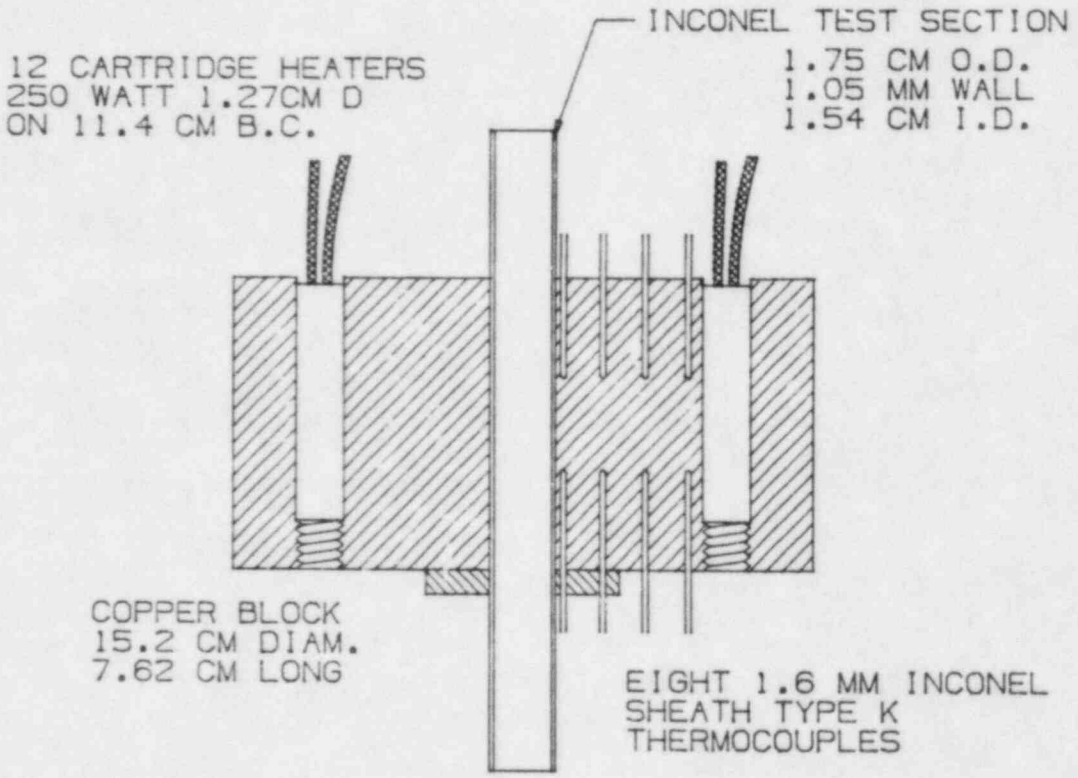

Figure 3-4. Inlet hot patch

the more difficult radiation techniques [3.3]. The selection of insulation over radiation was made when fixed quench front experiments were expected to dominate this program. Moving quench front experiments present some difficulties in calculating the test section heat loss due to the long time constant of the insulation. The effect of insulation temperature on wall heat flux during the cooling of the test section wall prior to the arrival of the quench front can be estimated, but the effect on wall heat flux during and after the passage of the quench front is difficult to quantify.

In order to determine the effect of the insulation's time constant on the wall heat flux, the test section was evacuated and heated to 600 C. After attaining steady state conditions, the test section power was turned off and the wall temperatures recorded as they decreased with time (figure 3-5). The wall thermocouples declined at an initial average rate of .37 C per second. This would correspond to a wall heat flux of 1.8 kw/m^2, 60 percent of the steady test section heat loss. Therefore, if during an experiment the wall temperature declined at a rate of .37 C per second, the specific heat released by the Inconel test section would be the heat lost to the insulation, and the wall heat flux would be equal to the electrical energy input to the Inconel. If the wall temperature increased

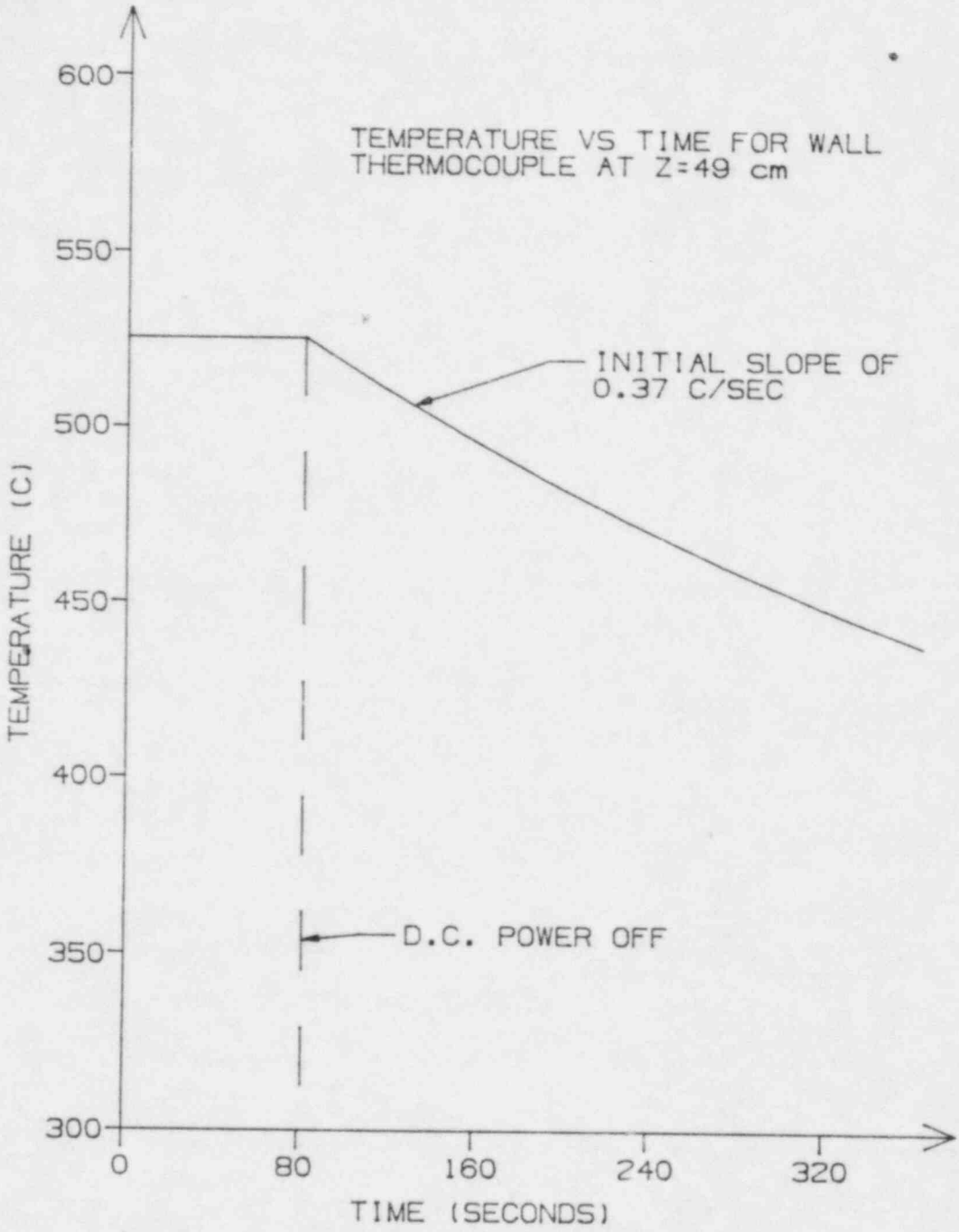

Figure 3-5. Determination of heat loss variation with time varying wall temperature.

early in the experiment, and decreased after reaching 50 to 75 C above its initial value, it would be much more difficult to determine the effect of the time varying heat losses. As a result, the heat losses are difficult to estimate for the moving quench front experiments. Fortunately the heat losses typically represent only 10 percent of the total heat flux, so that a 25 percent error in heat loss represents only a 2.5 percent error in wall heat flux.

With test section heat losses typically less than 2 watts per centimeter of length, the conduction of heat along the vapor ports and spacer support tubes from the test section into the insulation resulted in greater localized heat losses. Calculations indicating a heat loss of 3 to 4 watts per tube were confirmed when 4 watt trace heaters were wrapped around each tube. Prior to the installation of the trace heaters, the wall temperature profile was depressed by as much as 40 C at distances of 2.5 cm above and below the vapor ports, and 60 C in the vicinity of the three spacer support tubes. Installation of the trace heaters resulted in smooth wall temperature profiles at the power levels of 3 to 4 watts per trace heater.

The wall temperature measurements were obtained with 1.6 mm diameter, type K, Inconel sheathed thermocouples. The

thermocouple junctions were not grounded to the sheath in order to avoid electrical interference from the test section voltage. 18 thermocouples were placed at various locations between the hot patch outlet and the last vapor port. 3 more thermocouples were placed downstream of the last vapor port. Due to the risk of damage during welding, all wall thermocouples were clamped to the test section with wire bands. The consequences of the fin effect on the thermocouple, and the potential error in measurement, were determinaed to be of two types. Conduction of heat along the thermocouple would result in a lower junction temperature, and the thermal resistance between the wall and junction introduced a time delay when the wall temperature varied with time. In order to minimize the conduction effect, the insulation was prevented from contacting the thermocouple close to the junction, and the sheath was wrapped closely around the test section for the first one to two centimeters after the junction. This insured that the sheath close to the junction was at a nearly uniform temperature, eliminating conduction error.

The time constant of each thermocouple was determined experimentally by evacuating the test section at ambient conditions and then starting the D.C. power supply at a high power level. By recording the test section voltage and the

wall thermocouple measurement on a stripchart recorder, the time constant for the thermocouple's response to a ramp function was determined, as shown in figure 3-6. The time constants for the wall thermocouples were found to range from 2 to 3 seconds. This implied that the thermocouple junction was 2 to 3 seconds behind the actual wall temperature. During moving quench front experiments, the quench front typically progressed less than a centimeter in 3 seconds and it was determined that the errors that might result from a time constant effect would not be discernable.

3.4 Vapor Probe

The vapor probes used in this investigation were improved versions of the probe developed by Nijhawan et al. [3.1] at Lehigh University. The new probes retained the same operational concepts but with smaller diameter tubing, as shown in figure 3-7. Four primary requirements were identified in the previous work: (a) preventing sensor quenching by the droplets, (b) reducing radiation heat transfer from the hot wall to the sensor, (c) minimizing temperature equilization between liquid and vapor phases during the measurement process, and (d) operation at low to moderate qualities. The multiple probe objectives of this research effort necessitated incorporation of a fifth requirement, (e) minimal disruption of the flow as it

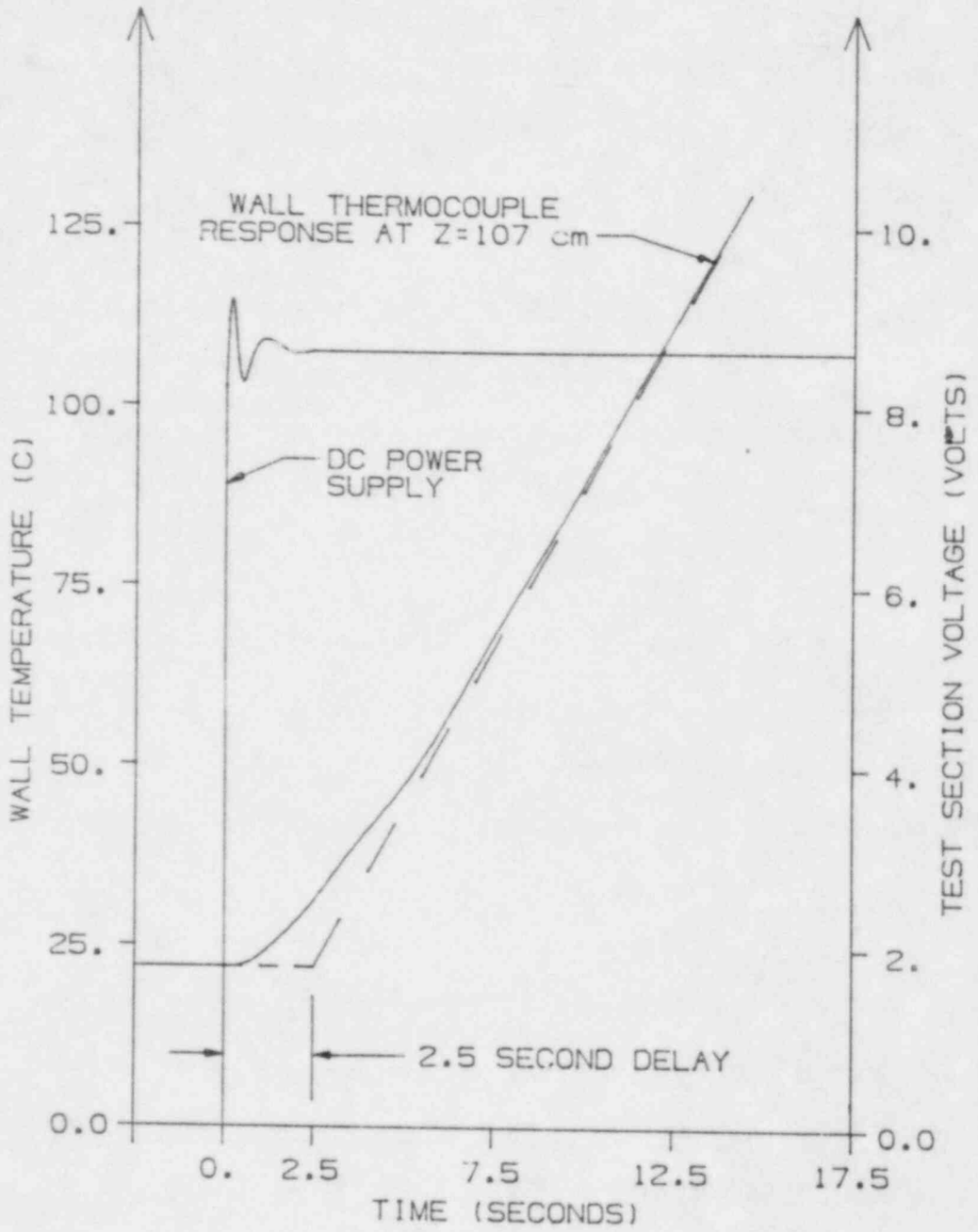

Figure 3-6. Determination of wall thermocouple time constant

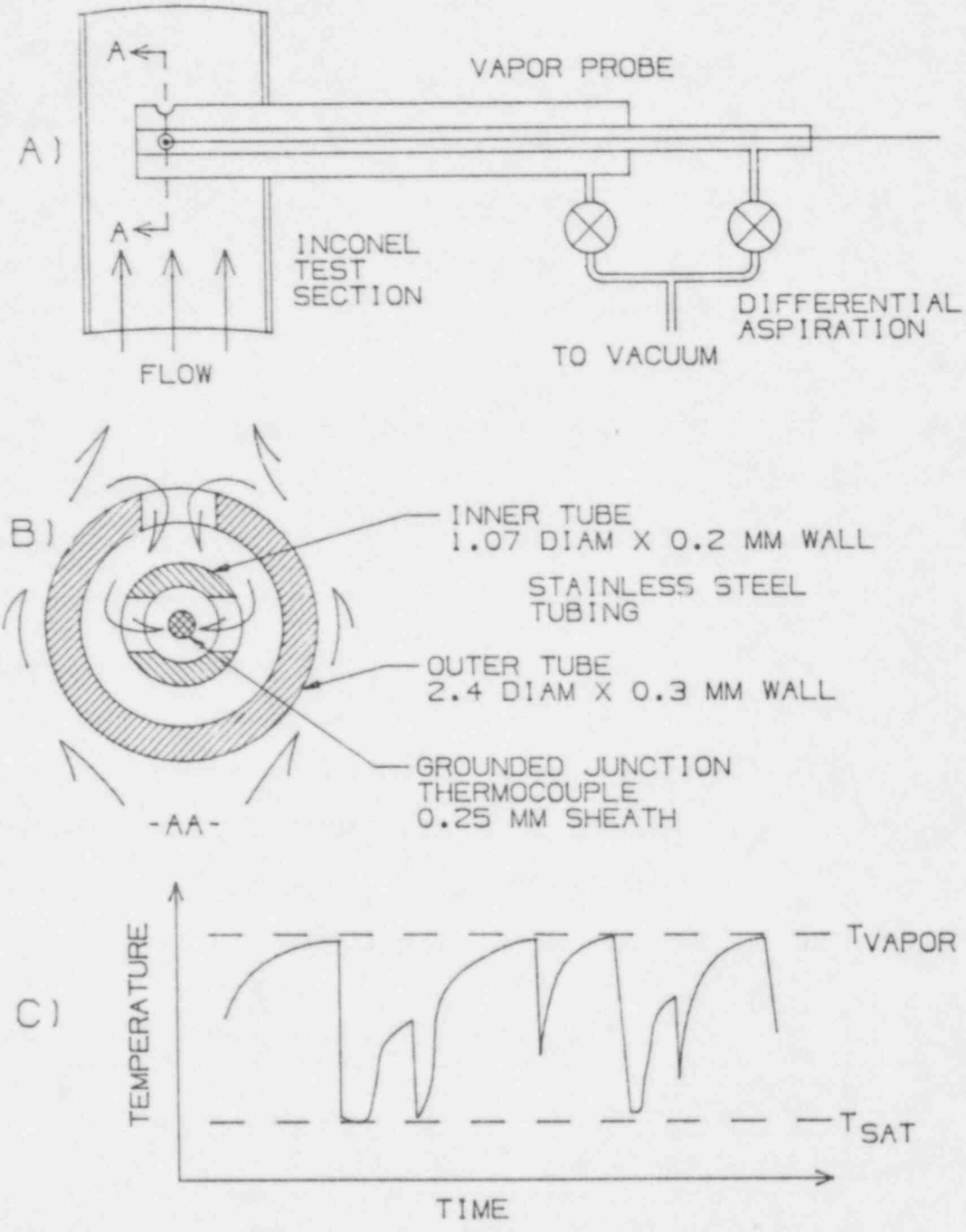

Figure 3-7. Differentially aspirated vapor probe

A) Vapor probe layout
B) Vapor probe construction
C) Vapor probe response

passed the vapor probe. The 6.4 mm outside diameter of the old vapor probes represented 42 percent of the test section internal diameter. This was felt to be unacceptable for the multiple probe experiments. The new vapor probes retained the geometry of the old probes, but utilized thin wall stainless steel hypodermic tubing and a 0.25 mm diameter thermocouple to enable a 62 percent reduction in outside probe diameter. The new probe diameter of 2.4 mm represented only 16 percent of the test section hydraulic diameter. Construction of the prototype probes with such small diameter tubing proved to be more difficult than expected. The exposed junction thermocouples were fragile and were eventually replaced with grounded junction thermocouples of the same diameter. A different technique was devised for connecting the probe to the aspiration lines on the production probe, resulting in much easier fabrication. Using this technique, further reduction in probe size is possible, although a smaller flow area may hamper fluid aspiration.

Difficulties with proper probe aspiration were encountered during the development phase of the investigation. Hydraulic analysis of the vapor probe showed that the pressure drop from the entrance of the probe to the control valves was small, and that choked flow was not the problem. Observation of the aspirated flow as it passed through clear plastic tubing revealed a

highly oscillatory flowrate. Experimentation revealed that the oscillations corresponded to the passing of liquid slugs through the micro-metering flow control valves. The vapor probe is conceptually a volumetric flow device in that the flow must be continuously passing the thermocouple junction for proper operation. If the volumetric flow rate should suddenly drop to near zero then whatever flow was in the vicinity of the junction would remain there, stagnating the measurement. The micro-metering needle valves feature an 0.48 mm orifice with a maximum liquid flow rate of 2 cubic centimeters per second. Whenever a liquid slug entered the valve, the probes volumetric flow rate would drop several orders of magnitude and thereby reduce the probe's effectiveness. This problem with the probe response was solved by using two valves and a separator on each aspiration line (fig. 3-8). The separator ensured that one valve always permitted a high volumetric flow of steam through the probe, while the other valve provided for constant drainage of the liquid phase. With the separators installed the vapor probe required very little adjustment for proper operation.

3.5 Differential Pressure Drop Measurement

The pressure drop along the test section was measured over a 50 cm region located upstream of the vapor probe. A Validyne differential pressure transducer produced an output of +_10

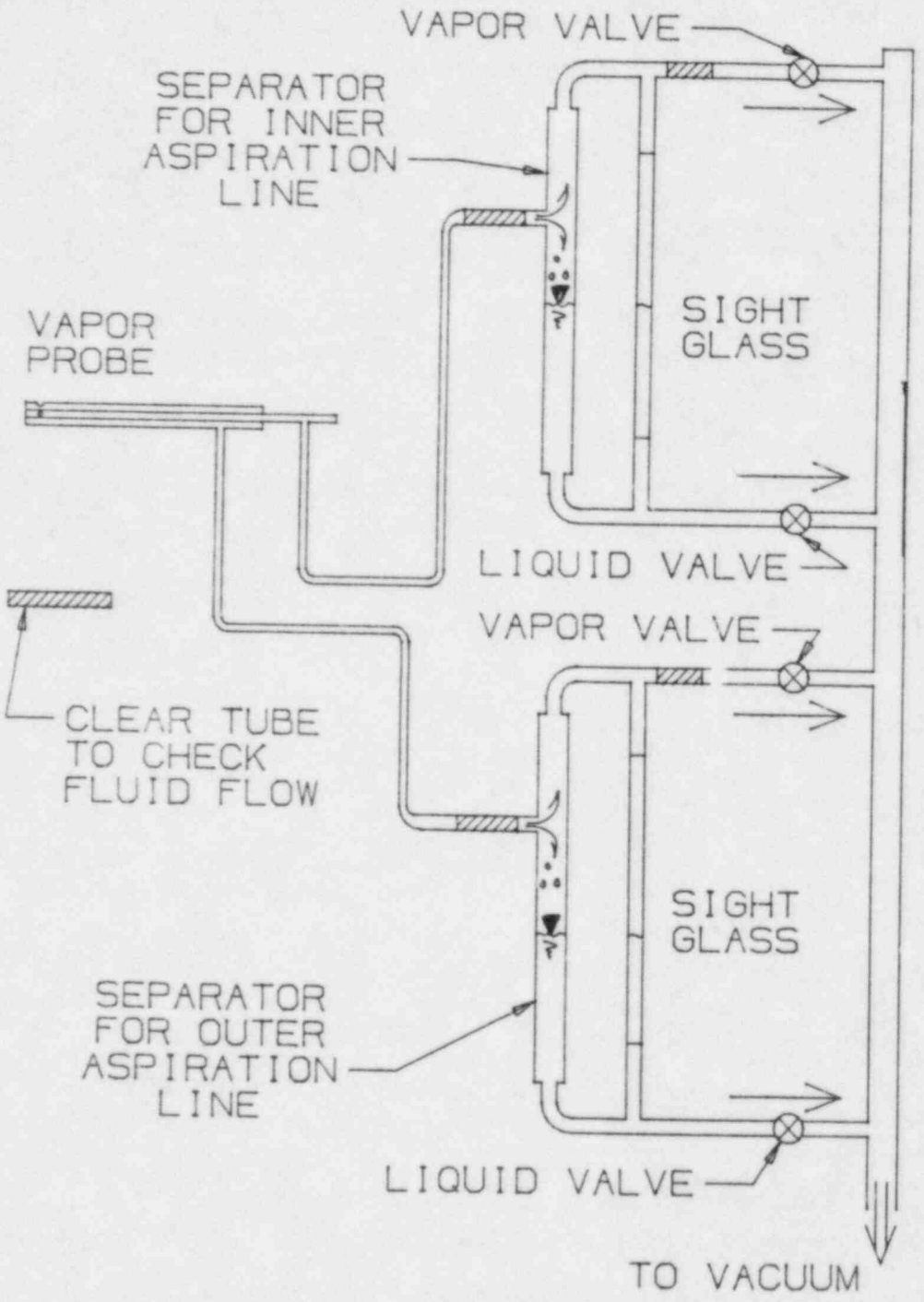

Figure 3-8. Vapor probe separators

vc :t proportional to its +_8600 N/m2 differential pressure range. The pressure taps utilized one of the spacer support tubes and the annular region between the vapor probe and the vapor port, for access to the flow, as illustrated in figure 3-9. The tubing between the pressure taps and the transducer required a single phase fluid throughout for proper measurement of the differential pressure. An argon purge system combined with trace heating of the tubing was used to ensure that the tubing was always filled with a gaseous phase. This permitted easy verification of the zero reading whenever the test section was empty.

3.6 Instrumentation and Data Acquisition

Data acquisition was performed by a Kaye Instruments Ramp Scanner and Processor capable of monitoring 104 channels. The unit was programmed to convert voltage measurements to the appropriate engineering units of the process variables. In addition, the unit could be programmed for alarm limits on any channel. Relays in the unit permitted the automatic shutdown of power during unanticipated transients. The unit scanned 20 channels every second and completed a scan of all 104 channels every 5.2 seconds. While the Ramp operated as a stand alone unit, it included two computer input/output ports which were connected to a Digital Equipment Corporation PDP 11-03 located

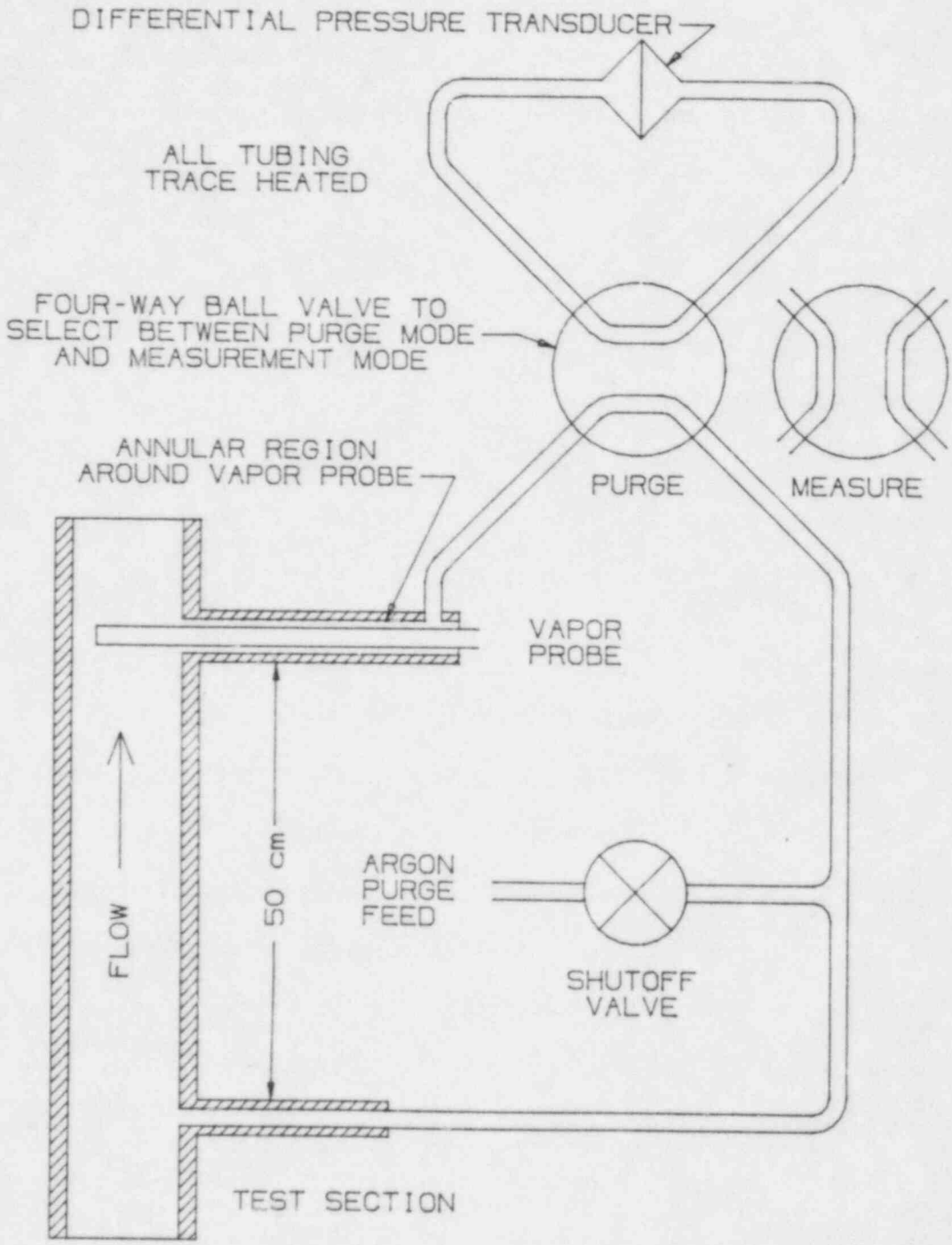

Figure 3-9. Measurement apparatus for differential pressure

in the lab (fig. 3-10). The computer provided three main functions: (1) real time monitoring of the experiment, (2) storage of the data on floppy disk, and (3) high speed analog to digital data acquisition with a Datel 16 channel A/D board. Programs were developed on the PDP 11-03 to receive data from the Ramp processor and scanner, perform thermodynamic calculations and high speed A/D conversion, display the relevant values on the terminal, and store the data on floppy disc. After an experiment, the data were transmitted to a DEC VAX 11/780, where the data were stored on hard discs. Data reduction was performed on the VAX due to the insufficient memory of the PDP 11-03.

Loop Instrumentation

Instrumentation of the two-phase loop consisted primarily of thermocouples and pressure transducers. The orifice flow meter was connected to a Validyne differential pressure transducer that produced a -10 v to +10 v signal proportional to the differential pressure. This signal fluctuated, and was inputted to the PDP 11-03 high speed a/d board to obtain accurate time averages. The voltages of the boiler's three-phase power supply were also inputted to the a/d board to enable accurate calculation of the true R.M.S. voltages. All other loop instrumentation was measured with the Ramp scanner.

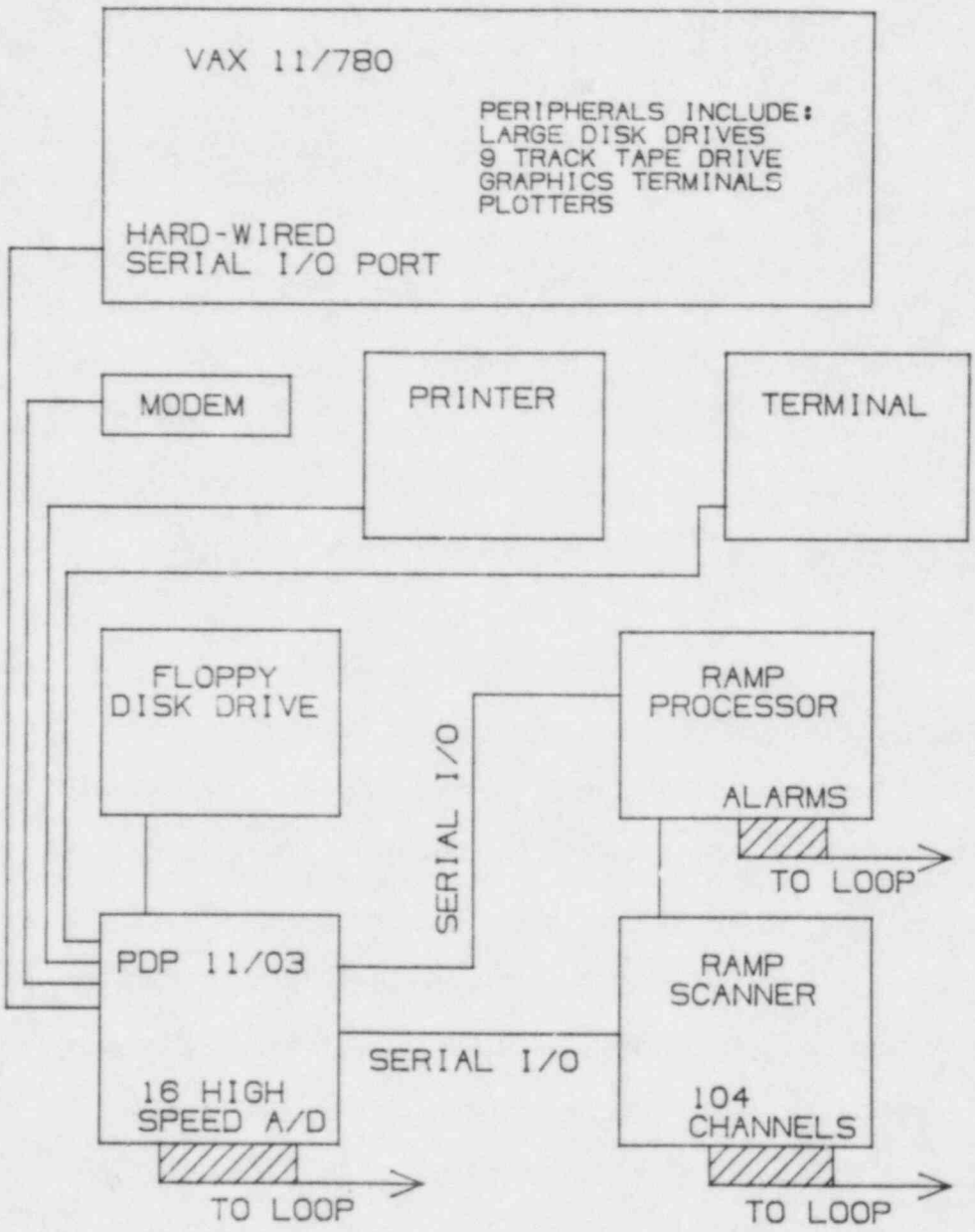

Figure 3-10. Block diagram of computer and data acquisition systems

Test Section Instrumentation

As mentioned previously, the test section included thermocouples on the test section wall and in the hot patches, power level measurements for the test section and hot patches, and pressure measurements at the test section inlet, spacer support tubes, and upper vapor port. All of these measurements were inputted to the Ramp scanner. In addition, the vapor probes were connected to stripchart recorders for uninterrupted display of the vapor temperature. A switching box with precise voltage references provided the stripchart with voltages equivalent to 200 C and 500 C for K type thermocouples. Prior to every experiment, these voltages were switched to the stripchart input to provide calibration references. A Validyne differential pressure transducer provided a pressure drop measurement across the 50 cm of tube upstream of the last vapor port. The transducer output was displayed on the same stripchart as the vapor probe, and was also inputted to the PDP 11-03 a/d board for high speed sampling. Due to the single-task limitation of the PDP 11-03 operating system, measurements of the pressure drop were obtained at 0.2 second intervals for only two continuous seconds during the complete 5.2 second data scanning cycle. The two total pressure measurements obtained at the same locations as the pressure drop measurements were

also displayed on the stripchart recorder to identify any oscillations in total pressure. This multiple stripchart configuration provided confirmation of the oscillatory flow patterns that occurred in some experiments.

3.7 Calibration

Mass Flux

Calibration of the rotameter was performed by maintaining a steady flow of water through the rotameter and into a container for mass measurement. This was performed over a range of flowrates on several occasions, in order to account for the slight non-linearity of the rotameter. Variation in results from different days was less than one percent, and the error in mass flowrate indicated by the rotameter is less than one percent. Attempts also were made to calibrate the orifice differential-pressure flowmeter. The orifice meter was accurate to one percent during calibration, but the differential pressure measurement often drifted 10 to 30 percent during experiments. An exact cause for the drift was not found, although the transducer's location relative to the pump was considered the probable cause of the drift. Attempts to correct the problem proved futile, and it was decided to use the flowrate indicated on the rotameter.

Inlet Quality

The boiler was calibrated by a series of heat balance experiments. The boiler heat loss was determined by pressurizing the loop to its maximum pressure, initiating flow at a high flowrate, and using the preheater to heat the fluid to within a few degrees of saturation temperature. Fluid thermocouples at the boiler inlet and test section inlet provided measurement of the fluid temperature drop and therefore heat loss to external surroundings. The fluid thermocouples had been tested previously, and were found to be within 0.2 C of 100 C during an atmospheric boiling test. The boiler wall temperatures were recorded along with the ambient temperature to determine the driving force for the heat loss. The experiment was repeated at lower temperatures to allow the calculation of a heat loss coefficient. Heat losses from the boiler inlet to the test section inlet were typically 150 watts.

Initial attempts at measuring the resistance of the Inconel tube proved inaccurate due to the low resistance of the tubing (8 milliohm per phase). The boiler power was found by flowing room temperature water into the boiler at maximum mass flow rate and maximum system pressure, and heating the water to within a few degrees of saturation. Power input to the fluid was over 9 kw, a factor of 60 over the heat losses, and was

sufficiently large to calculate the total power output from the power supply. Recording the R.M.S. values of the power supply voltages on the PDP 11-03 computer permitted a back calculation of the boiler resistance. This experiment was repeated at different power distributions between the phases, and the net power to the fluid was found to be reproducible to within 1/2 of one percent. At high power levels, the net boiler power error was less than one percent, but when the power level was less than 2 kw the error would exceed one percent due to the +_10 W error on the heat losses.

Wall Heat Flux

Test section power was calculated from the voltage drop across the test section, and the voltage drop across a 50 micro-ohm shunt located in the test section DC power supply. The shunt voltage yielded the current flowing through the test section to within 1/2 percent. The power level was confirmed by performing a single-phase heat transfer experiment similar to the net boiler power experiment. Heat losses were measured by evacuating and then heating the test section to a steady state temperature. Repeating this experiment at different power levels permitted the derivation of a heat loss formula, enabling the heat losses to be calculated as a function of the wall and ambient temperatures. The hot patches contained

cartridge heaters of known resistance, and required no power calibration tests. The heat losses for the hot patches were obtained with the same experimental procedure used in deriving the test section heat loss formula.

Pressure Drop

The differential pressure transducer used for the pressure drop measurements was calibrated by filling the test section with argon, thereby generating a zero point, and then flooding the test section with water to obtain a known differential pressure.

System Pressure

The total pressure measurements were obtained with Statham strain gauge pressure transducers. The transducers were calibrated with a Helicoid precision test gauge, resulting in measurement uncertainty of less than 3 kPa.

3.8 Experimental Procedure

The original goal of this experimental program was to obtain vapor temperature measurements at three axial positions downstream of a fixed CHF point. Starting with the test section flooded with argon at the same pressure as the loop, the test section, the hot patch, and the top patch were preheated

to temperatures in the range of 550 to 575 C. During this preheating stage, which required one hour if the test section started at ambient conditions, the operators brought the two-phase loop up to the desired operating conditions with flow through the test section bypass. At this time the instrumentation was checked out and the data acquisition programs on the computer commenced the real time monitoring of both the loop facility and the test section. When the various systems had reached steady state conditions, the boiler power was adjusted to obtain the desired test section inlet quality, while flow was passing through the bypass. When the inlet quality, mass flux, and system pressure were at the desired values, the following procedure would be executed to divert flow from the bypass into the test section:

(1) the test section outlet valve was opened

(2) the test section inlet valve was opened

(3) the test section argon feed valve was closed

(4) the bypass shutoff valve was closed

This sequency of events, taking approximately 3 seconds, minimized pressure transients in the loop and therefore allowed the loop to restabilize at the same mass flux, pressure, and flow quality within 5 to 10 seconds. During this brief period the test section power was adjusted to a target value

determined prior to the experiment. Under the original fixed-CHF experimental concept, the operators would wait until the wall temperature stabilized, and then record a data point. While maintaining the post-CHF flow conditions in the test section, the operators could vary any of the four inlet conditions; mass flux, inlet quality, pressure, and wall heat flux. When the wall temperature profile stabilized another data point would be taken.

Initial fixed-CHF experiments were attempted with only one vapor probe in an attempt to verify previous data. During this phase of the program, it was discovered that the fixed-CHF experiments were limited to a narrow range of inlet conditions. After considerable experimentation, the limitations were found to be due to two phenomena, the probe intrusive effect, and a possibly faulty braze joint in both hot patches. A few experiments were attempted with two probes, but concerns over the probe intrusive effect resulted in abandoning the multi-probe objective.

Evaluation of the experiment and data acquisition capabilities led to the decision that the program should focus on moving quench front experiments. The data acquisition program was modified extensively to minimize the time between data scans for the moving quench front experiments, with a complete

set of measurements obtained every 5.2 seconds. The moving quench front experiments were performed with only one vapor probe, located at the last vapor port. The only modifications to the fixed-CHF procedure were to maintain the hot patch at the saturation temperature so that the hot patch was adiabatic, and to hold the test section power level constant throughout an experimental run to permit easier interpretation of the reduced data. The target power level was usually selected to produce maximum wall temperatures of 600 to 650 C. The four variables of the experiment, pressure, inlet quality, mass flux, and heat flux, were established using the same procedure as the fixed-CHF experiments, prior to diverting the flow from the bypass to the test section. As the quench front began to propagate up the test section, the vapor probe was adjusted to optimize probe response. One operator was responsible for the vapor probe response, and the other monitored the progress of the experiment on the terminal and noted on the vapor probe stripchart the average flowrate indicated by the rotameter. The flow oscillations observed at the rotameter seldom exceeded 5 percent of the flowrate. The resulting error in measurement was an absolute error of ± 0.4 kg/m^{2}sec due to the "eye-ball average" plus an additional ± 1 percent of the flowrate for rotameter uncertainties, resulting in a total mass flux

uncertainty of +_(0.4kg/m^2sec + 0.01*G). During the production runs of the project, this was the primary mode of operation.

4. RANGE OF DATA

A total of 154 production experiments were run during this investigation, of which 144 runs were moving quench front experiments and 10 runs were fixed-CHF experiments. The range of conditions attempted during this investigation were:

Mass flux (G)	13 to 85 $Kg/m^2/sec$
Pressure (P)	240 to 570 kPa
Inlet flow quality (Xin)	0 to 70 percent
Wall heat flux (q''_w)	18 to 57 Kw/m^2

Error estimates, detailed in Appendix C, indicate the following degrees of uncertainty in the experimental conditions:

Mass flux (G)	$\pm$(0.4kg/m^2/sec + 0.01xG)
Pressure (P)	$\pm$ 3 kPa
Inlet flow quality (Xin)	$\pm$ 0.008 (low Xin) to
	$\pm$ 0.04 (high Xin)
Wall heat flux (q''_w)	$\pm$ 3%

The inlet quality and mass flux for these 154 runs are plotted in figure 4-1. The shaded area represents inlet conditions which could not be obtained due to limitations on the maximum boiler power. Attempts to generate inlet conditions in this region resulted in wall heat fluxes that exceeded the

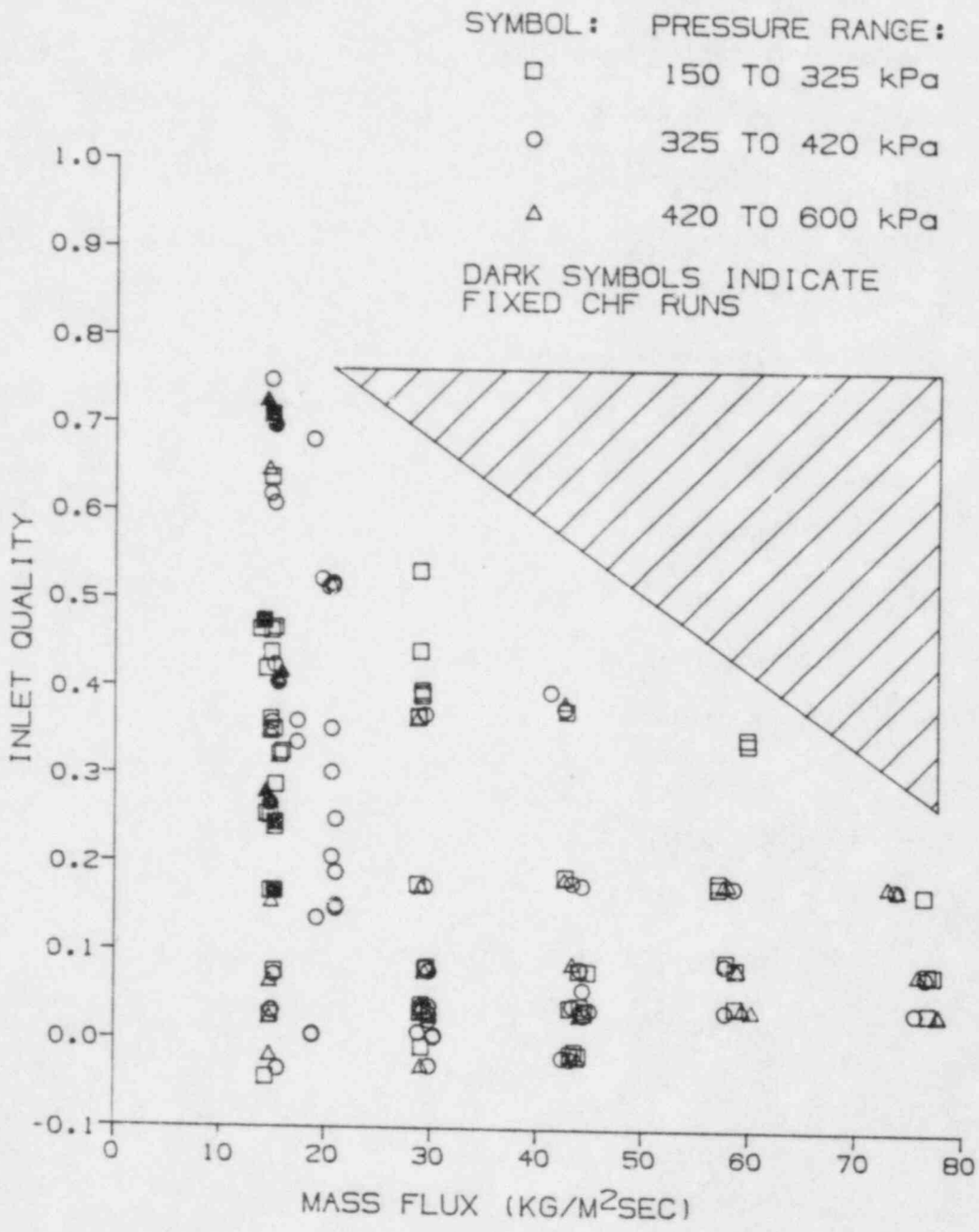

Figure 4-1. Mass flux and inlet quality for all production runs

critical heat flux, resulting in boiler dryout and rapid increases in boiler wall temperatures. During such excursions, the boiler wall would rise by as much as 75 C per second, resulting in automatic boiler shutdown by the data acquisition system. The permanent programming in the data acquisition system required two consecutive over temperature measurements before turning the boiler off, resulting in a delay of 5 to 10 seconds. On one occasion the boiler wall temperature exceeded 800 C, prompting a decision to cease further attempts to run in this region. Analysis with MacBeth's correlation for critical heat flux [4-1] showed that at the higher power levels corresponding to this region, the boiler wall heat flux was often 75 percent of the predicted critical heat flux.

For the 154 production runs, a rating system was developed to characterize the vapor probe response and the steadiness of the flow:

1-7 were moving quench front runs:

1- Steady flow pattern with excellent vapor probe response. Vapor probe interpretation error typically less than +_5 C.

2- Minor oscillation in flow pattern with excellent vapor probe response. While minor flow pattern oscillations were observed in the sight glass, the impact on the

data appeared to be negligible. Vapor probe interpretation error typically +_5 C.

3- Steady flow pattern with fair vapor probe response. Vapor probe interpretation error typically less than +_15 C.

4- Minor flow pattern oscillation with fair vapor probe response. Vapor probe interpretation error typically less than +_20 C.

5- Minor flow pattern oscillation with poor vapor probe response. Vapor probe interpretation error typically +_25 C.

6- Oscillatory run. Flow pattern was observed to oscillate severely. Many runs oscillated from bubbly flow to dispersed droplet flow. Excellent vapor probe response yields limited qualitative data.

7- Oscillatory run similar to rating 6, but without vapor probe response. These runs did not yield any data.

11- 17 were fixed-CHF runs. Subtract ten from their rating and use the corresponding moving quench front rating description.

The 24 runs with a rating of 1, plotted in figure 4-2, featured low mass fluxes, and were primarily with medium to

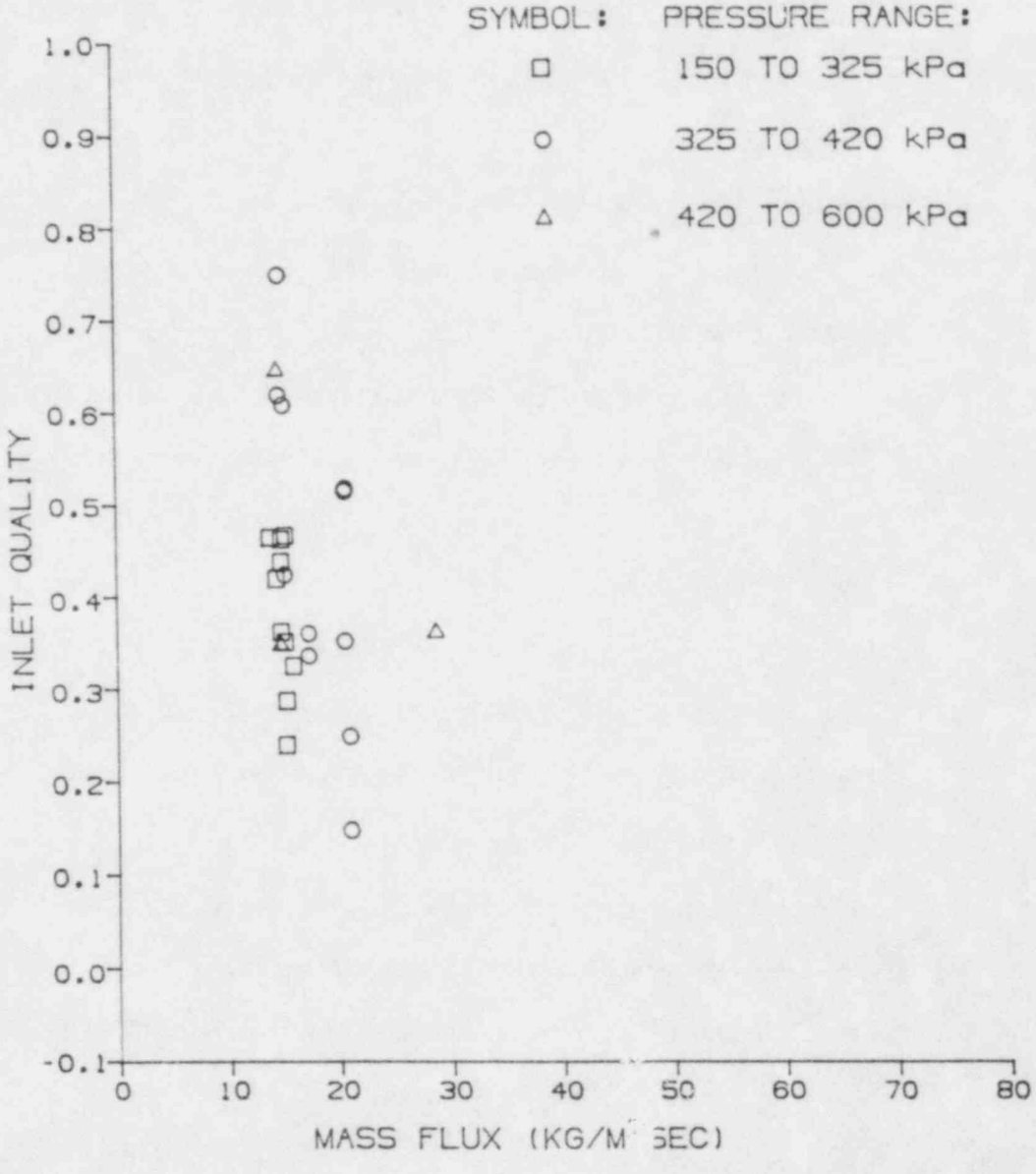

Figure 4-2. Mass flux and inlet quality for runs with rating of 1

high inlet qualities. All runs that demonstrated steady flow were rated 1, 3, 11 or 13, and are plotted in figure 4-3. It is important to observe that the runs at lower qualities and higher mass fluxes are all in the medium to high pressure ranges. The runs that featured minor flow oscillations that were judged to not significantly alter the data are plotted in figure 4-4. While all mass fluxes and qualities are represented in these groups, it should be noted that only one run in the high pressure range had an inlet quality greater than 20 percent. Runs that exhibited severe oscillations were rated 6, 7, 16, or 17, and are plotted in figure 4-5. These runs demonstrated a direct dependence of the vapor temperature on the flow pattern, and were not reduced due to difficulty in quantifying the inlet flow quality as a function of time. Qualitative observations from the oscillating runs are presented in Appendix A.

Rating the 154 production runs resulted in 579 data points being obtained from the 123 runs that did not oscillate severely. A data point includes complete axial information on the wall temperatures, wall heat fluxes, and flow equilibrium qualities, the location of the quench front with its associated CHF quality, and the vapor temperature at the vapor probe. The mass flux and CHF quality for the 579 points are plotted in

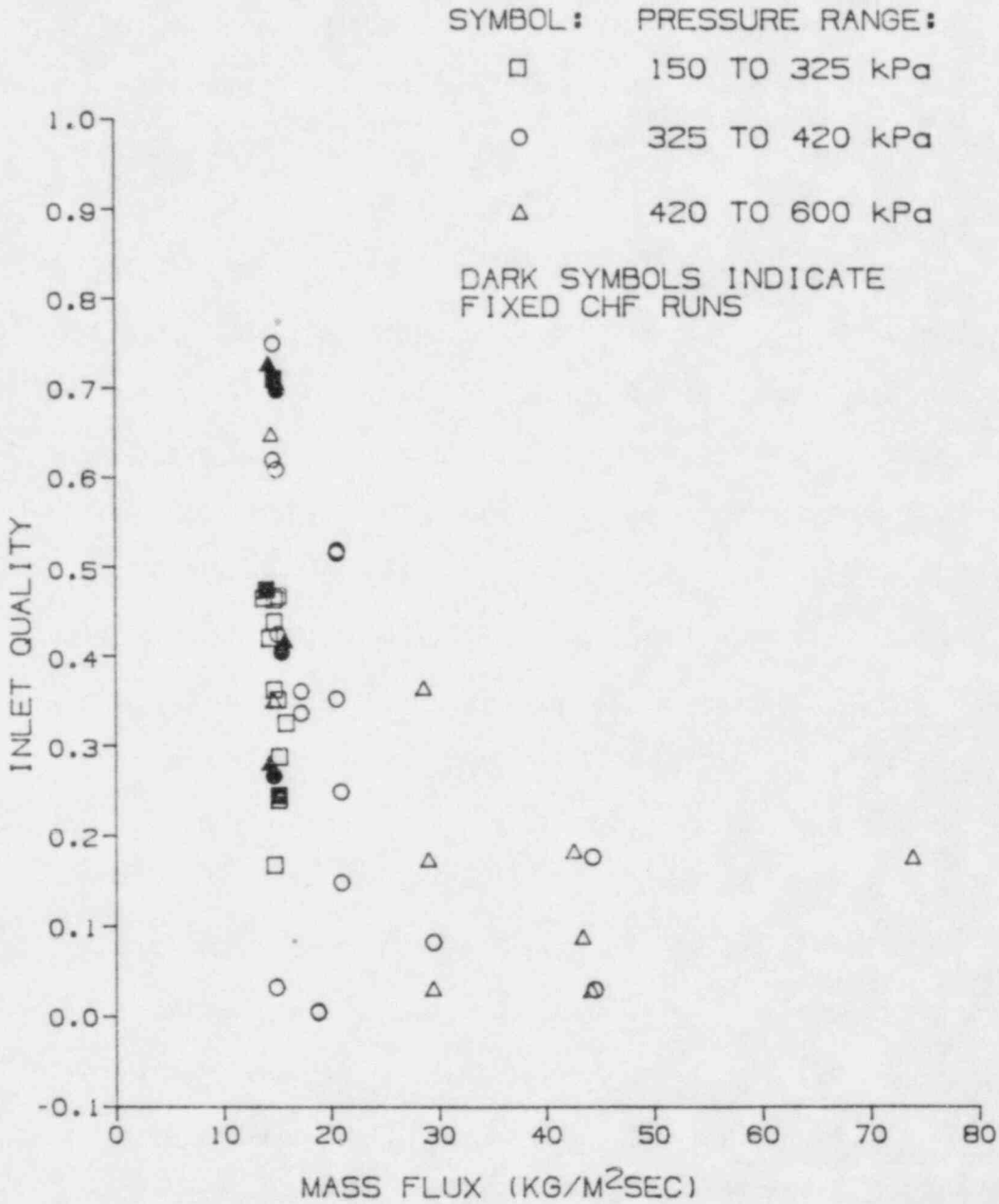

Figure 4-3. Mass flux and inlet quality for runs with rating of 1, 3, 11, 13

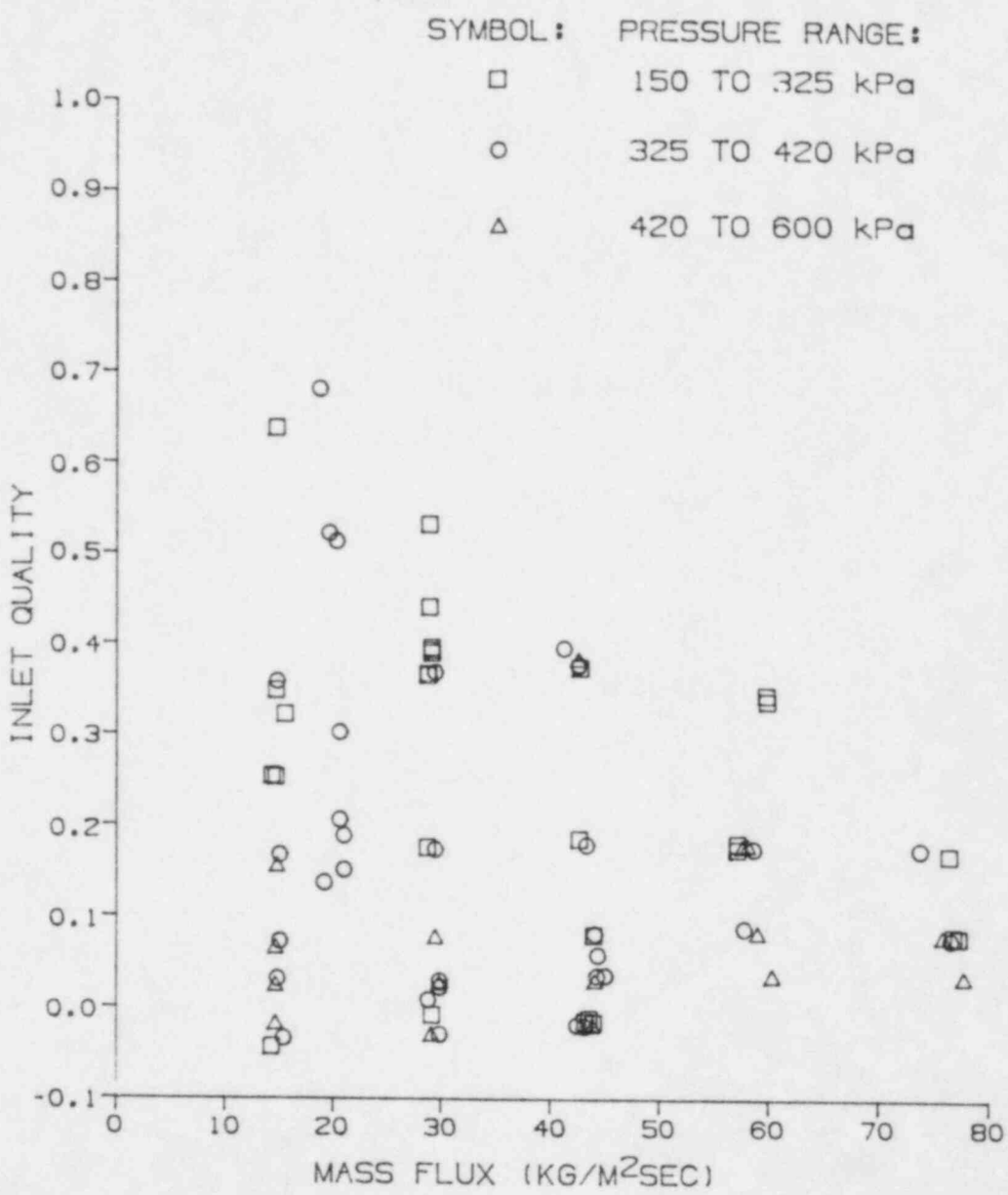

Figure 4-4. Mass flux and inlet quality for runs with rating of 2, 4, 5, 12, 14, 15

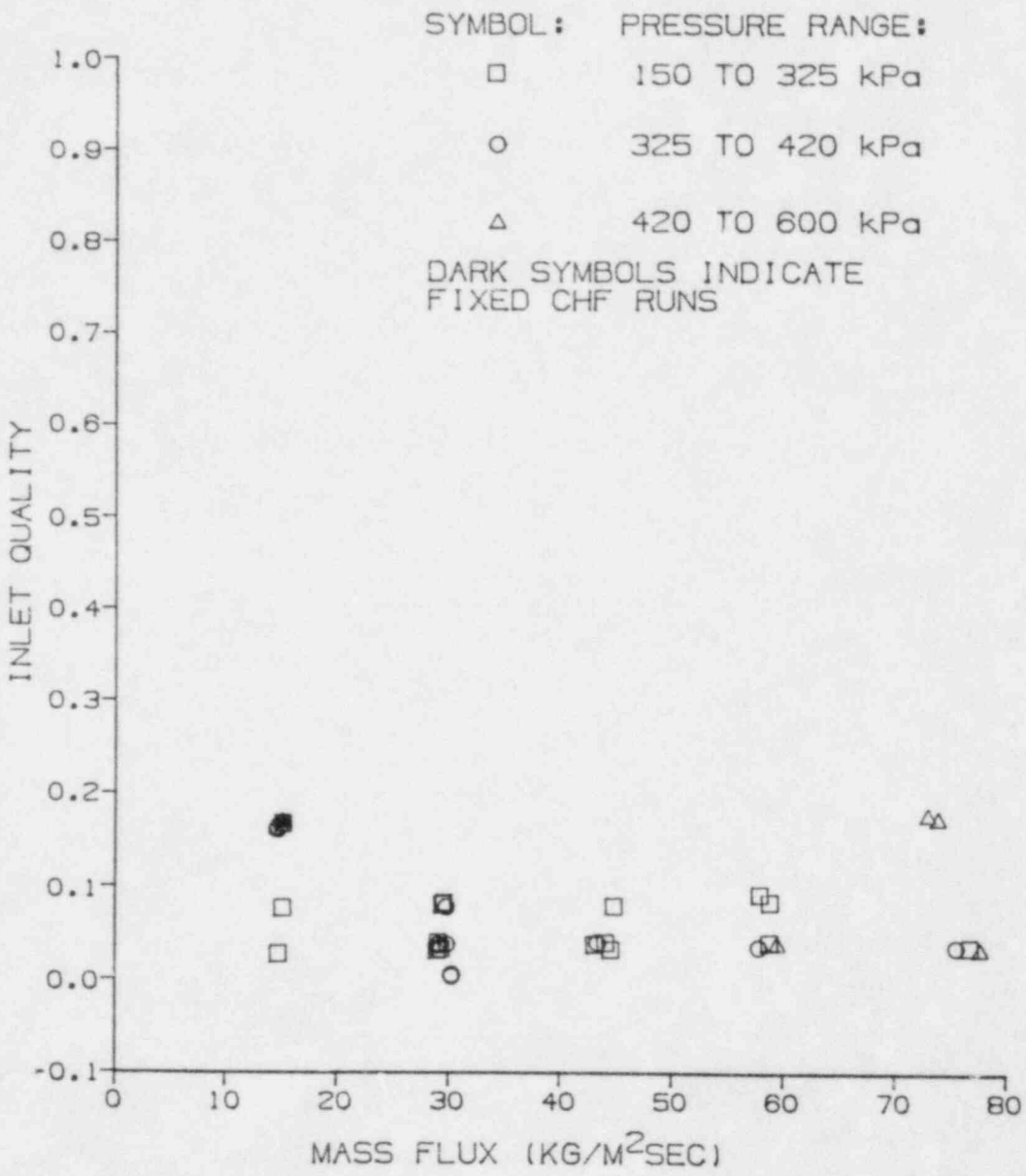

Figure 4-5. Mass flux and inlet quality for runs with rating of 6, 7, 16, 17

figure 4-6. Six separate plots, figures 4-7 to 4-12, of the same 579 points grouped by ranges of mass flux and plotted by CHF quality and distance between the quench front and the vapor probe reveals the loss of data resulting from the probe intrusive effect. The greater the quantity of liquid present in the test section, the greater the tendency towards preferential quenching at the probe. Once a quench region was established downstream of the vapor probe, a descending quench front would move upstream of the vapor probe, resulting in a reduced or zero vapor probe measurement. Any data obtained after the descending quench front passed the probe was judged to be invalid and no attempt was made to quantify the resulting reduction in vapor superheat.

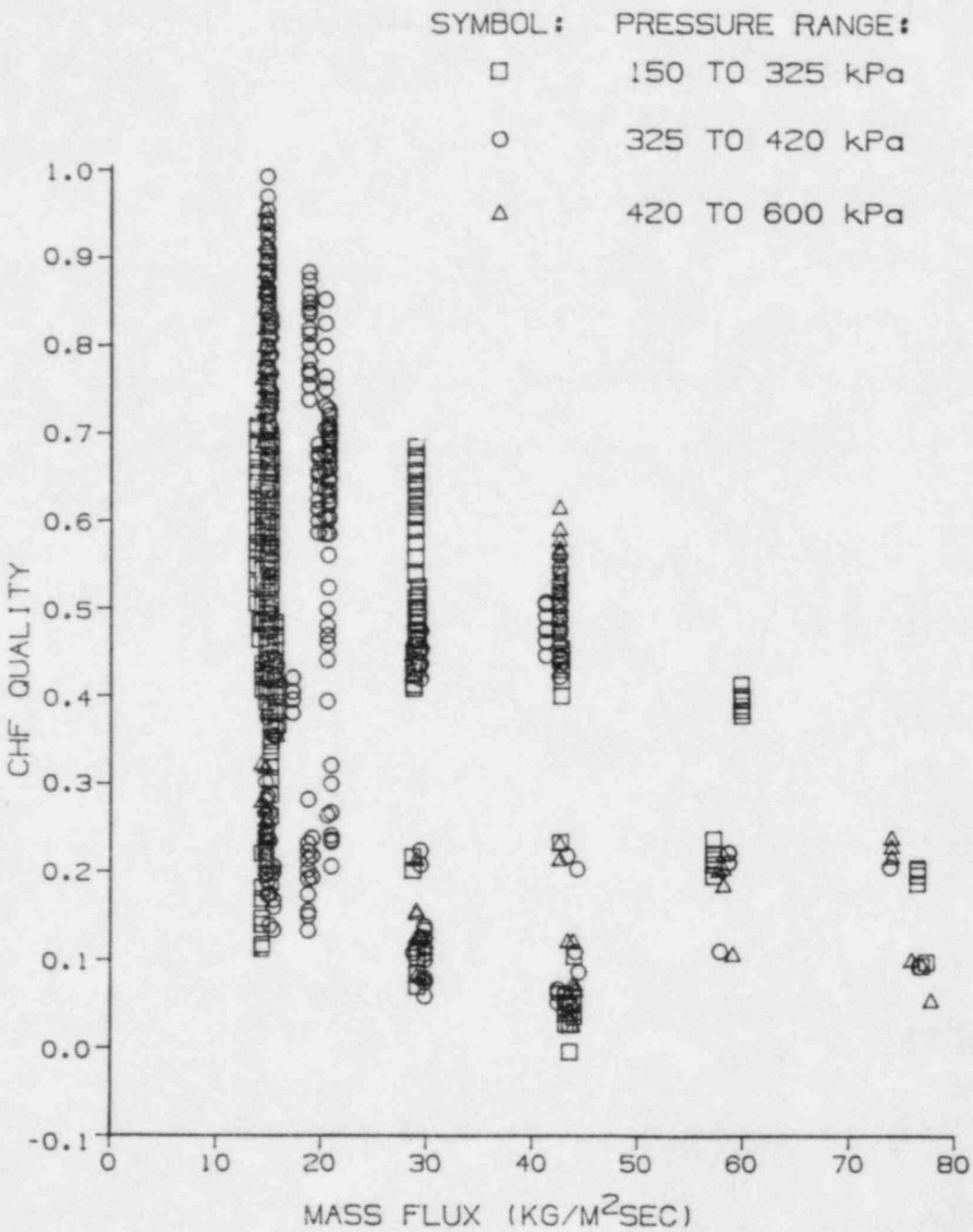

Figure 4-6. Mass flux and CHF quality for all reported data points

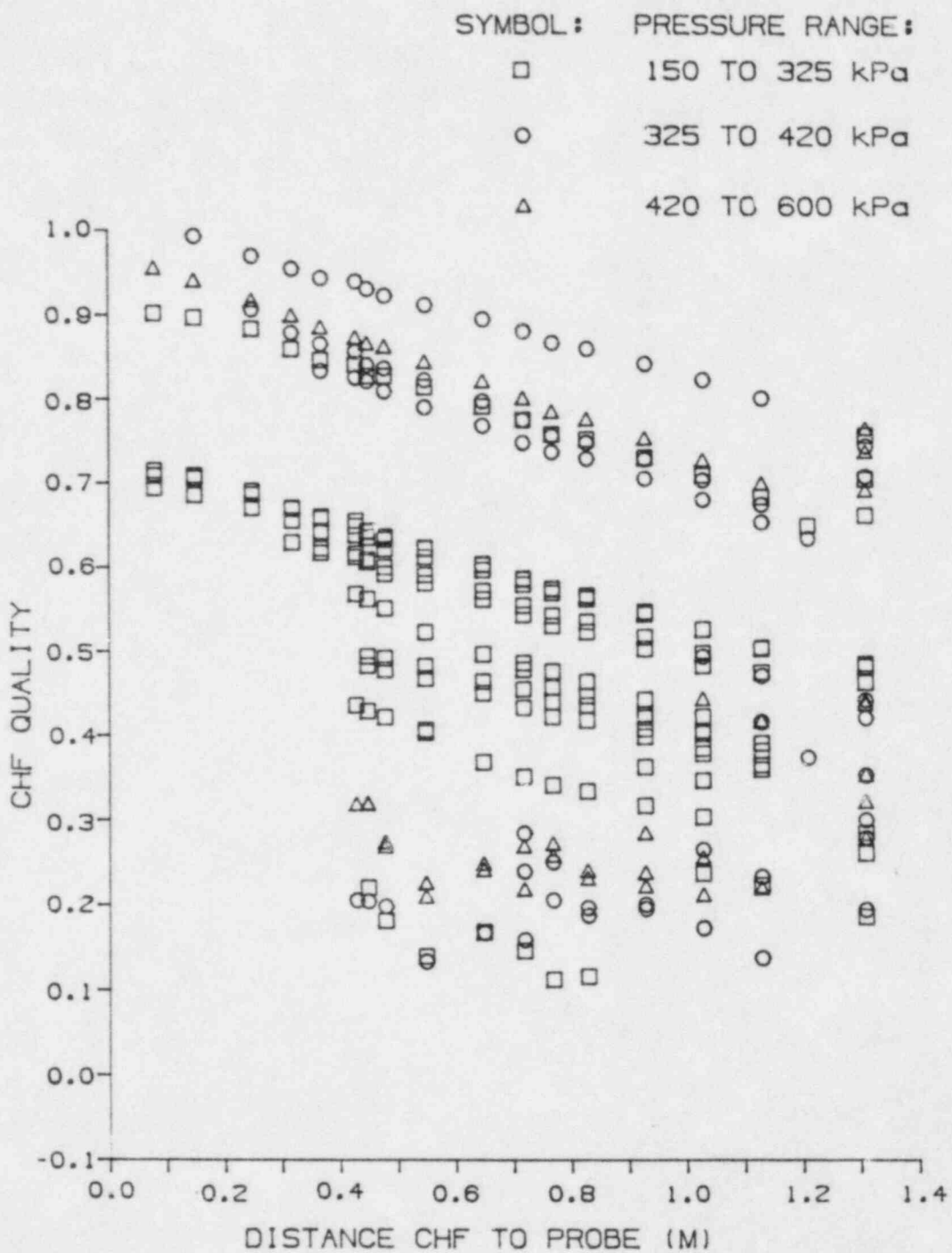

Figure 4-7. Distance vs. CHF quality for all data points with G between 12 and 16 kg/m^2 sec

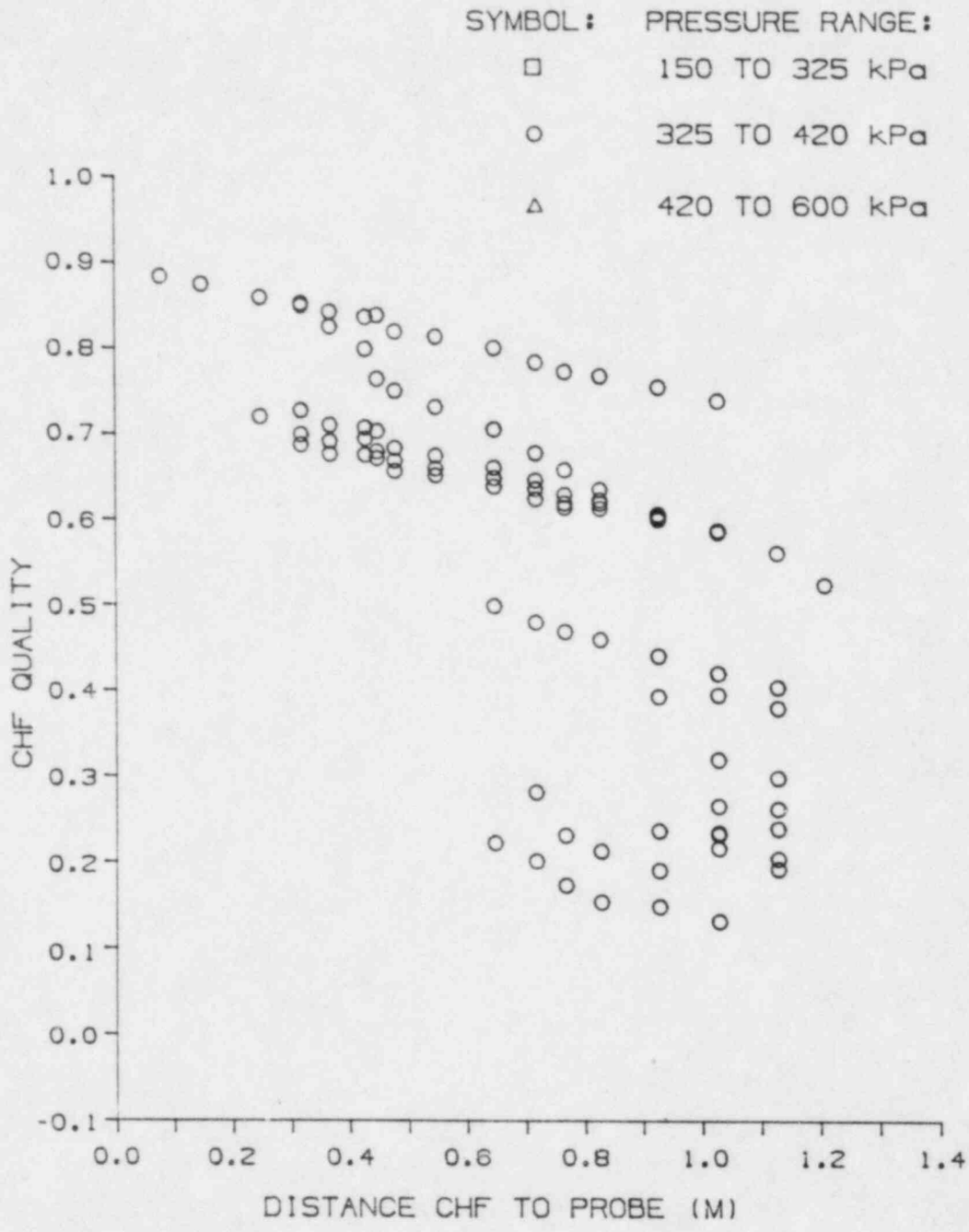

Figure 4-8. Distance vs. CHF quality for all data points with G between 16 and 25 kg/m^2 sec

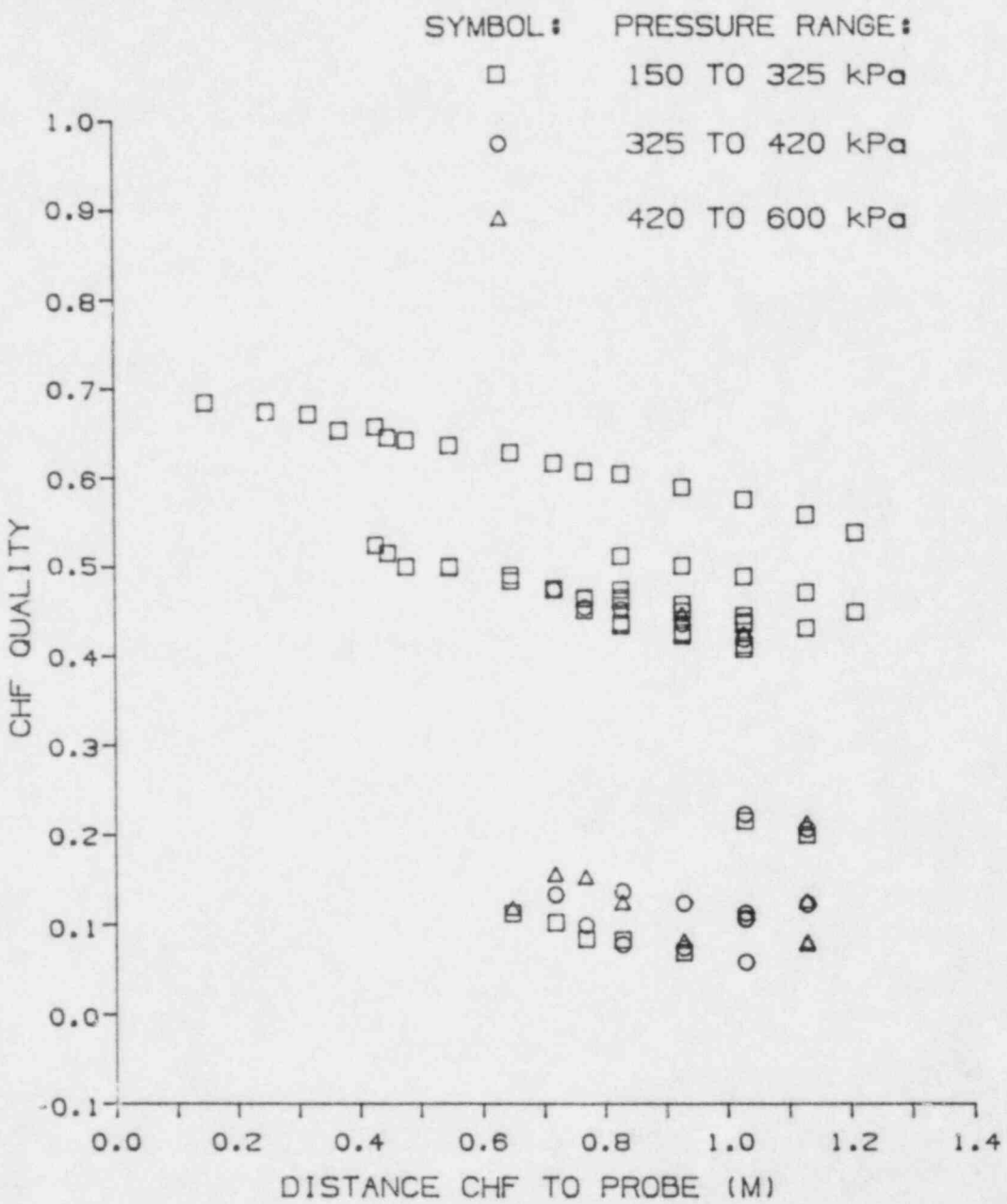

Figure 4-9. Distance vs. CHF quality for all data points with G between 25 and 35 kg/m^2 sec

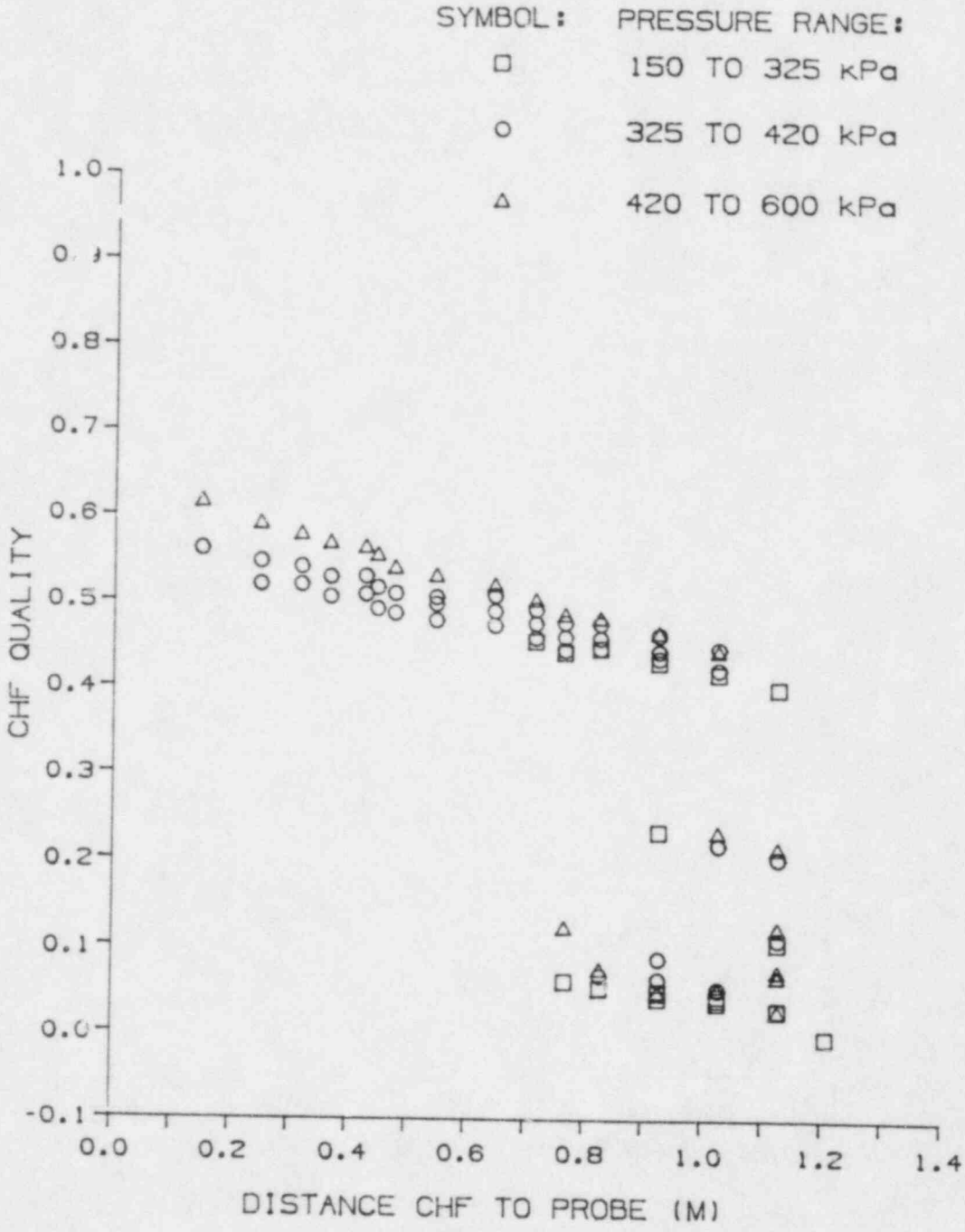

Figure 4-10. Distance vs. CHF quality for all data points with G between 35 and 50 kg/m^2 sec

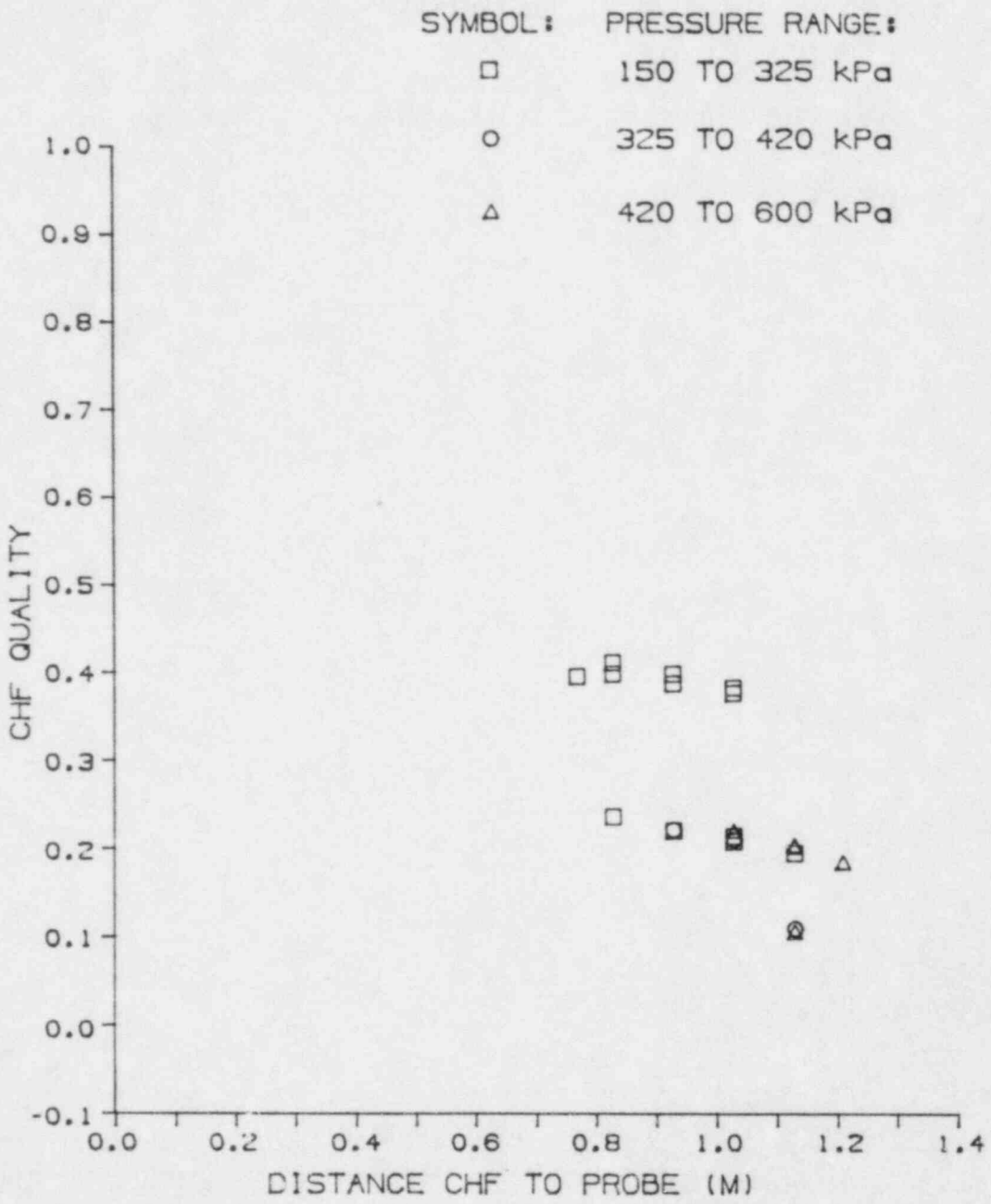

Figure 4-11. Distance vs. CHF quality for all data points with G between 50 and 65 kg/m^2 sec

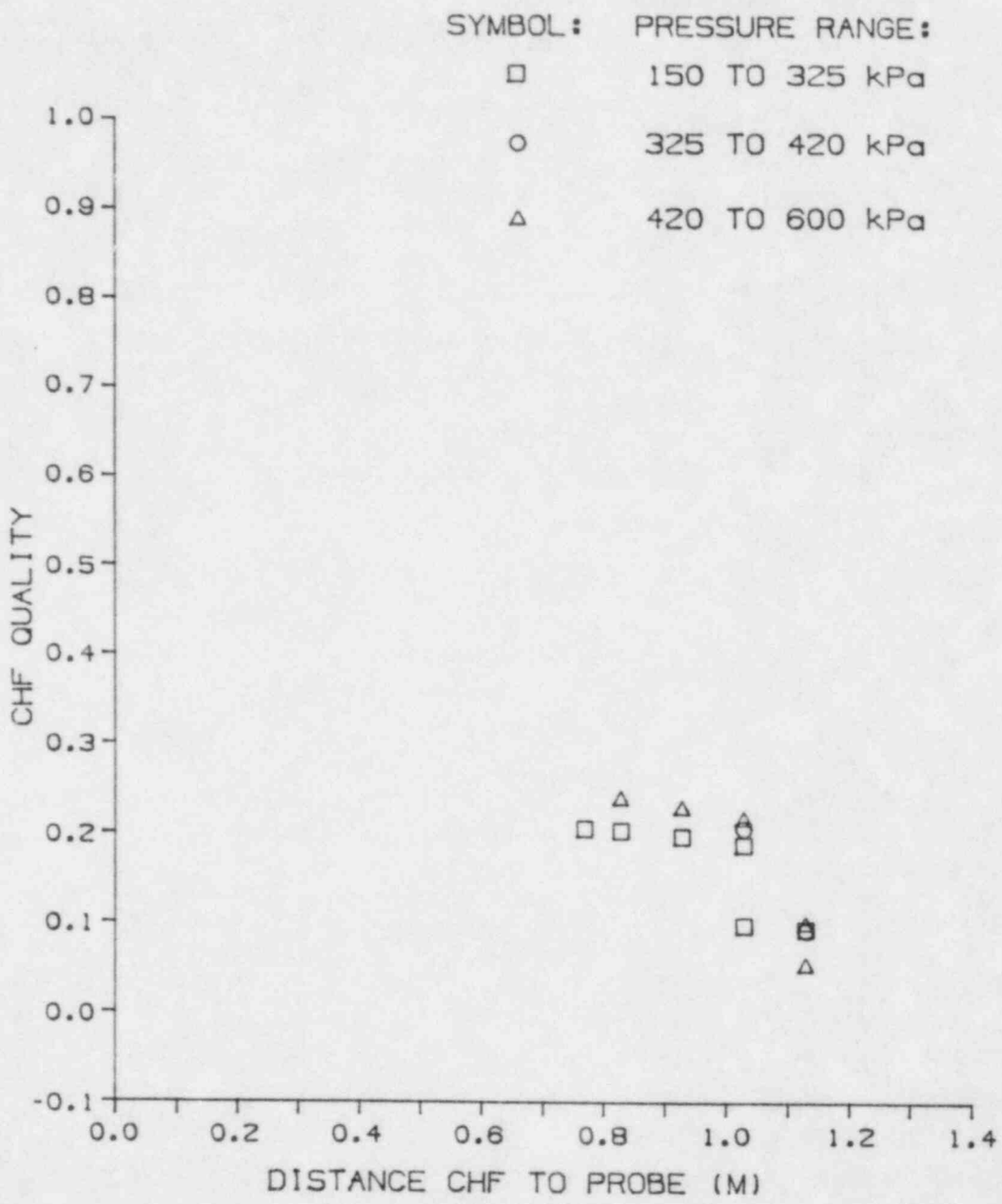

Figure 4-12. Distance vs. CHF quality for all data points with G between 65 and 85 kg/m^2 sec

5. DATA REDUCTION

5.1 Overview of Procedure

The data reduction process developed for the moving quench front experiments involved four steps: (1) preliminary calculations of inlet conditions and plotting of the raw data, (2) evaluation of the raw data and assignment of a rating, (3) reduction of the vapor probe data for those runs judged to be steady or exhibiting minor oscillations in flow pattern, and (4) complete data reduction of experiments with steady or minor oscillations in flow pattern. The limited quantity of fixed-CHF experiments used the same process, with only minor changes in the execution of step 4.

5.2 Preliminary Calculations and Plots

Execution of the primary data reduction program performed the following tasks, (1) calculation of the inlet conditions, (2) determination of the average electrical heat flux, and (3) generation of four plots featuring both raw and calculated values. The mass flux was calculated based on the flowrate manually recorded by the operators on the vapor probe stripchart. The test section inlet pressure was calculated by averaging the measurements obtained every 5.2 seconds during the experiment. The design of the two phase loop ensured that the inlet pressure did not drift significantly during an experiment, eliminating

the need to determine the inlet pressure as a function of time. The boiler power measured at the beginning of the experiment was used to calculate the test section inlet quality. The boiler power was not varied during the experiment.

An energy balance was performed on the hot patch for every data scan, and the net value averaged. For the moving quench front experiments, the net value was very close to zero, resulting in little or no change in flow quality from hot patch inlet to hot patch outlet. For the fixed-CHF experiments, the change in flow quality due to the hot patch was as large as 10 percent and varied with time. The average wall heat flux during the experiment was calculated to provide a preliminary indication of the heat flux encountered in the event that an attempt was made to duplicate the experiment before it was completely reduced.

The preliminary data reduction phase generated four raw data plots to provide a quick indication of the quality of a run. Examples are shown in figures 5-1 through 5-5. The first plot, figure 5-1, plots the wall temperature versus axial position. Every third data scan was plotted, resulting in a wall temperature profile every 15.6 seconds. All of the plots produced during the data reduction phase present temperatures in terms of superheats (excess above fluid saturation temperature). Figure 5-1 is from an experiment at low mass flux and high quality,

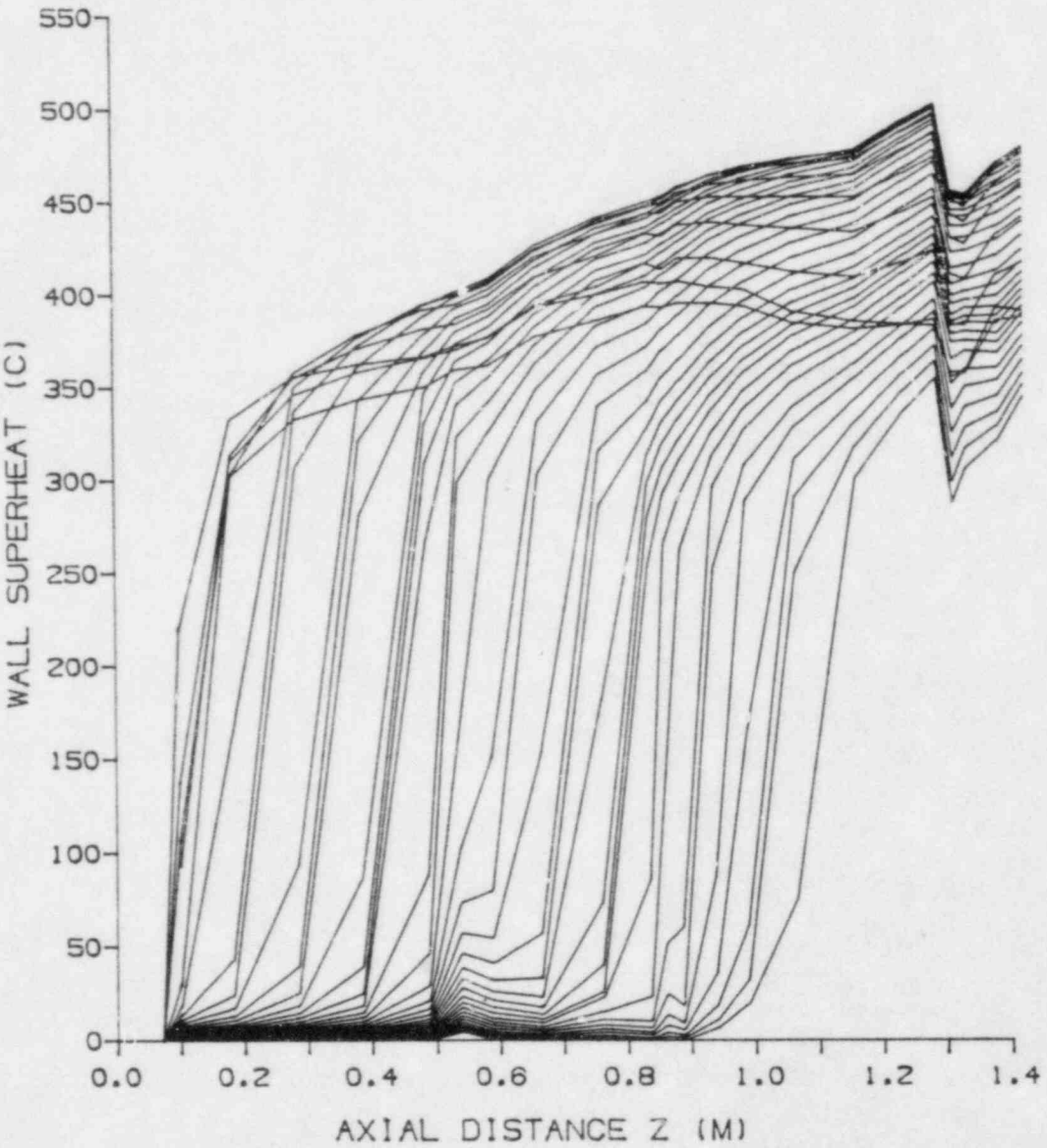

Figure 5-1. Wall temperature profile obtained every third raw data "snapshot" for run 100

while figure 5-2 is from an experiment which suffered from the probe induced quench with descending quench front.

Figure 5-3 presents the time history of each wall thermocouple plotted in figure 5-1 that was quenched by the ascending quench front. The temperature and time corresponding to the occurrence of critical heat flux at each thermocouple is indicated by the circles. Critical heat flux was determined by using IMSL interpolation routines on the computer to obtain the instant when the rate of wall temperature decrease was greatest, which corresponds to the maximum heat flux.

Figure 5-4 is a multi-plot to assist in the evaluation of the experiment. The triangles represent the time and location of wall thermocouple quenches. The line represents a least squares fit to these points. The slope of this line provides an indication of the quench front velocity. The circles represent the wall heat flux based on electrical power only. Heat losses and sensible heat contributions are not included. This plot provides an indication of the power supply operation during an experiment, specifically temperature-limit power trips ($\dot{q}=0$) and operator intervention. The plus signs indicate the raw differential pressure measurements. The vertical line represents the time when either of the pressure taps quenched.

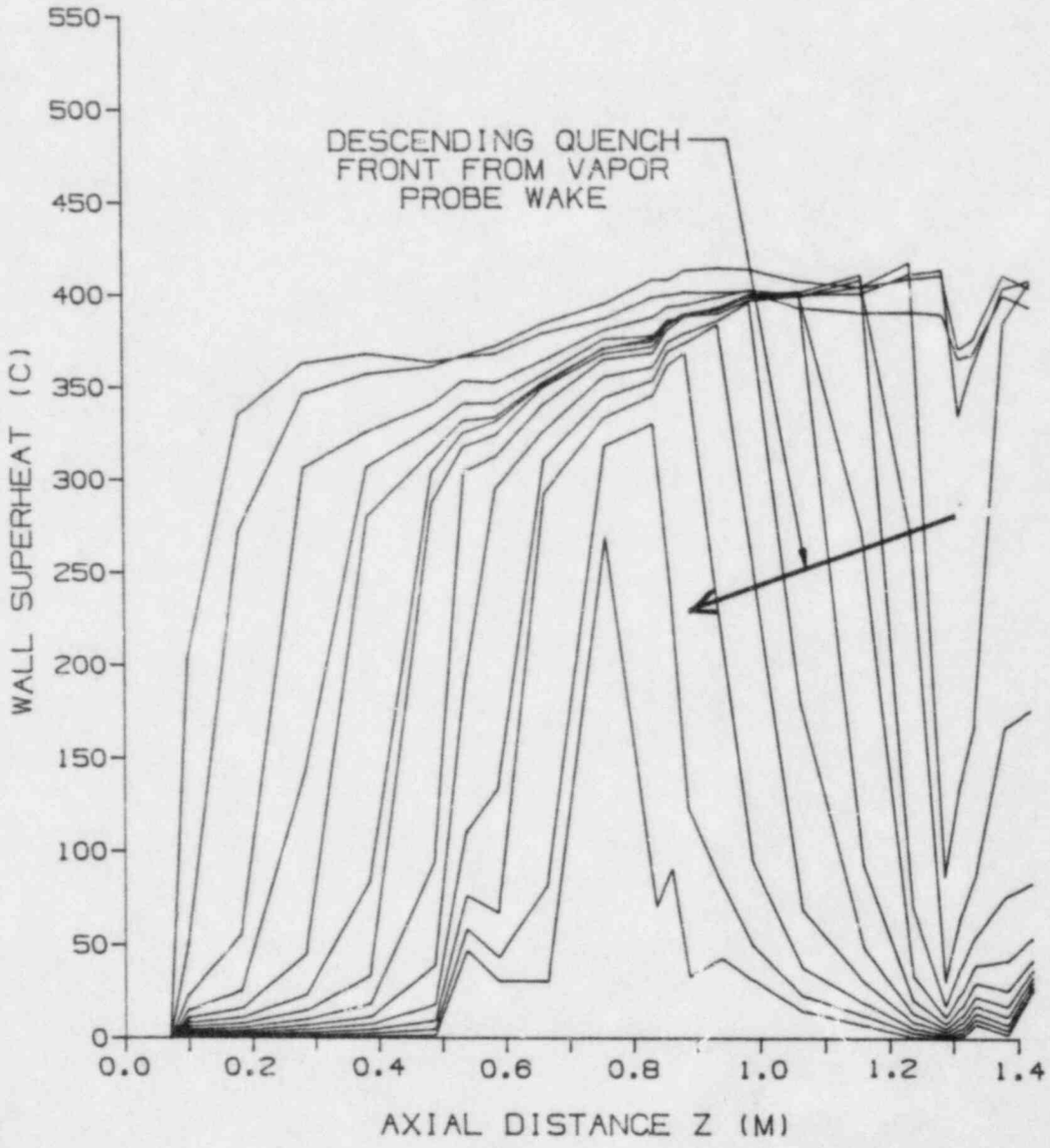

Figure 5-2. Wall temperature profile vs. time for run 146 demonstrating vapor probe wake effect

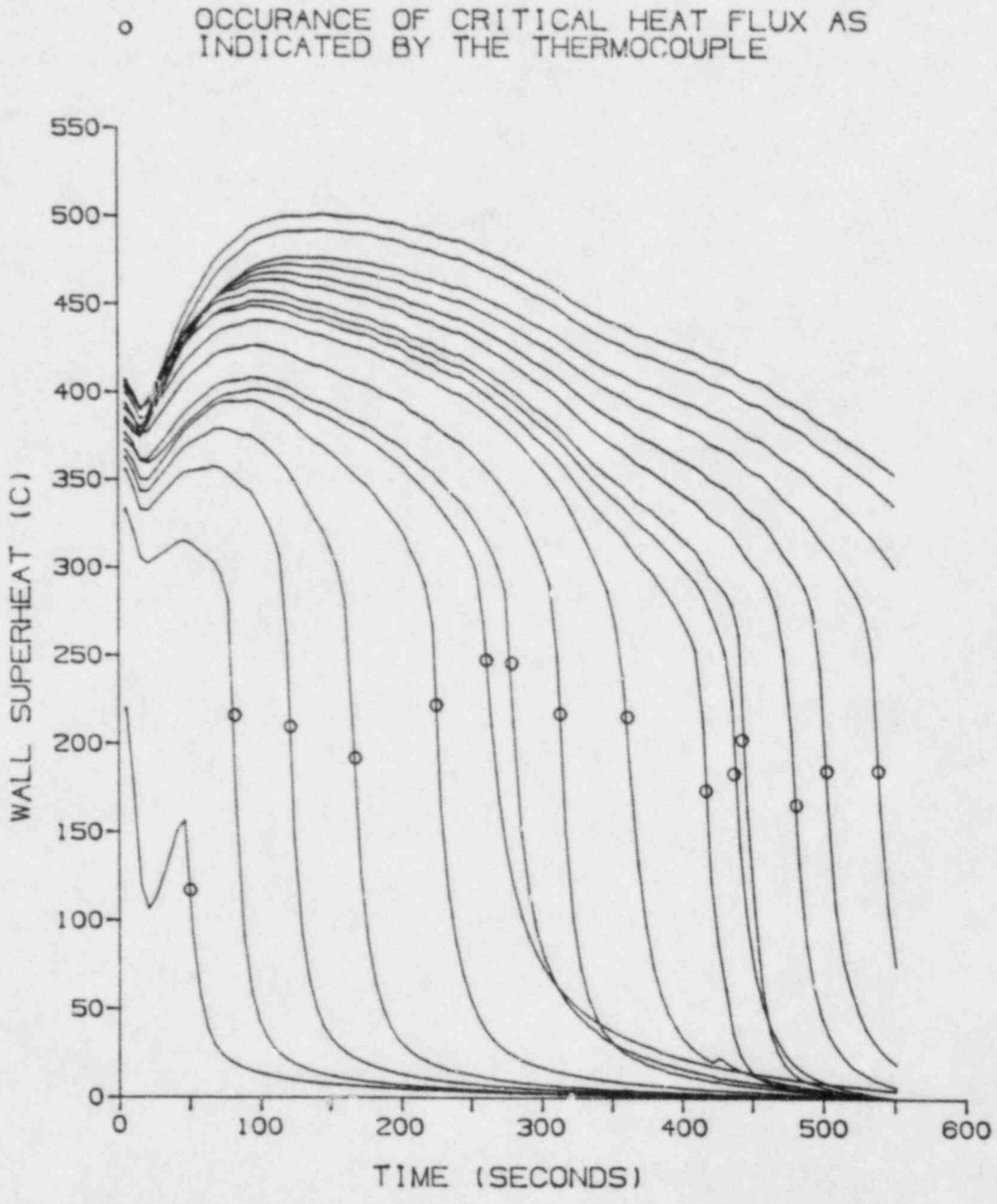

Figure 5-3. Wall temperatures vs. time for all thermocouples between the hot patch and vapor probe for run 100

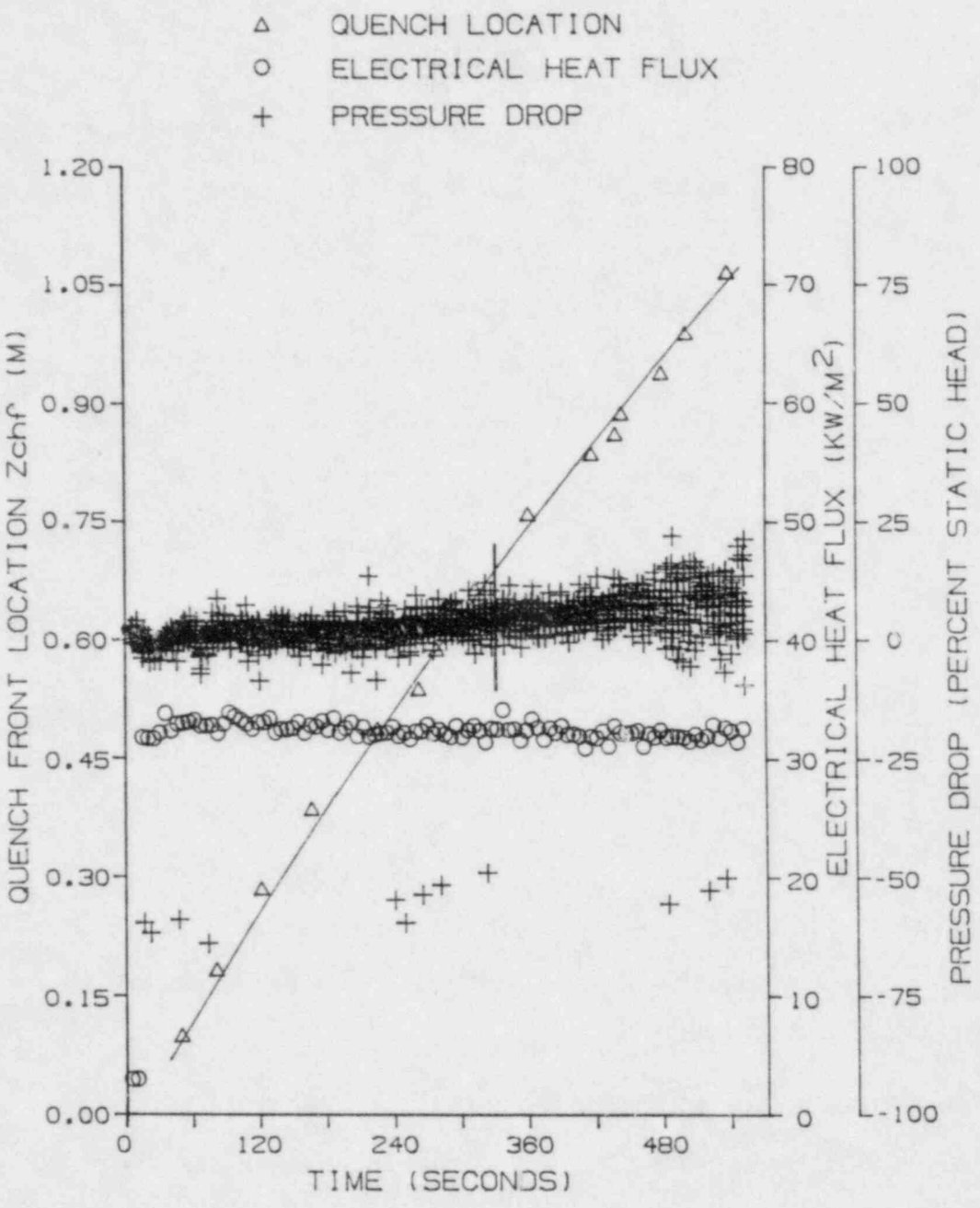

Figure 5-4. Multi-plot for run 100

In order to assist the classification of an experiment's flow pattern, figure 5-5 presents the product of two probabilities, (1) the probability of a given delta pressure measurement occurring, and (2) the probability that the previous or next delta pressure measurement was within a specified range of the current delta pressure measurement. For example, on the curve with a 2 percent window, for any measurement with a value of 2.5% static head, this would be the probability that an adjacent (in time) delta pressure measurement was within the range of 0.5-4.5% static head (2.5% +_2.0% [WINDOW]). This plot aids in determining if an experiment's flow pattern was steady or oscillating.

5.3 Evaluating the Rating of the Experiment

The quality of the vapor probe response and the severity or lack of oscillations in the flow pattern governed the rating of each experiment. Four sources of information were used in the evaluation: (1) observations noted by the operators, based on the flow pattern visible in the sight glass located at the boiler outlet, (2) quality and characteristics of the vapor probe response and pressure drop measurement recorded on the strip-chart, (3) appearance of the wall temperature versus time plot, and (4) appearance of the probability of pressure drop plot. The quality of the vapor probe response was based primarily on

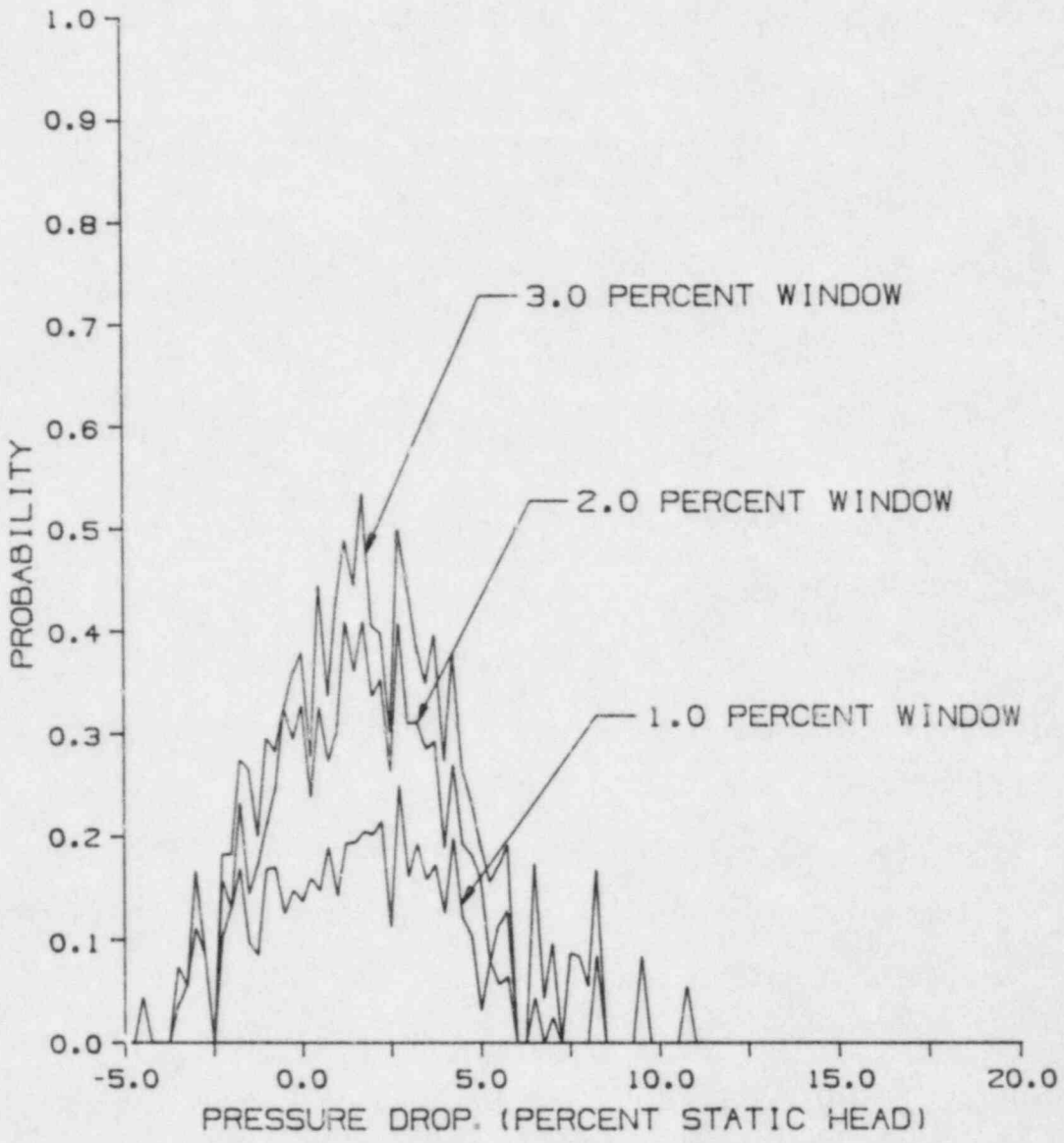

Figure 5-5. Probability of pressure drop measurement for run 100

the stripchart. Knowledge of the time when a descending quench front passed the probe, obtained in the preliminary data reduction step, assisted in differentiating between poor probe response and the localized quenching that occurred in some experiments.

The severity of flow oscillations was often graphically illustrated by the three different data representations (2) through (4). If the flow was steady, resulting in a constant void fraction, the probability of differential pressure plot would appear as in figure 5-6a. For oscillating flows where the void fraction oscillated between two values, the plot would appear as in figure 5-6b. Operator observations consistently confirmed the conclusions drawn from the plots.

Figures 5-7, 5-8, 5-9 demonstrate the appearance of a class 1 run featuring steady flow and excellent vapor probe response. Figure 5-7 illustrates the steady decline in wall temperatures resulting from a steady flow pattern. The pressure drop probability plot, figure 5-8, indicates a near constant pressure drop and therefore steady flow pattern. The raw pressure drop measurement, along with the vapor probe measurement in figure 5-9, confirms that this run was steady. A class 2 experiment with minor oscillations in flow pattern and good vapor probe response is illustrated in figures 5-10, 5-11, and 5-12. The ripple in

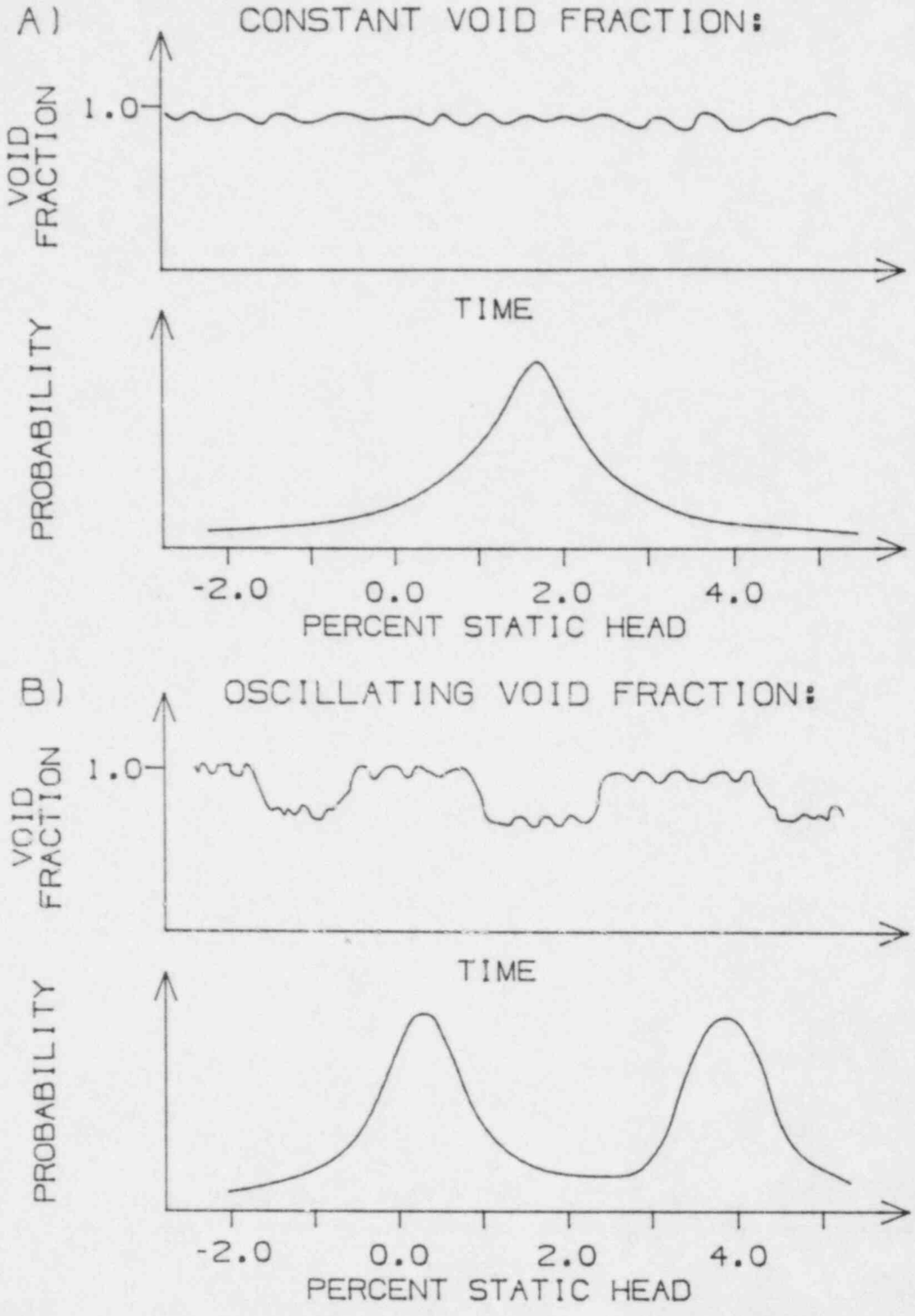

Figure 5-6. Relationship between void fraction and probability of differential pressure measurements

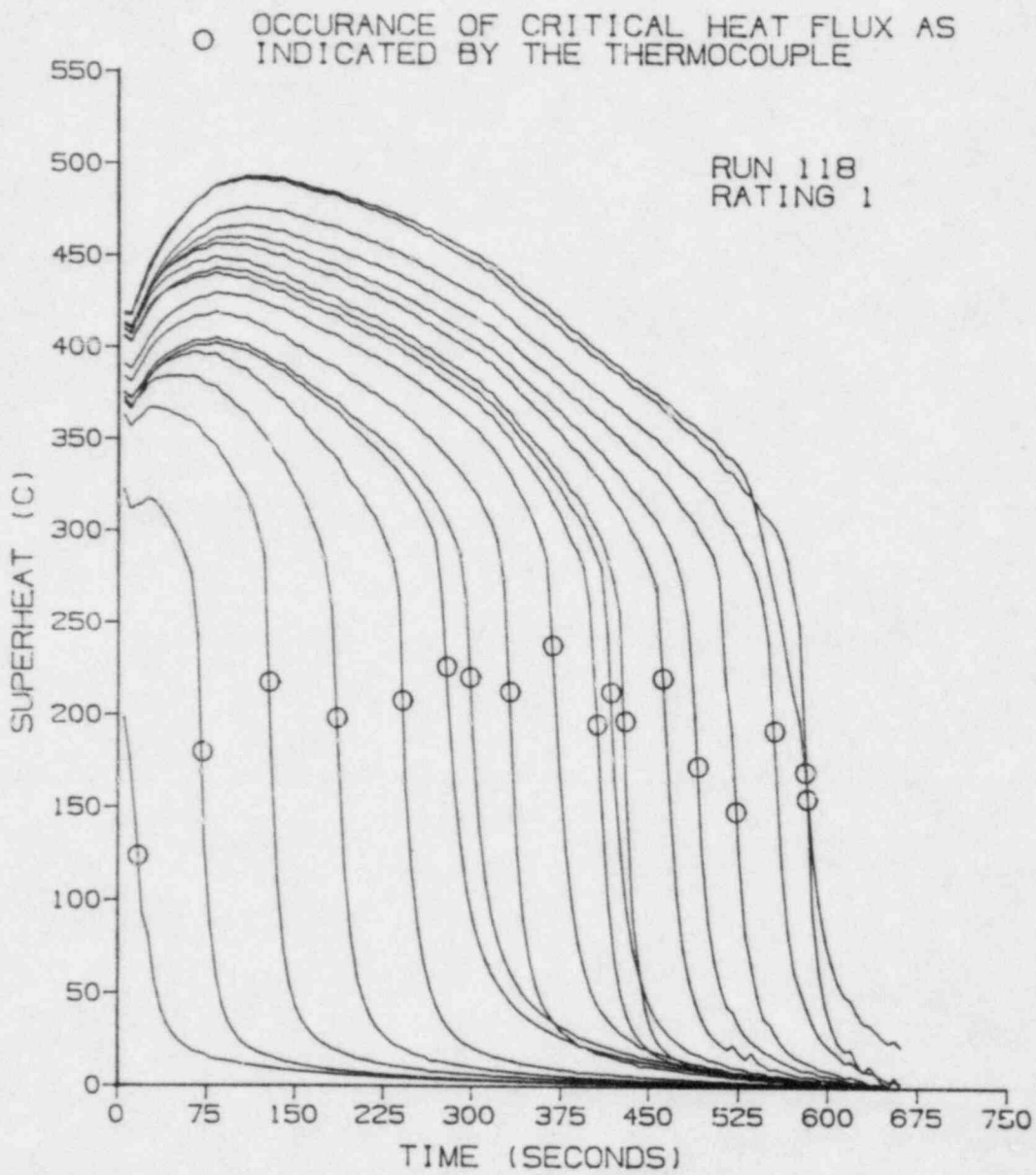

Figure 5-7. Wall temperature vs. time for a typical run with a rating of 1

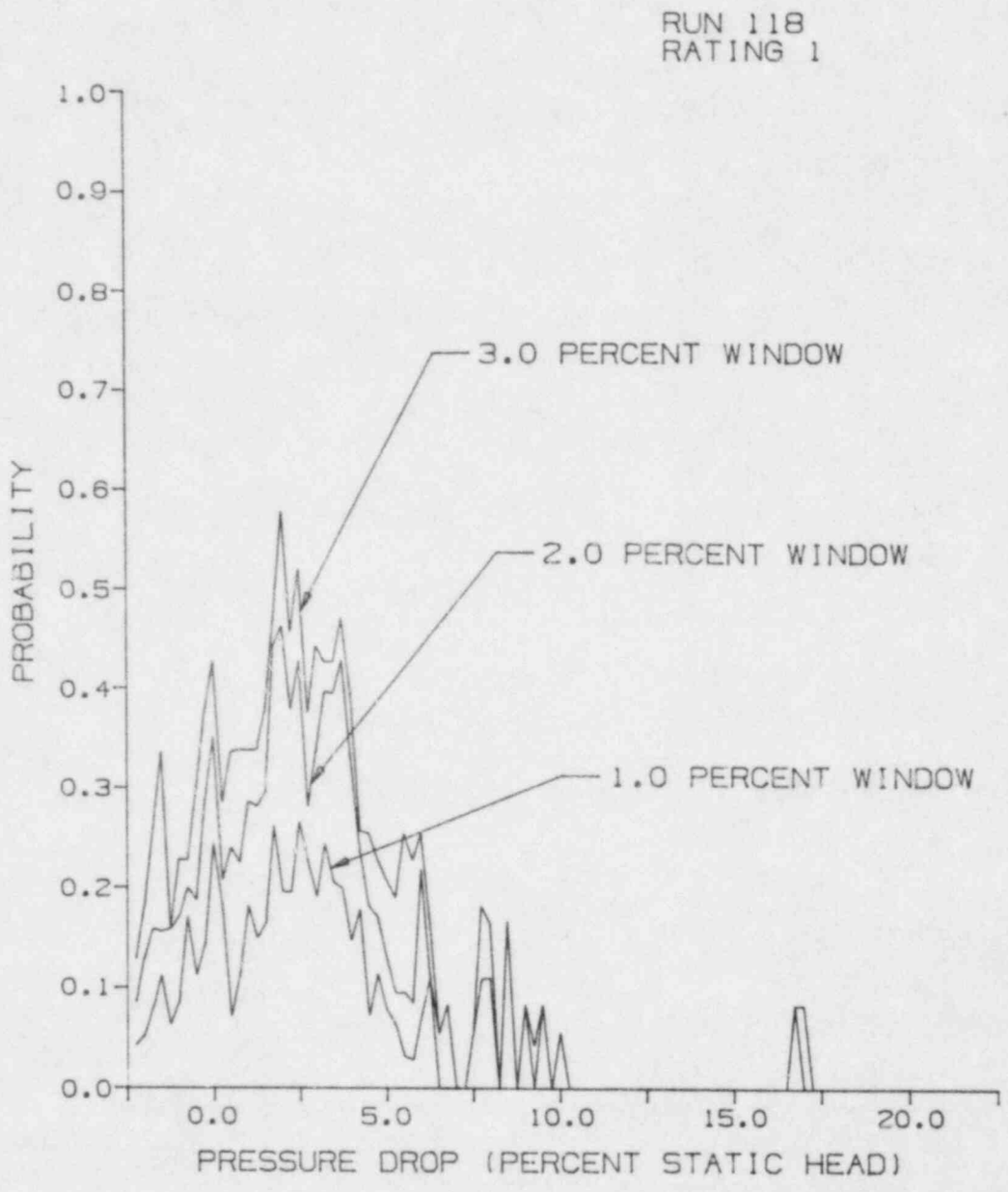

Figure 5-8. Probability of pressure drop for a typical run with a rating of 1

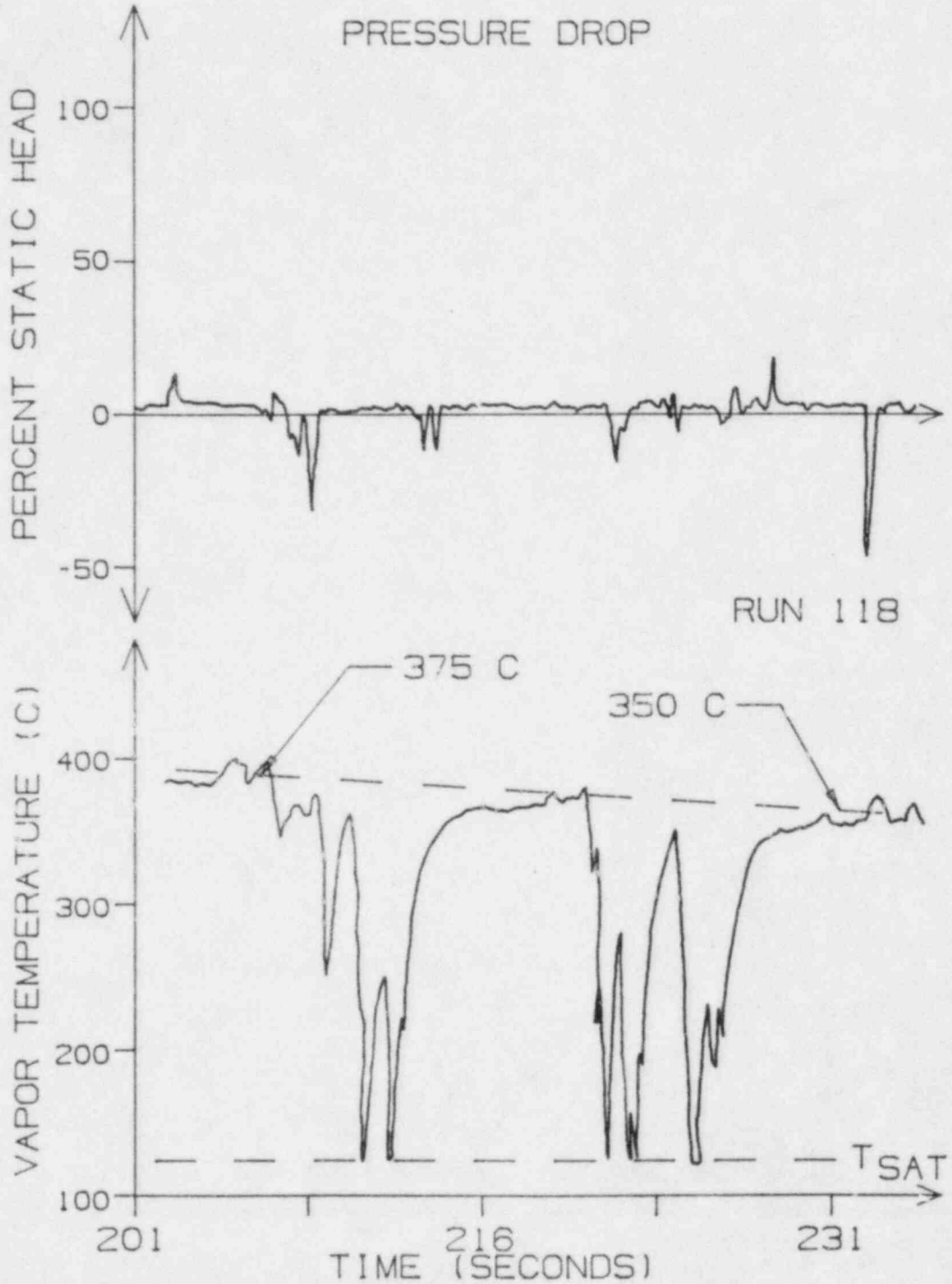

Figure 5-9. Vapor probe and pressure drop stripchart for a typical run with a rating of 1 (run 118)

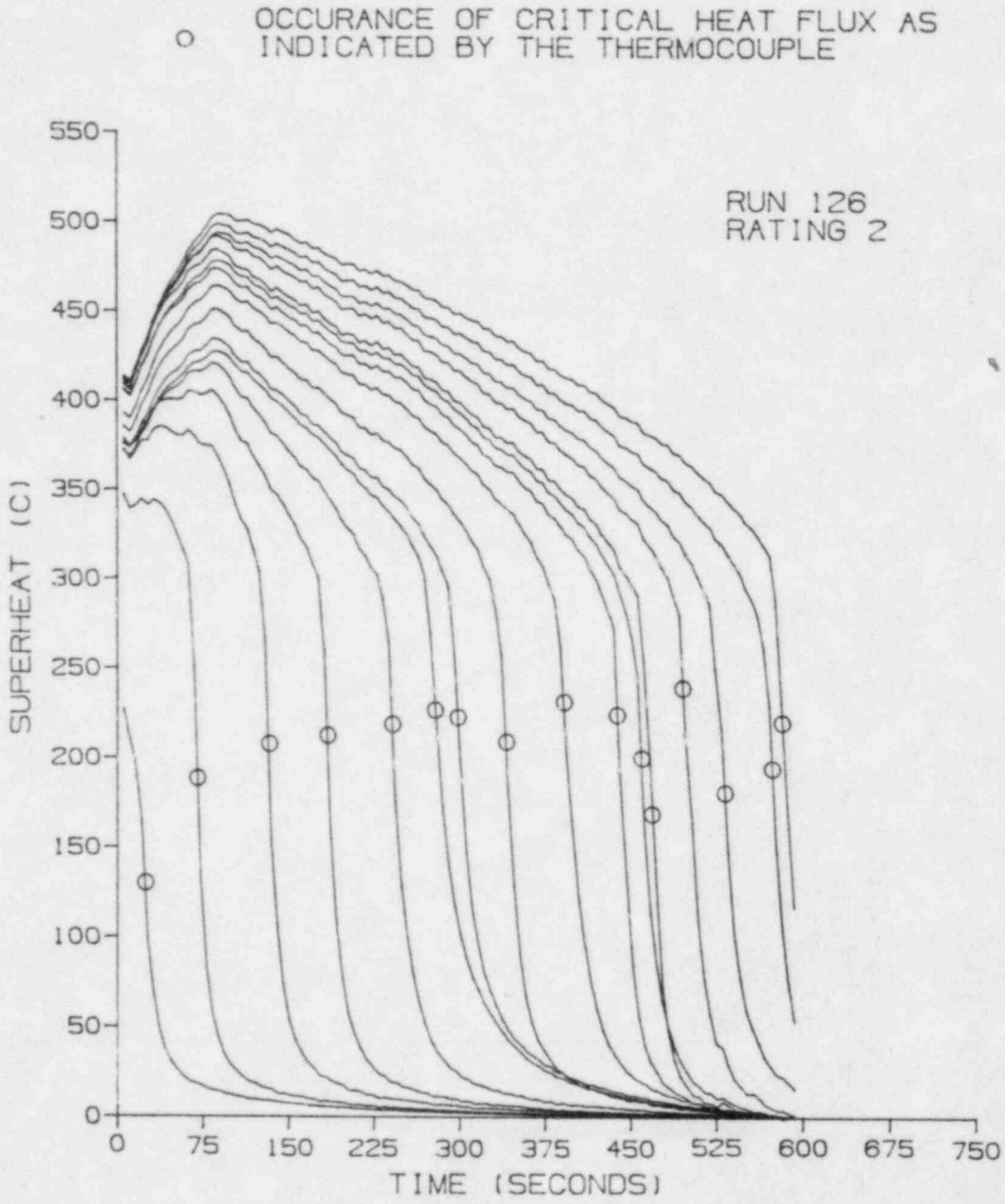

Figure 5-10. Wall temperature vs. time for a typical run with a rating of 2

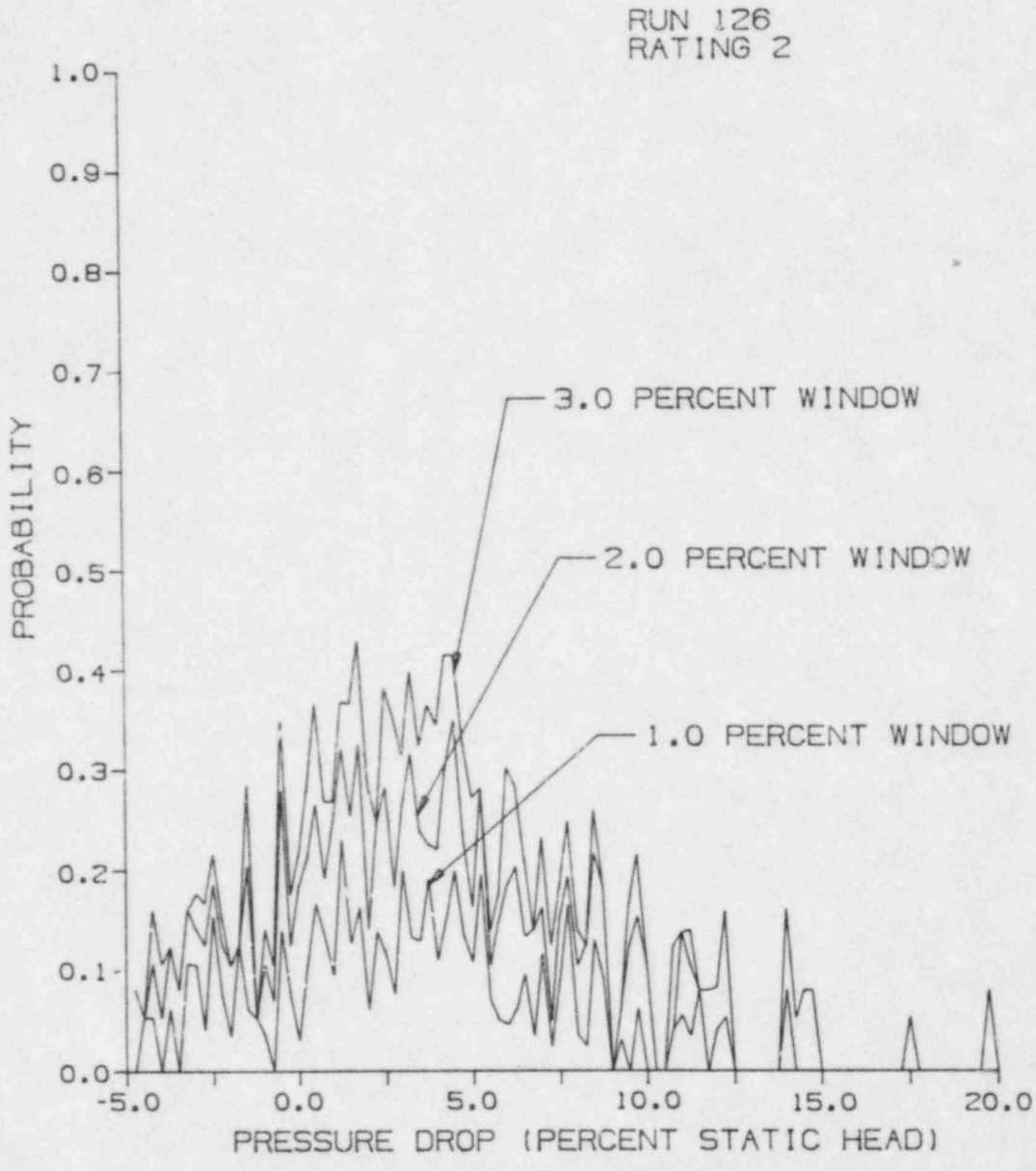

Figure 5-11. Probability of pressure drop for a typical run with a rating of 2

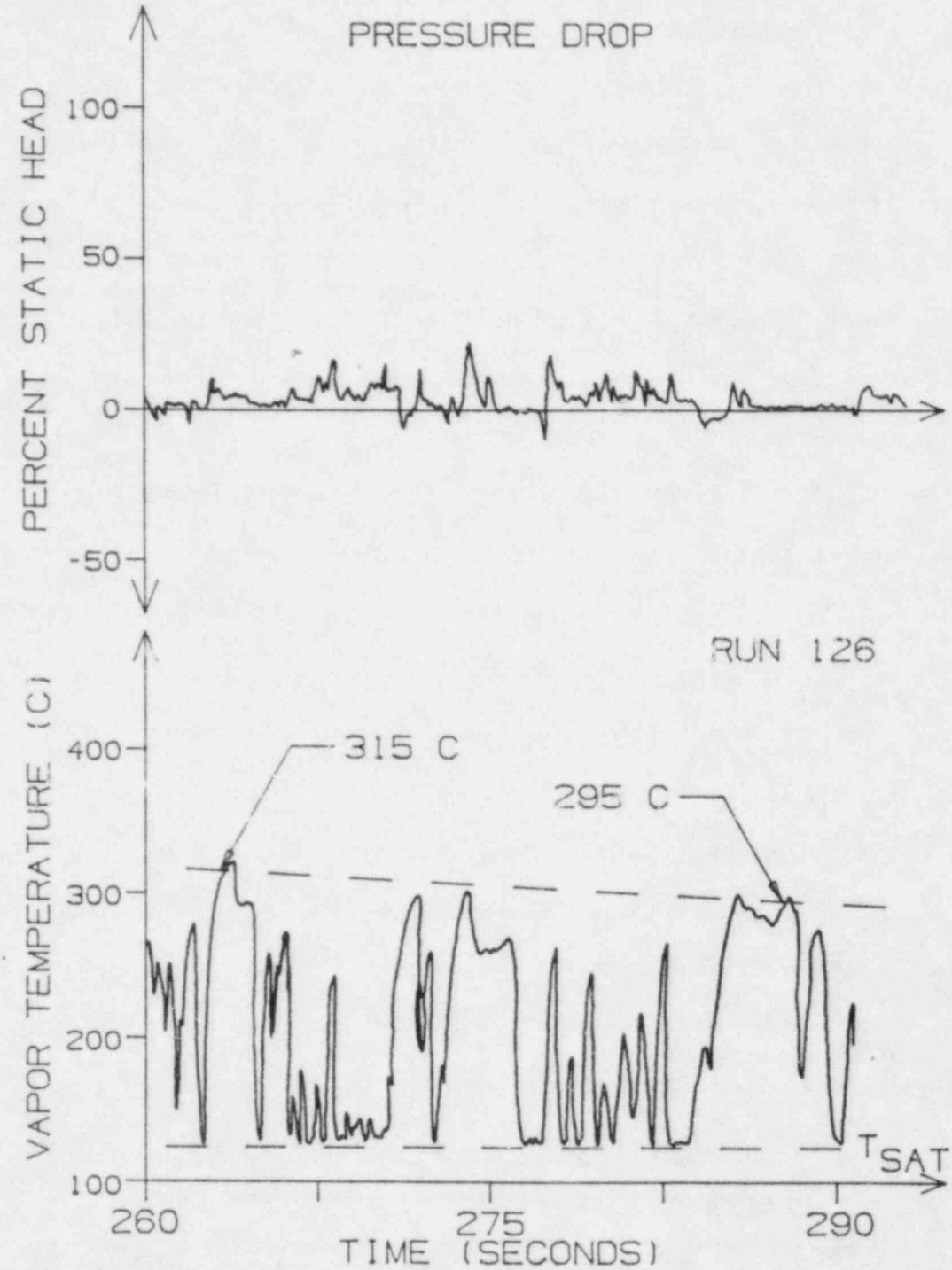

Figure 5-12. Vapor probe and pressure drop stripchart for a typical run with a rating of 2 (run 126)

the wall temperature plots, a flattened probability chart, and the characteristics of the vapor probe and pressure drop strip-chart demonstrate the quality of class 2 experiments. The severity of flow oscillations in class 6 experiments is shown in figures 5-13, 5-14, and 5-15. Observations of the flow pattern visible in the sight glass often revealed that the flow pattern at the boiler outlet would oscillate between bubbly flow and annular flow. The class 6 experiments were not reduced. After classifying all of the experiments, serial numbers were assigned to each run based on its rating, as shown in table 5-1.

TABLE 5-1

Evans/Webb reduced data serial numbers

100-123	Rating class 1, moving quench front data
124-139	Rating class 2, moving quench front data
140-152	Rating class 3, moving quench front data
153-202	Rating class 4, moving quench front data
203-213	Rating class 5, moving quench front data
214-222	Rating class 11, fixed quench front data
300-316	Rating class 6, moving quench front data
317	Rating class 16, fixed quench front data
318-329	Rating class 7, moving quench front data

Only runs 100 to 222 are reducible and therefore they are the only runs released. Runs 300-329 were not released as data, but

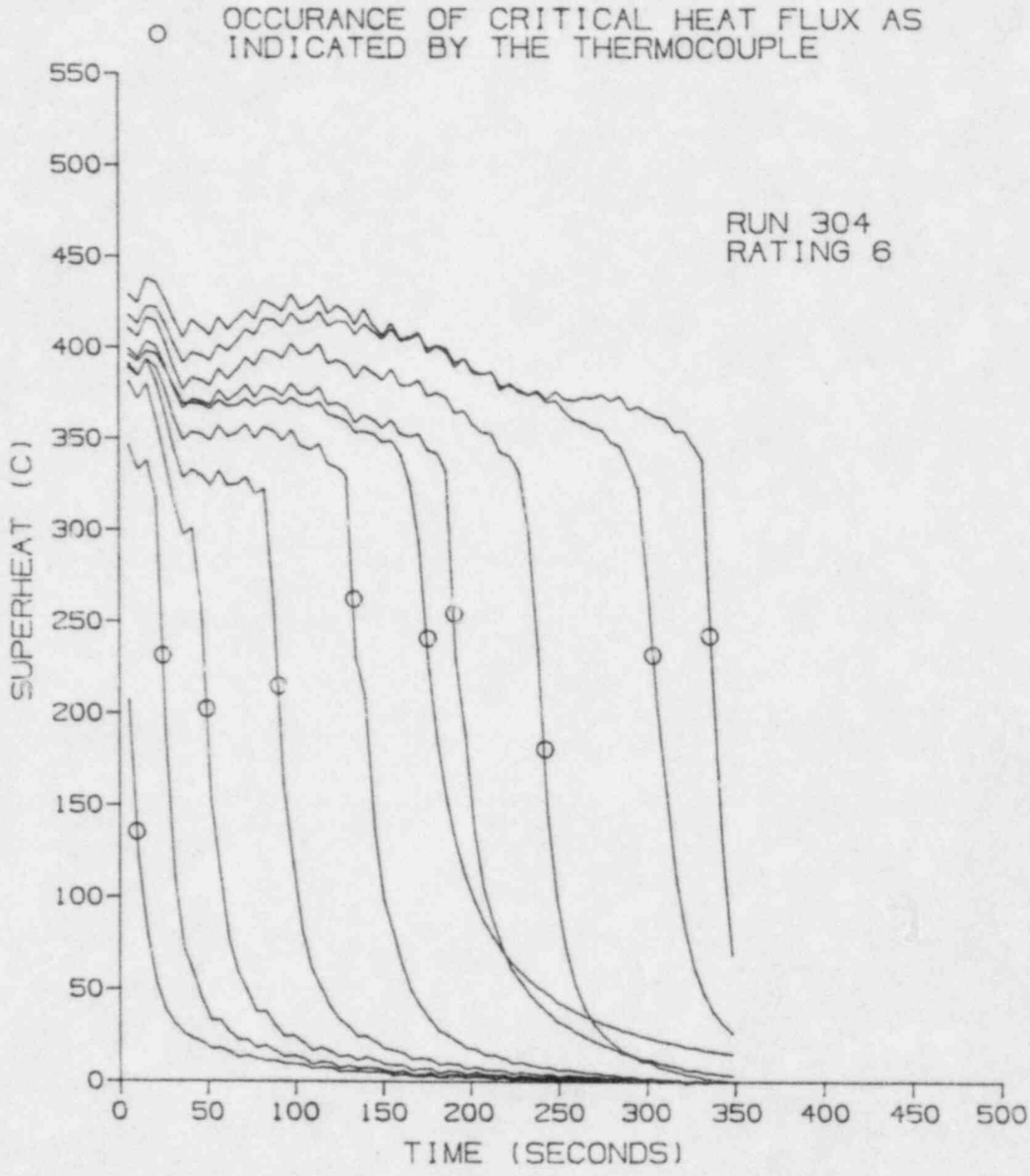

Figure 5-13. Wall temperature vs. time for a typical run with a rating of 6

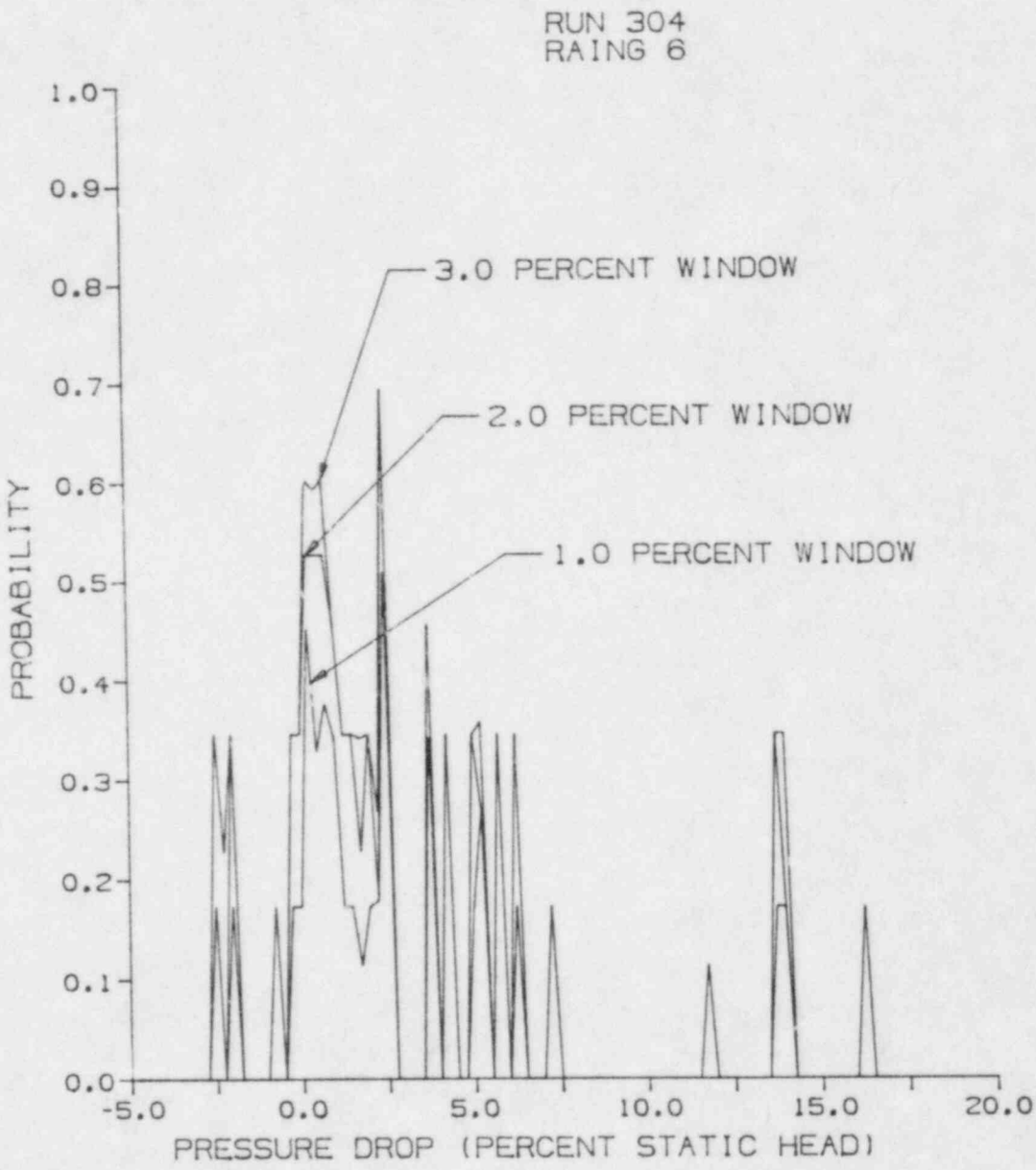

Figure 5-14. Probability of pressure drop for a typical run with a rating of 6

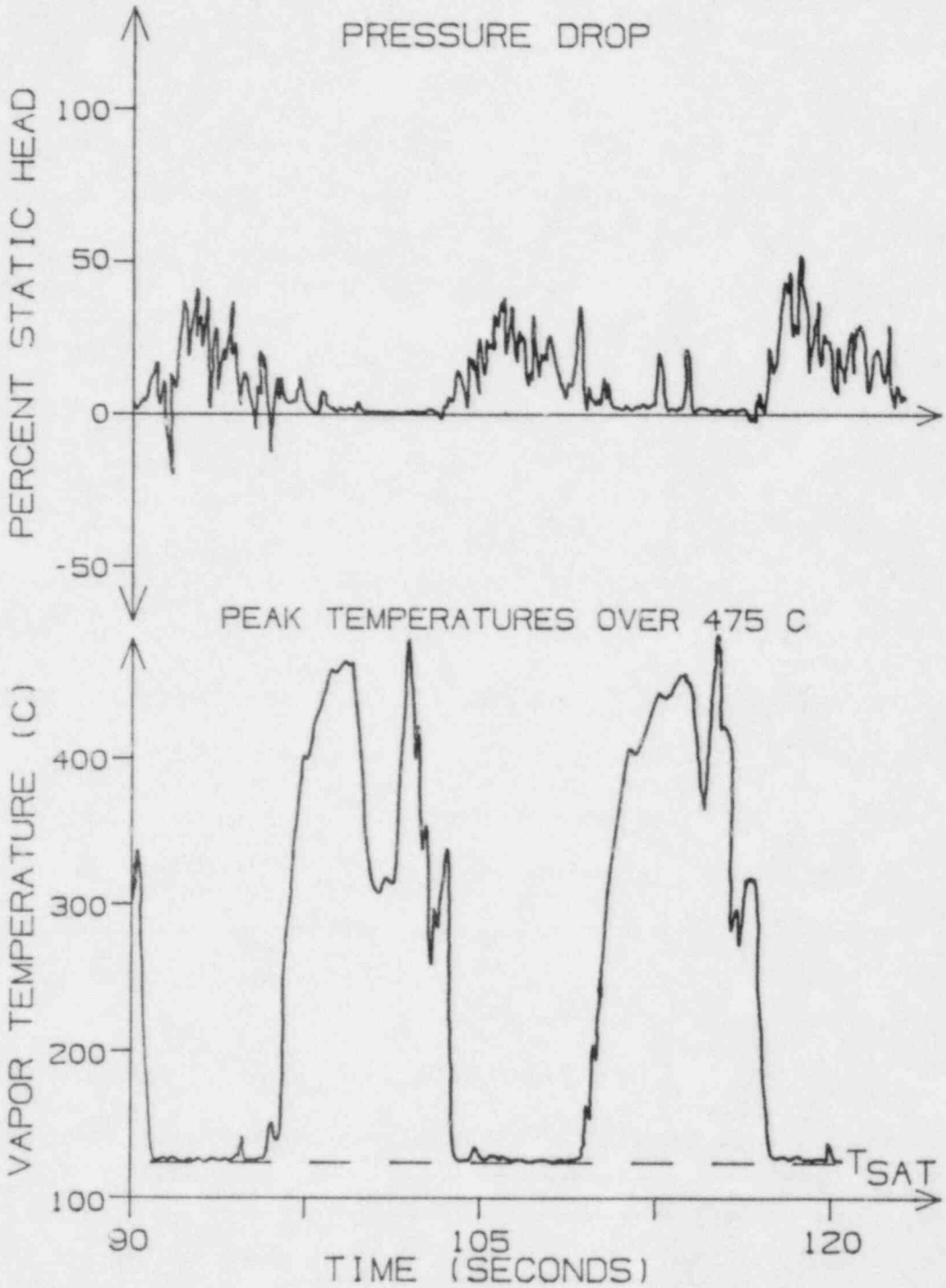

Figure 5-15. Vapor probe and pressure drop stripchart for a typical run with a rating of 6 (run 304)

observations from these runs are reported in Appendix A. In addition, 42 pre-production runs were not given serial numbers.

5.4 Reduction of the Vapor Probe Data

If an experiment had a rating of 1 to 5 or 11 to 15, then the next step in the data reduction process was the interpretation of the vapor probe stripchart. This process began with plotting the time base on the stripchart, and verification of the saturation temperature. A smooth curve was then drawn through an average of the peak vapor measurements. A series of points were selected to provide enough information to represent the vapor superheat as a series of linear interpolations during the data reduction process. The time and vapor superheat measurements for these points were entered into a program that provided for the proper storage of the vapor data points. These points were then used in the final data reduction program.

5.5 Final Data Reduction

The format of the final data reduction was governed by the criteria used to select valid data points for the moving quench front experiments. Some of the moving quench front experiments lasted over 10 minutes, with quench front velocities as low as 1.3 mm per second. The raw data for these experiments often included more than 100 raw data scans. Reporting such a large

volume of data was thought to be unnecessary. It was decided that a useful criteria for generating individual data points involved reporting all of the necessary information obtained at the instant corresponding to the quench of a wall thermocouple. The quench front was determined to be passing a particular thermocouple when the time derivative for that thermocouple reading reached its maximum, corresponding to a maximum rate of temperature decrease and maximum surface heat flux. The time derivative was based on an IMSL interpolation routine available on the computer. Therefore, the data points reported for moving quench front experiments correspond to the instant when a wall thermocouple quenched and a vapor superheat measurement was available. Criteria were established to ensure that the vapor superheat measurement was not corrupted by the initial transients or a descending quench front.

For fixed-CHF experiments, two or three data points were generated at times corresponding to approximately 30, 60, and 90 percent of the total time of the run. Including the 25 data points from fixed-CHF experiments, a total of 579 data points were generated from the 118 experiments with ratings of 1 to 5 and 11 to 15. The inlet conditions, location of CHF and its associated quality, vapor temperature at the vapor probe, and complete axial information on the wall temperatures, wall heat

fluxes, and flow equilibrium qualities for all 579 data points have been tabulated in volume II. A sample tabulation for run 100, and an explanation of the calculations used in this final data reduction process are located in Appendix D. In addition to the tabulation, plots were generated on the computer to graphically display the data obtained from each of the 118 runs. The following plots from run 100 illustrate typical data obtained during this investigation.

Figure 5-16 is a plot of the wall temperature profile for the data points obtained from this experiment. The circles represent the location of the quench front for each temperature profile.

Figure 5-17 is a plot of wall heat flux versus time as calculated at each of the thermocouples located between the test section inlet and the vapor probe. Calculation of the local wall heat flux includes time varying heat losses and the storage and release of sensible heat in the test section wall. A more detailed discussion of wall heat flux is located in Appendix D. The spikes represent the release of sensible heat from the wall when the quench front passed each thermocouple. The spikes are not uniformly spaced due to the varying distances between the wall thermocouples.

Figure 5-18 is a plot of the wall heat flux calculated at the wall thermocouple 2 cm upstream of the vapor port. The

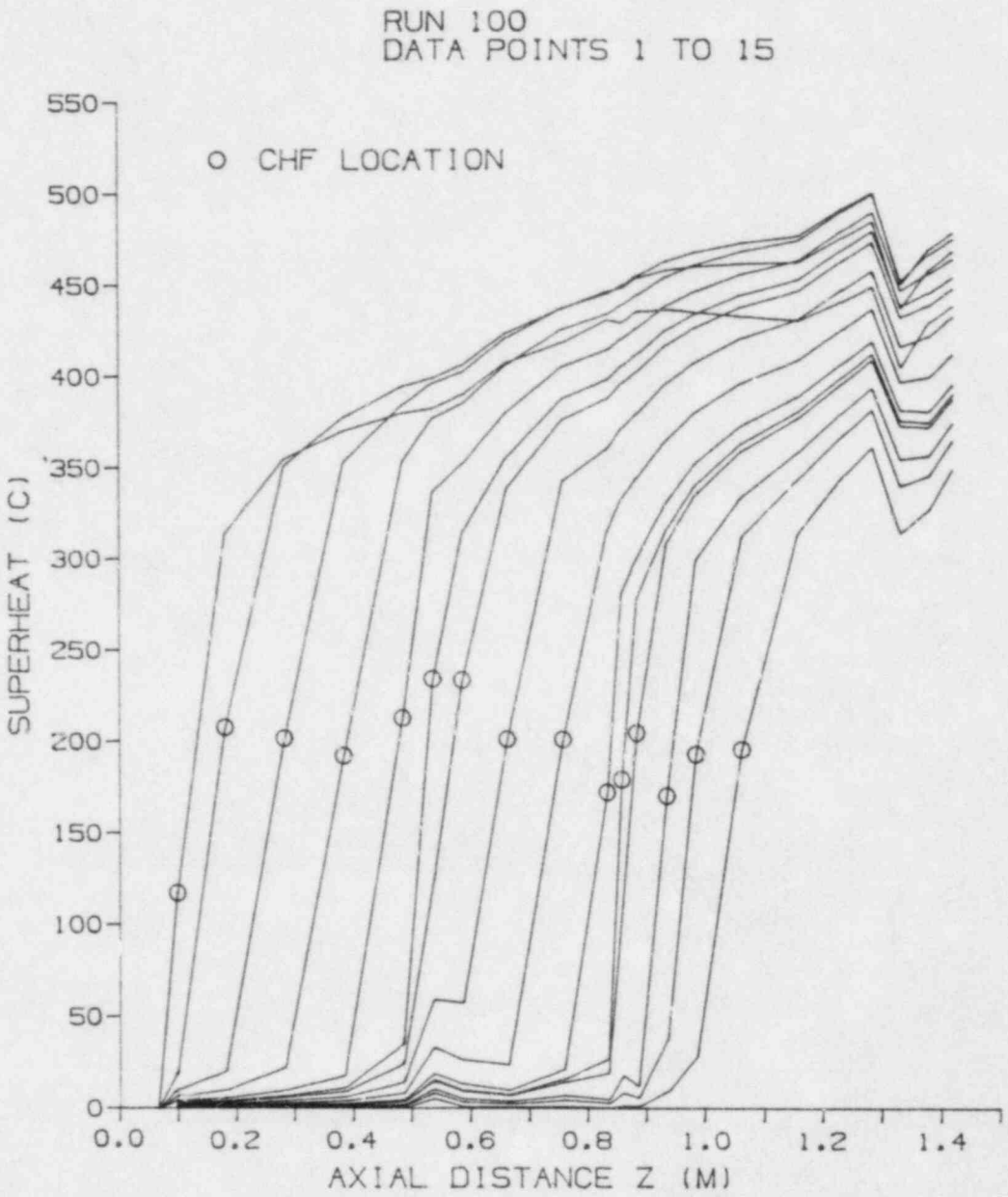

Figure 5-16. Wall temperature profile for the 15 data points reported from run 100

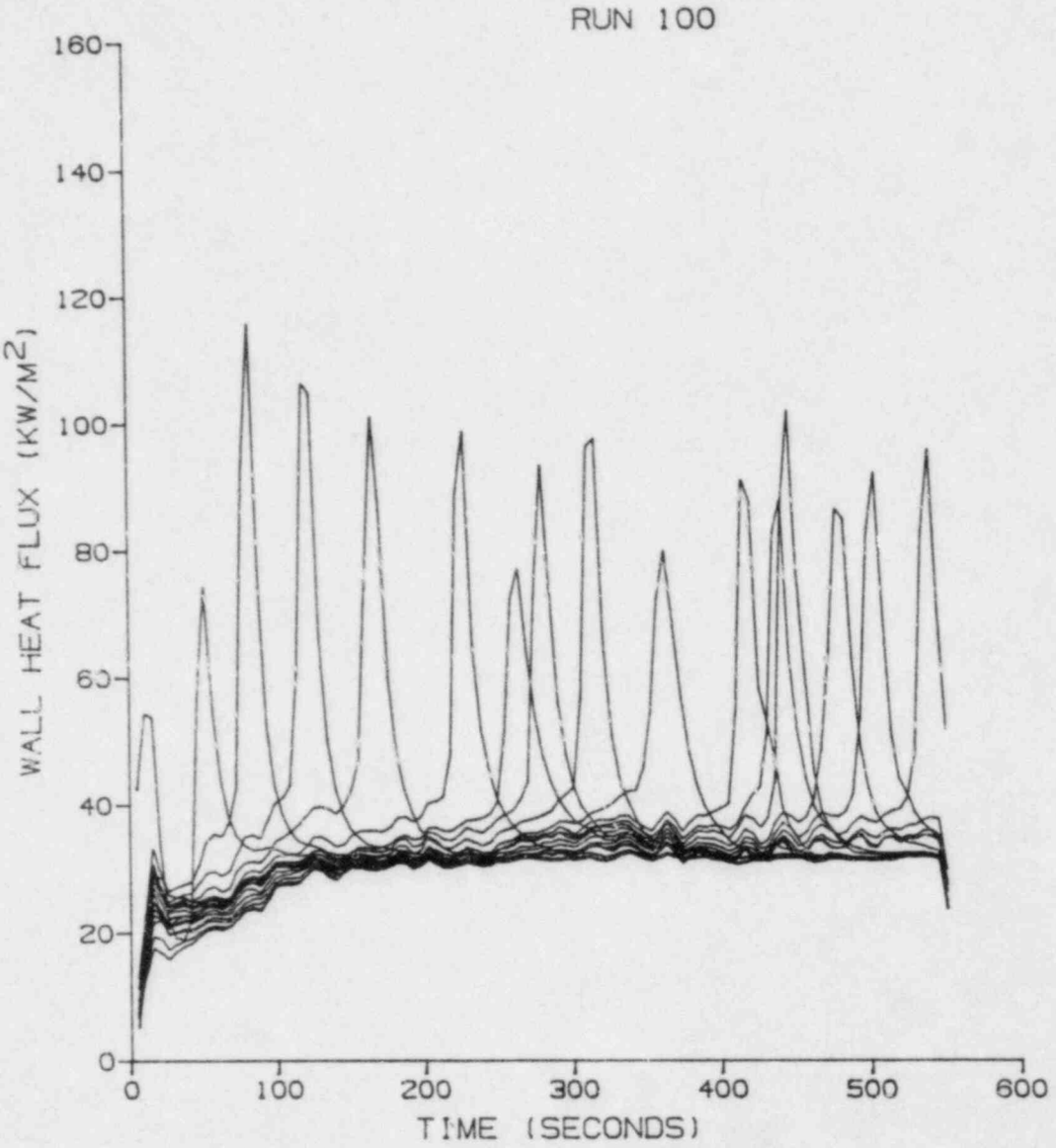

Figure 5-17. Wall heat flux vs. time at the 18 thermocouples between the hot patch and the vapor probe

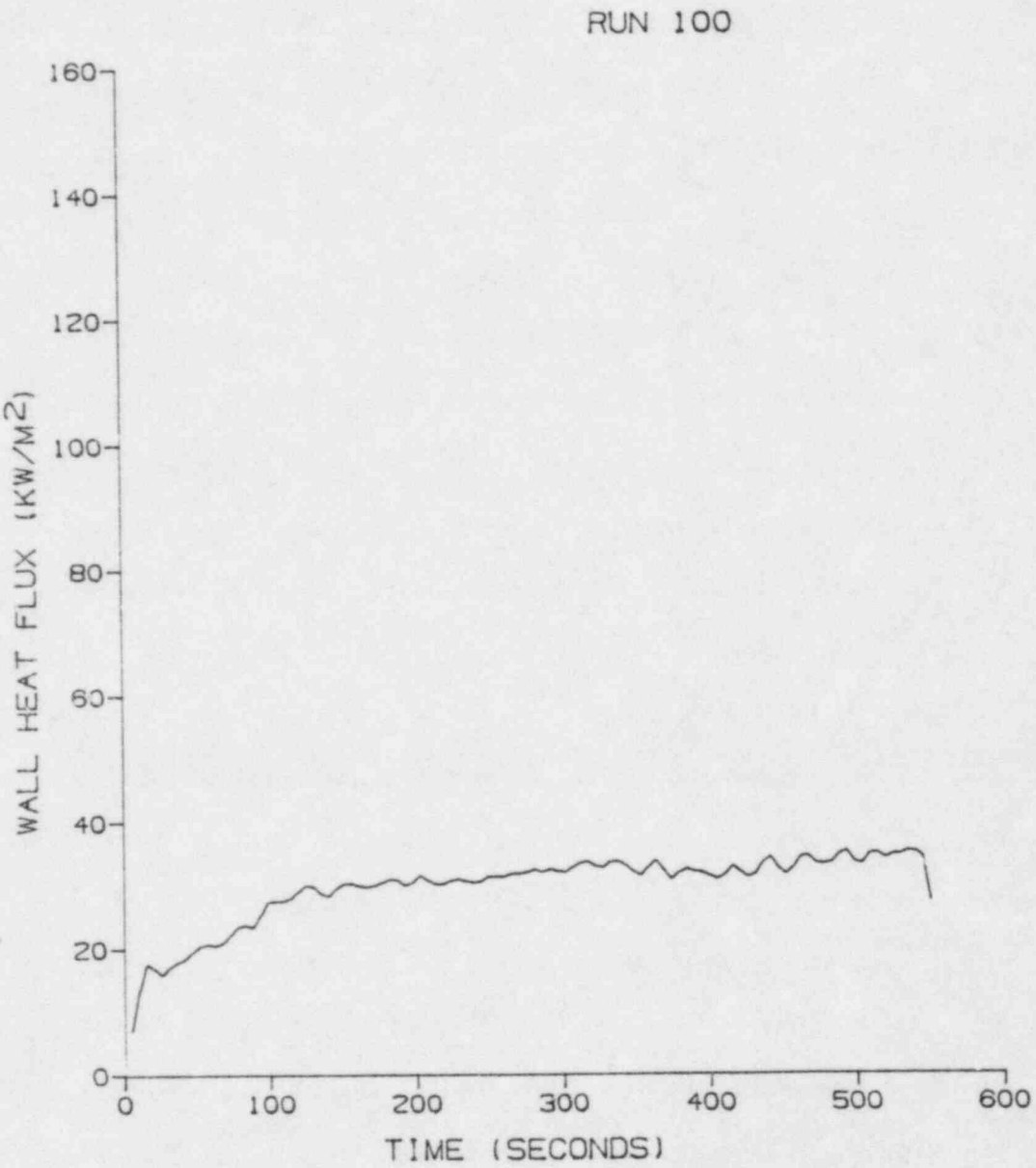

Figure 5-18. Wall heat flux at the vapor probe vs. time for run 100

wall heat flux at this location is the wall heat flux used in the effective convective heat transfer coefficient calculations at the vapor probe. Measurements precisely at the vapor probe are corrupted by the variation in test section electrical resistance in the vapor port weld area, the fin effect of the vapor port to external surroundings, and the local variation in wall volume and therefore sensible heat.

Figure 5-19 is a plot of the vapor superheat measured by the vapor probe, and the wall superheat 2.5 cm upstream of the vapor probe. The line represents the vapor temperature which would result if the actual quality of the flow downstream of the quench front was frozen at the quench front equilibrium quality.

For moving quench front experiments figure 5-20 represents the data presented in the previous plot, cross plotted against the distance between the quench front and the vapor probe. The wall and vapor superheats for each of the data points obtained from this experiment are plotted as a function of the distance between the wall thermocouple which was quenched and the measurement location. Notice that the wall measurement is always 2.5 cm closer to the quench front than the vapor measurement.

In figure 5-21, the equilibrium quality along the test section is plotted as a function of distance for each of the data points. The step increase in quality for each curve represents the addition of sensible heat from the inconel to the flow at

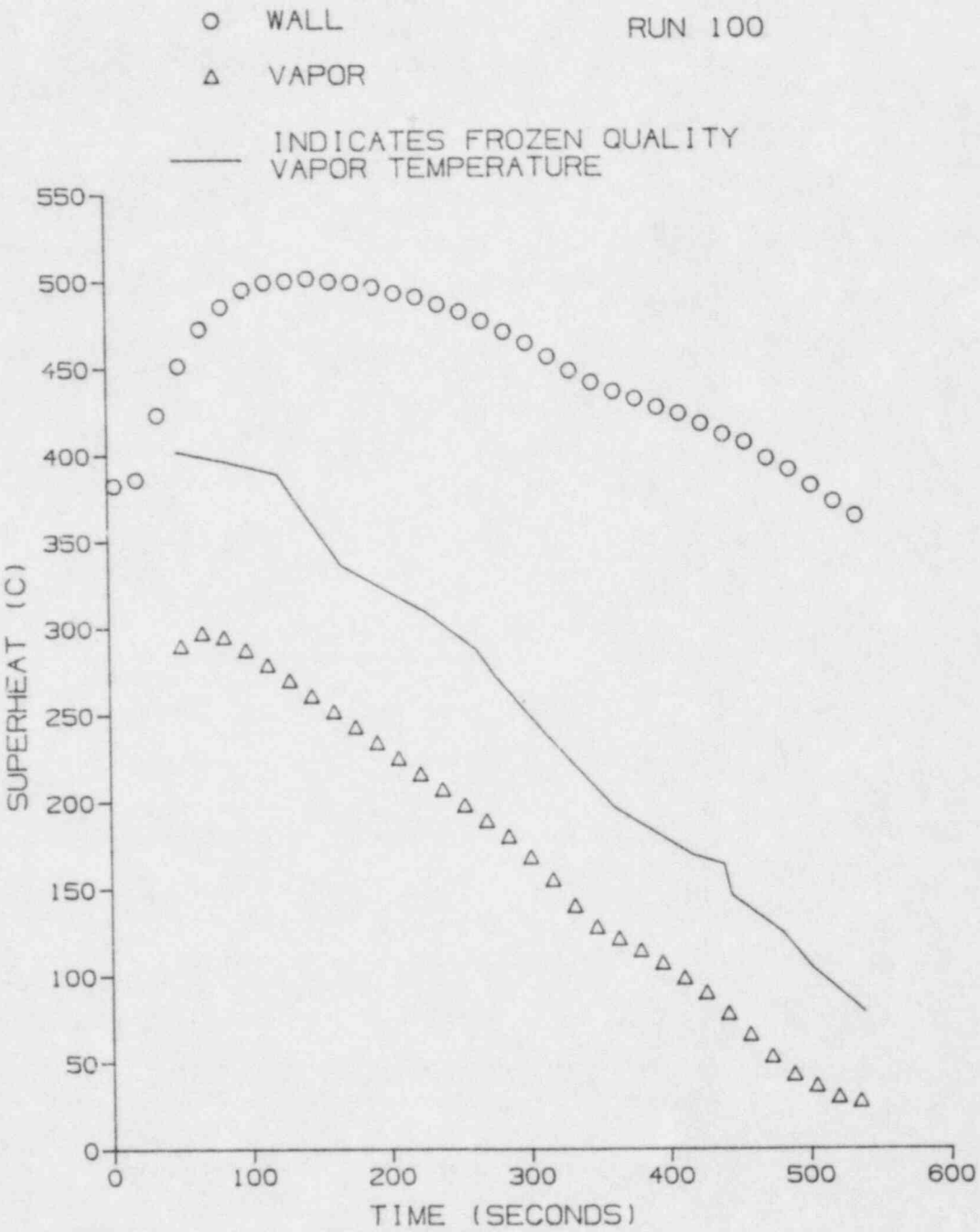

Figure 5-19. Wall and vapor temperatures at the vapor probe vs. time for run 100

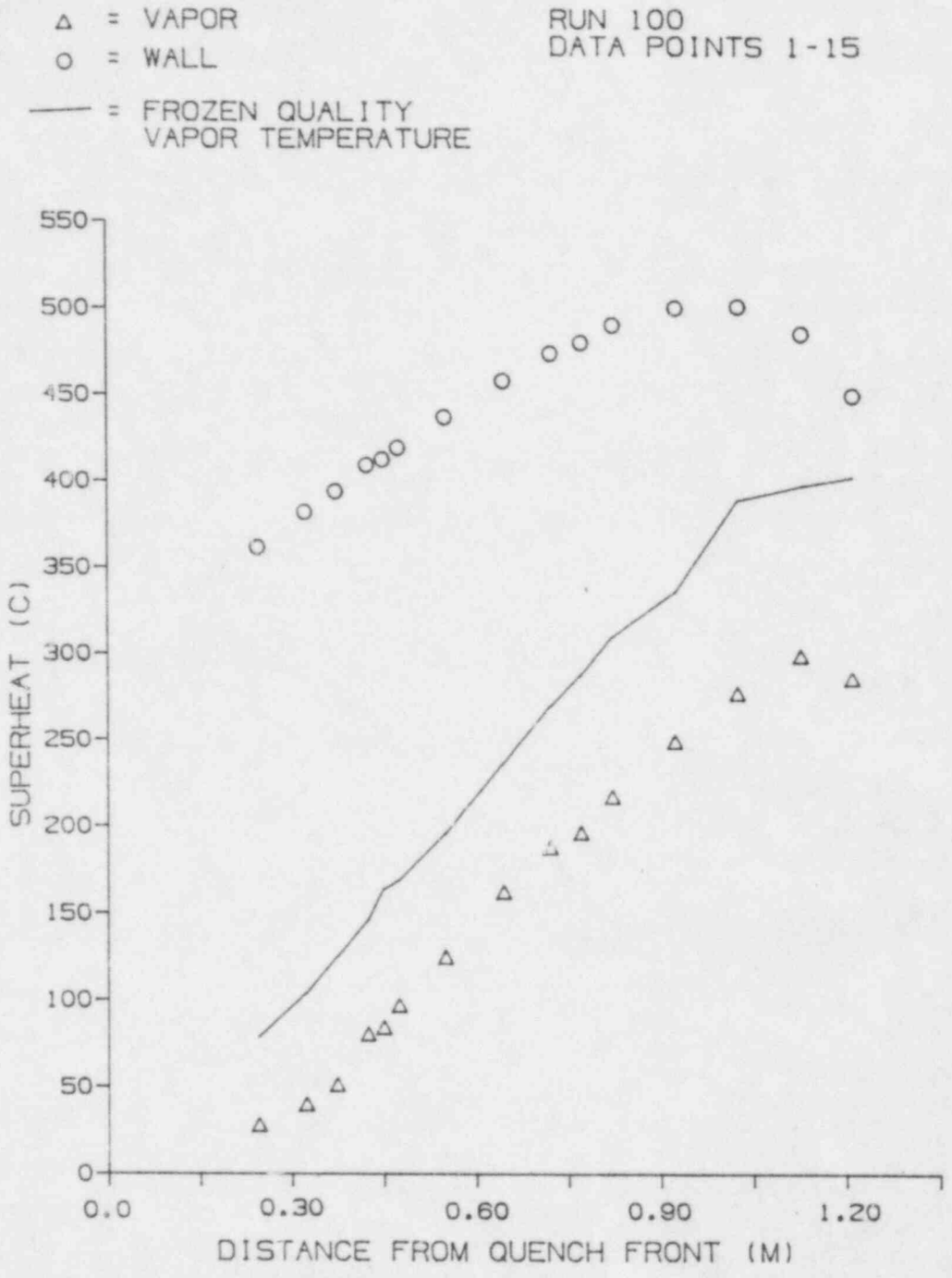

Figure 5-20. Temperatures at the vapor probe as a function of distance from the quench front

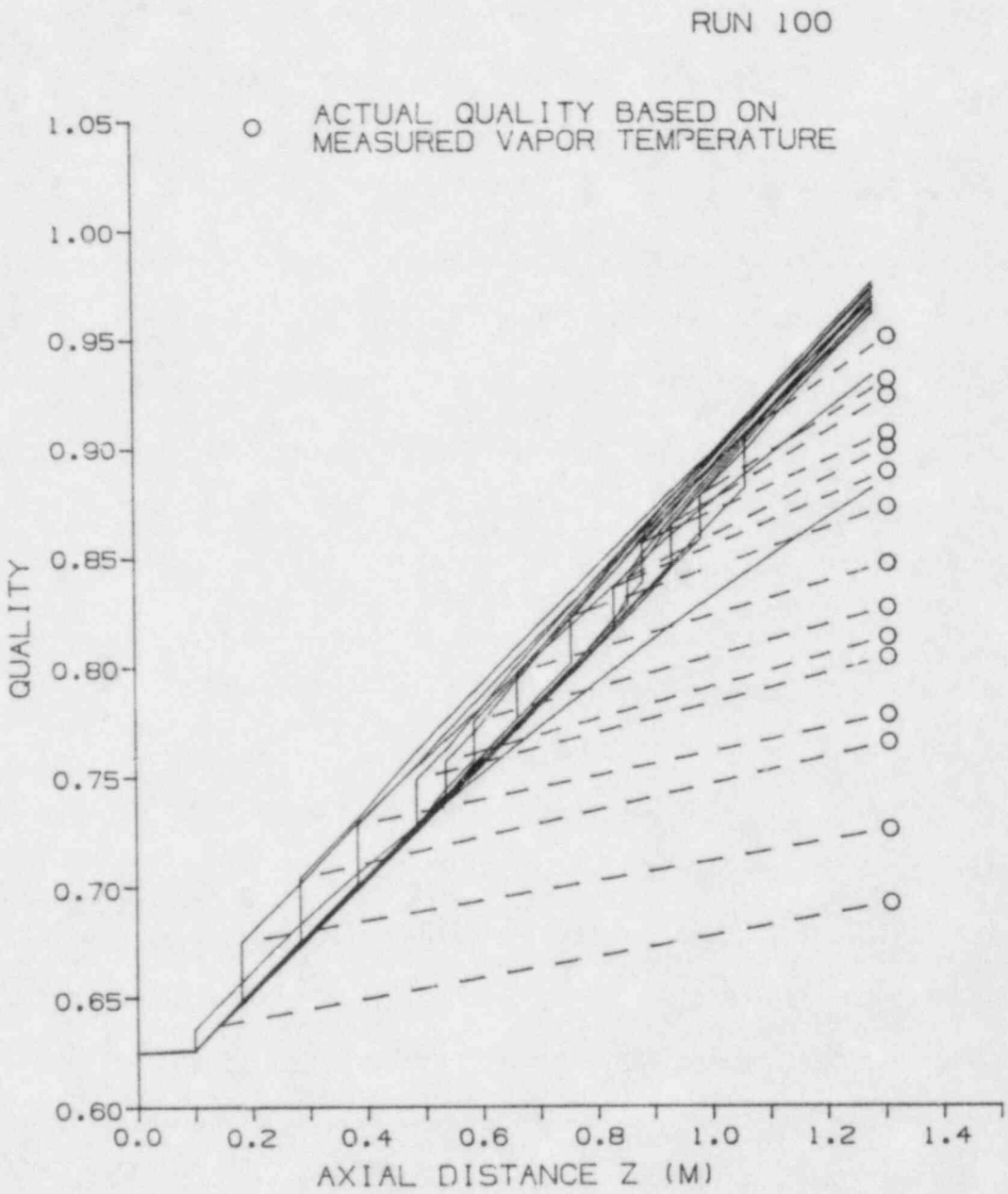

Figure 5-21. Qualities vs. distance for the 15 data points reported from run 100

the quench front. The circles plotted at a distance of 1.23 m are the actual qualities based on the vapor temperature. The dashed line between the top of the step increase in quality at the CHF location and the actual quality measurement is for visual reference only, and does not represent any data.

Figure 5-22 is a plot of (1) the CHF quality as the quench front propagates up the test section, (2) the equilibrium quality at the probe vs. time, and (3) the actual quality at the probe vs. time. The minimum possible actual quality at the vapor probe is usually the CHF quality, except in low quality experiments when, because of the limited quantity of vapor present, the vapor temperature would have to exceed the wall temperature for the actual quality to equal the CHF quality. For all runs the actual quality could never be less than the CHF quality without violating thermodynamic constraints.

Figure 5-23 is a plot of the effective wall to vapor convective heat transfer coefficient. This is calculated by dividing the wall heat flux at the thermocouple 2.5 cm upstream of the vapor probe by the difference between the wall temperature at the same location and the vapor temperature measured by the probe.

Figure 5-24 presents the same data as plotted above, but only for the data points reported versus the distance between the quench front and the vapor probe for that data point. This particular run demonstrates a slight reduction in the convective

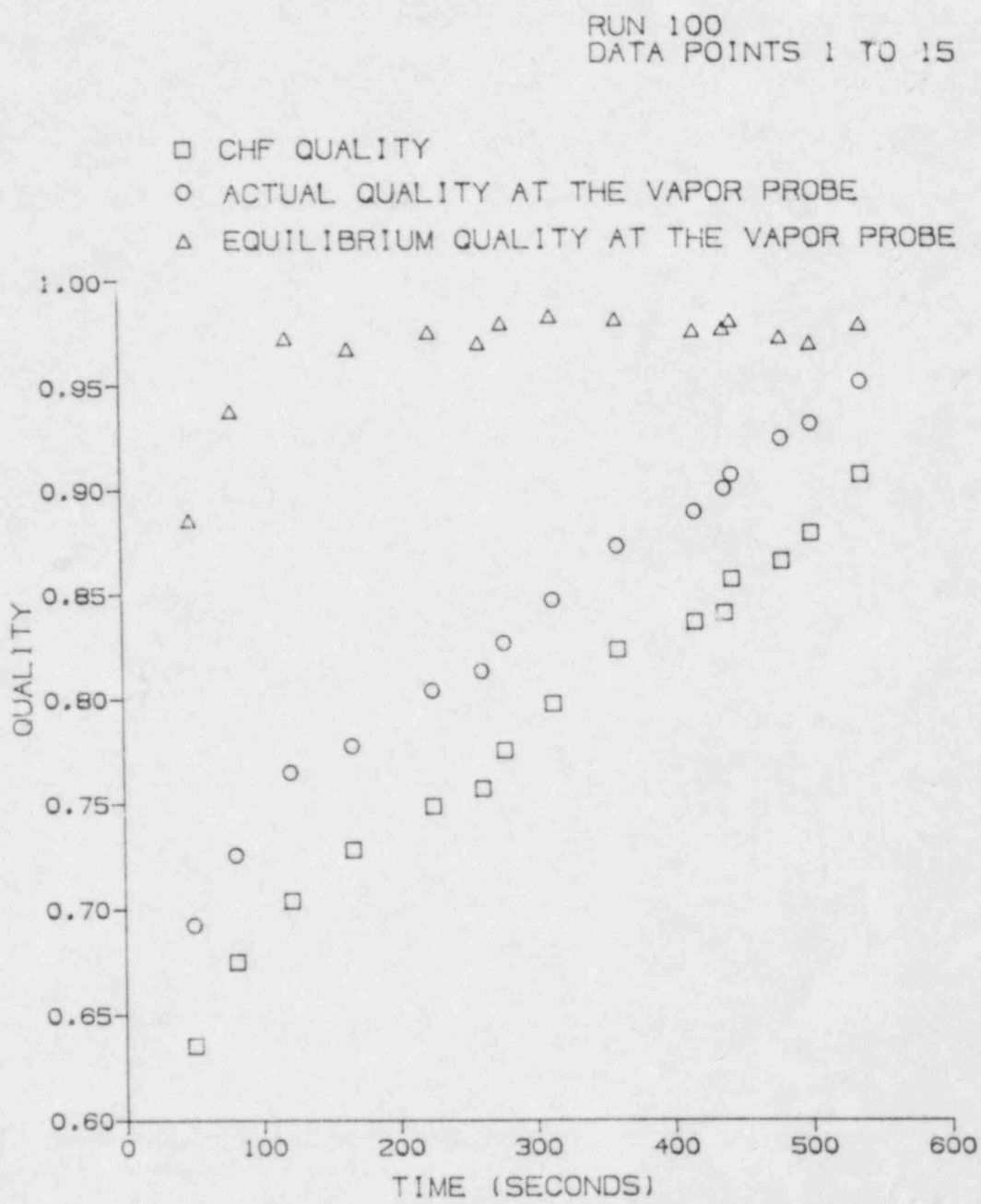

Figure 5-22. CHF quality, actual quality at the vapor probe, and equilibrium quality at the vapor probe vs. time for the 15 data points reported from run 100

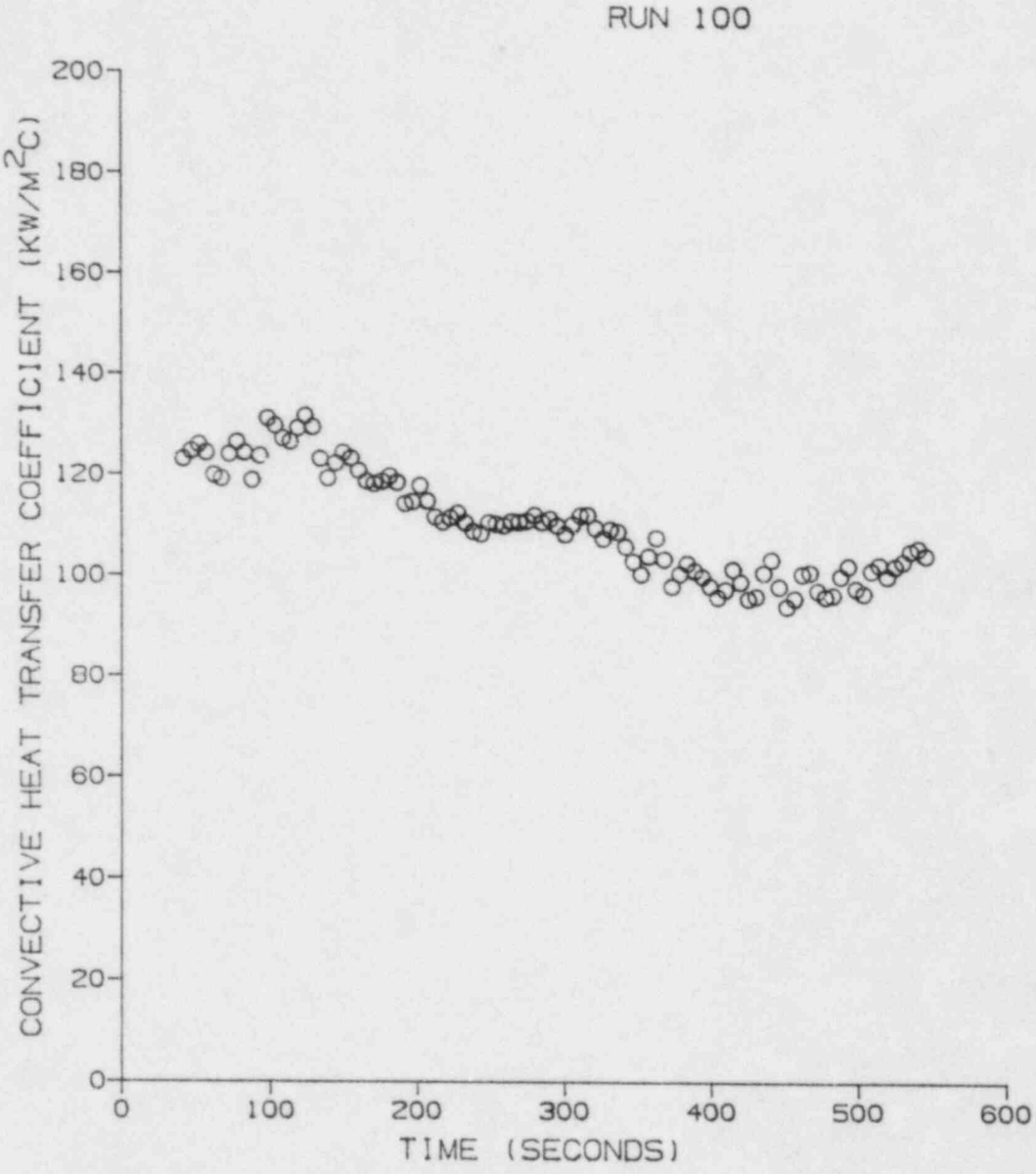

Figure 5-23. Convective heat transfer coefficient at the vapor probe vs. time for run 100

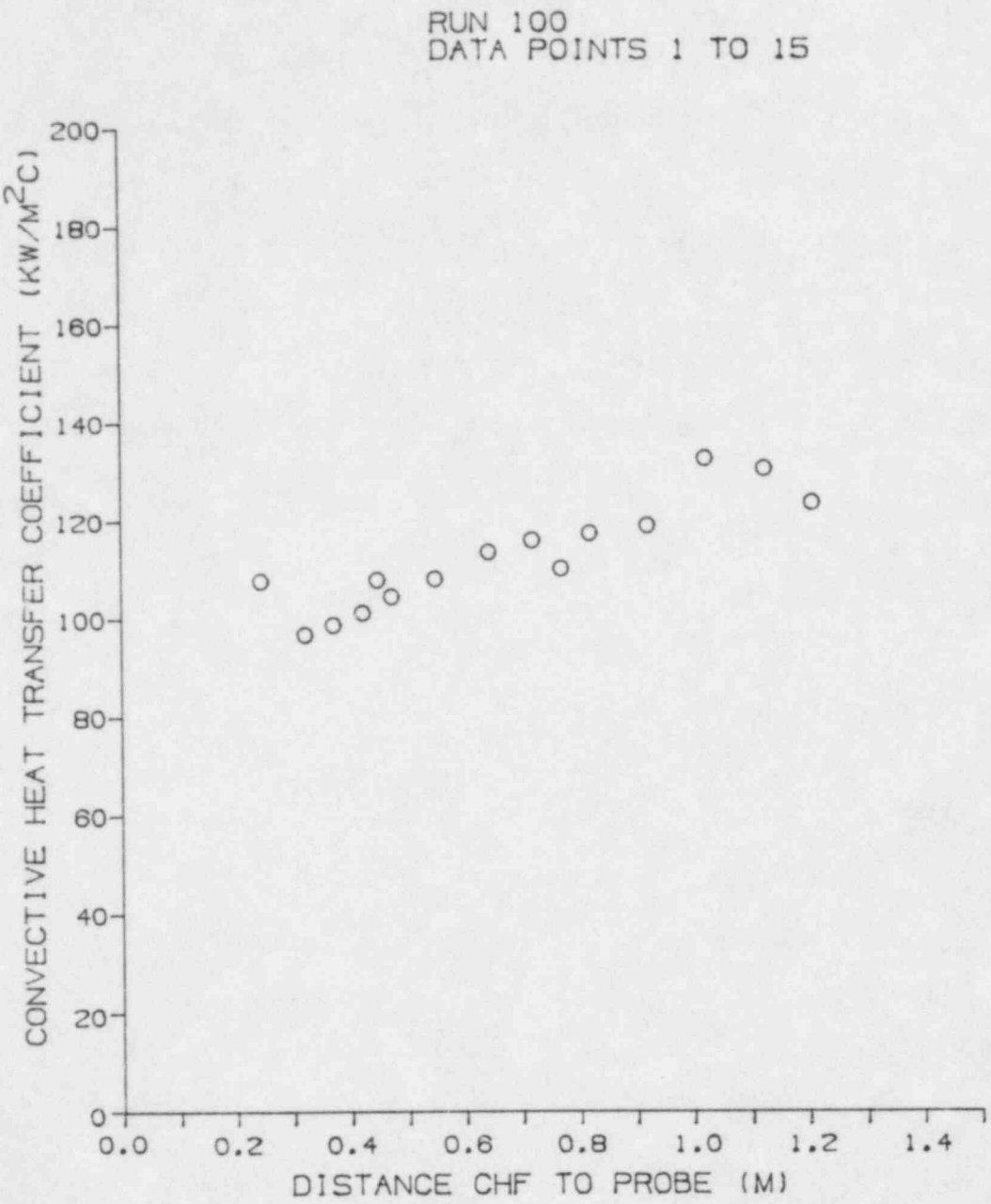

Figure 5-24. Convective heat transfer coefficient at the vapor probe vs. distance from CHF to the probe for the 15 data points reported from run 100

heat transfer coefficient as the quench front neared the vapor probe. While some runs demonstrated the same trend, many runs did not. This particular run was at a low mass flux and high quality, and the reduction in vapor velocity at the probe as the quench front approached the vapor probe, as demonstrated by the decreasing frictional pressure drop in figure 6-4, was probably responsible for the decrease in the convective heat transfer coefficient. Many other runs at different inlet conditions indicated a more constant convective heat transfer coefficient.

6. VOID FRACTION EVALUATION

While the main purpose of the test program was determination of the vapor superheat, or thermodynamic non-equilibrium, in convective film boiling, pressure drop measurements were obtained simultaneously in an attempt to estimate the corresponding void fractions. For this measurement, a differential pressure transducer was installed between the vapor port and the upstream spacer support tube as shown in figure 3-3. Thus the time dependent total pressure drop was measured in the convective film boiling regime.

The objective of the pressure drop measurement was to estimate the void fraction in convective film boiling. The total pressure drop is the sum of friction, acceleration, and gravity components:

$$dp_f + dp_{acc} + dp_g = dp_t \tag{6.1}$$

6.1 Friction Pressure Drop

Correlations for frictional pressure drop are numerous. Recently, Beattie and Whalley [6.1] have proposed a simple yet accurate model for two-phase frictional pressure drop using a hybrid model for the two-phase viscosity. The two-phase Fanning friction factor is calculated by the Colebrook equation with a two-phase Reynolds number based on this viscosity. The appropriate formulae are:

$$\frac{dp_f}{dz} = \frac{2f}{D_i}\frac{G^2}{\bar{\rho}} \tag{6.2}$$

$$\frac{1}{f^{\frac{1}{2}}} = 3.48 - 4\log_{10}(2\,\varepsilon/D + 9.35/(Re\,f^{\frac{1}{2}})) \tag{6.3}$$

$$Re = \frac{DG}{\mu} \tag{6.4}$$

$$\mu = \mu_\ell(1-\alpha_h)(1+2.5\ \alpha_h) + u_v\alpha_h \tag{6.5}$$

The viscosity equations include consideration of the flow pattern and are a hybrid of viscosity relationships in bubble and annular flow. This model was compared with data in the HFTS [6.2] data bank. Despite the simple form, this correlation gives comparable results to the HTFS and Barcoczy [6.3] correlations, and is superior to such methods as Martinelli-Nelson [6.4] and Thom [6.5] for vertical steam-water flow. Other fluids and orientations show similar results. This frictional pressure drop method has been adopted in the present evaluation.

In the application of these models, the quality variation between the two pressure taps must be specified in order to determine the total frictional pressure drop. Three different models for the variation in quality with axial distance can be incorporated into the calculation. As shown in figure 6-1, the models are (1) frozen quality at the CHF quality, (2) equilibrium quality along the test section, (3) equilibrium quality from Z_{CHF} until the equilibrium quality matches the actual quality measured by the vapor probe, and frozen quality from that location to the vapor probe. The frictional pressure drop calculations were performed for each of the three quality models. Comparisons of the results for each model will be presented later. Numerical integration with small step sizes between the pressure taps was used to calculate the pressure drop.

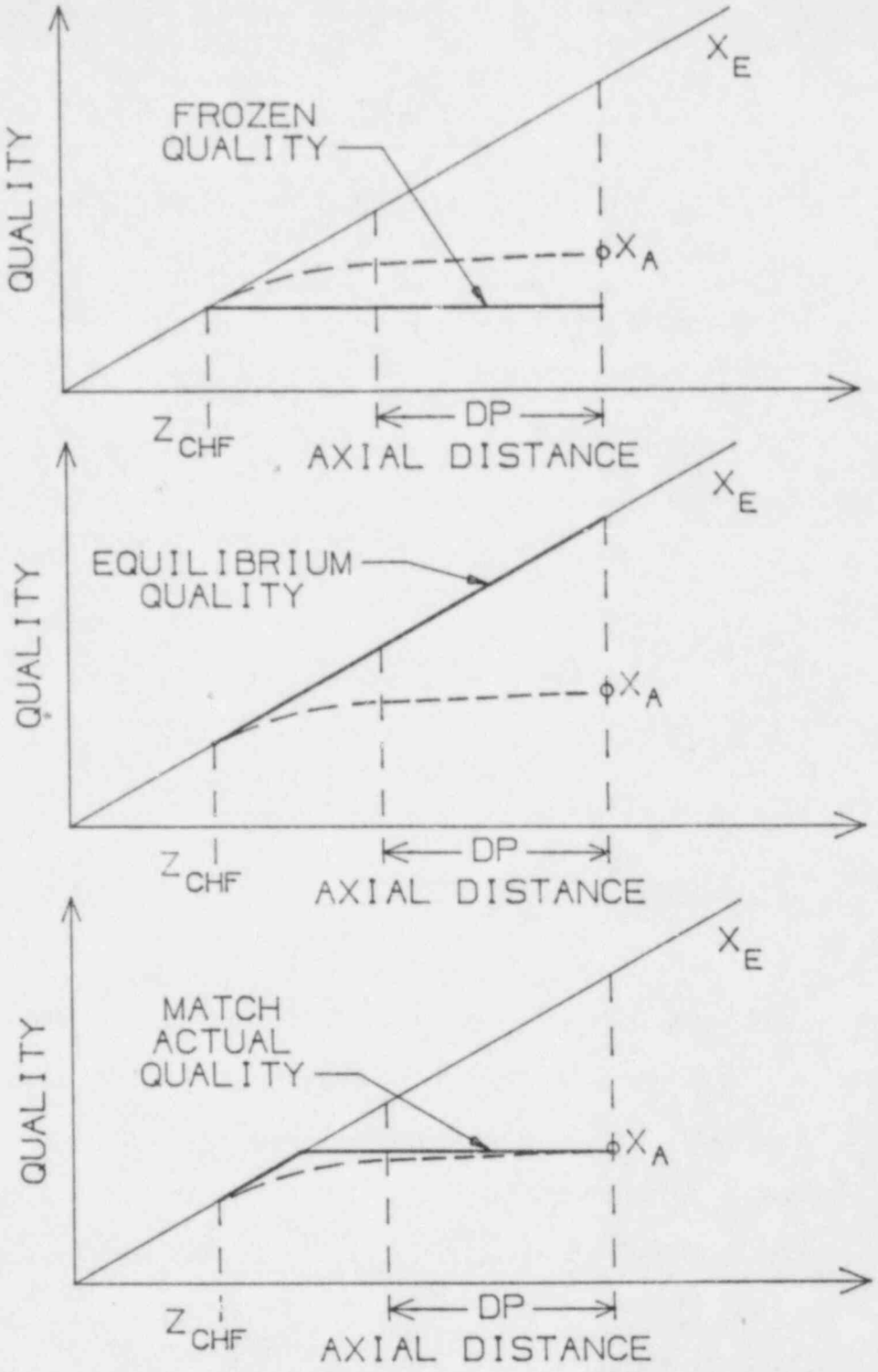

Figure 6-1. Models of flow quality

6.2 Acceleration

The acceleration pressure drop between the two pressure taps is simply the momentum change of the flow (Hsu and Graham, [6.6])

$$\frac{dp_{acc}}{dZ} = \frac{d}{dz}\left[\frac{1}{A}\int_A (\rho_\ell(1-\alpha)V_\ell^2 + \rho_v\alpha V_v^2)dA\right] \tag{6.6}$$

Using area average nomenclature,

$$\frac{dp_{acc}}{dZ} = \frac{d}{dZ}\left\{\left\langle \rho_\ell(1-\alpha)V_\ell^2\right\rangle + \left\langle \rho_v\alpha V_v^2\right\rangle\right\} \tag{6.7}$$

where

$$\langle\ \rangle \equiv \frac{1}{A}\int dA$$

In general,

$$C_L = \frac{\langle \rho_\ell(1-\alpha)V_\ell^2\rangle}{\langle\rho_\ell\rangle\ \langle 1-\alpha\rangle\ \langle V_\ell\rangle^2} \neq 1$$

The same form holds for the vapor quantities. Therefore, evaluation of the acceleration pressure drop could proceed from radially averaged quantities if C_L and C_v were known. However, at the present time no models for C_L and C_v have been proposed. Assuming that C_L and C_v are equal to 1.0 has been shown to be unacceptable by Andeen and Griffith [6.7], especially at low pressures. Instead, the use of a homogeneous model gives a better prediction of the momentum flux of the flow than using a slip model. While the homogeneous model gives a better

calculational answer, this result does not imply homogeneous flow but rather that compensating errors are included in the model.

Therefore the acceleration pressure drop in the flow is evaluated by

$$\frac{dp_{acc}}{dZ} = \frac{d}{dz}\left\langle \left\{ \rho_\ell (1-\alpha_h) V_{\ell h}^2 + \rho_v \alpha_h V_{vhj}^2 \right\} \right\rangle$$

or rewriting the expression

$$\frac{dp_{acc}}{dZ} = \frac{d}{dz}\left[G^2 \left\langle \left\{ \frac{(1-x)}{\rho_\ell} + \frac{x}{\rho_v} \right\} \right\rangle \right]$$

and the actual quality is used.

6.3 Gravity

The gravitational pressure drop component for vertical upward flow is given by

$$\frac{dp_g}{dz} = -g \left[\langle \rho_\ell (1-\alpha) \rangle + \langle \rho_v \alpha \rangle \right]$$

The liquid density is constant across the flow, and assuming

$$\langle \rho_v \alpha \rangle = \langle \rho_v \rangle \langle \alpha \rangle$$

and that $\langle \alpha \rangle$ is given by the relationship between the actual and equilibrium quality, i.e.

$$\frac{X_a}{X_e} = \frac{i_{fg}}{i_v(P, T_v) - i_{ls}}$$

the gravitational pressure drop component is

$$\frac{dp_g}{dZ} \cong - g \left(\rho_\ell(1-\langle\alpha\rangle) + \rho_v\langle\alpha\rangle\right)$$

Note that this pressure drop component is the only component dependent on the actual void fraction.

6.4 Void Fraction Determination

The area average void fraction, $\langle\alpha\rangle$, can now be determined from the total pressure drop measured during the tests by using the pressure drop component methods outlined above. The general procedure is to subtract the frictional and acceleration components, which are not a function of the actual void fraction, from the total pressure drop. The result is the gravity component which can be used to evaluate the average value of $\langle\alpha\rangle$ between the pressure taps.

The pressure drop measurements used in the void fraction calculation were obtained throughout each run, but only the data obtained prior to the quenching of either pressure tap are used. The quenching of a pressure tap indicated that either the ascending or descending quench front had moved into the measurement region. Since the entire measurement region then would not be in post-CHF flow, the analysis used would no longer be valid. The raw data obtained for a typical class 1 run, prior to the quenching of a pressure tap, is shown in figure 6-2. Figure 6-3 shows the strip-chart recordings of the differential pressure measurement for the same run at times corresponding to A, B, C, and D on figure 6-2. The scatter apparent in figure 6-2 is primarily due to the severe

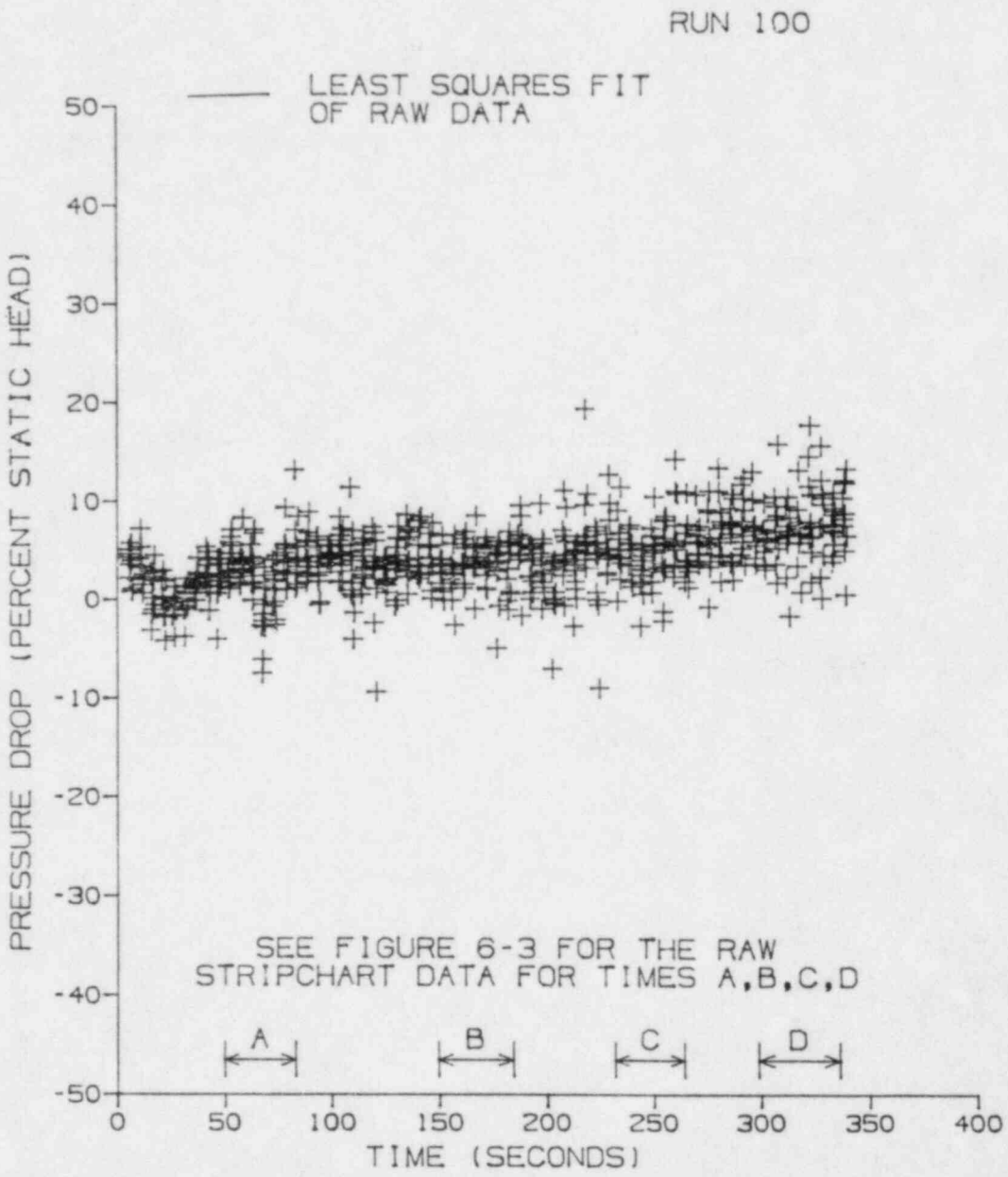

Figure 6-2. Pressure drop data vs. time for run 100

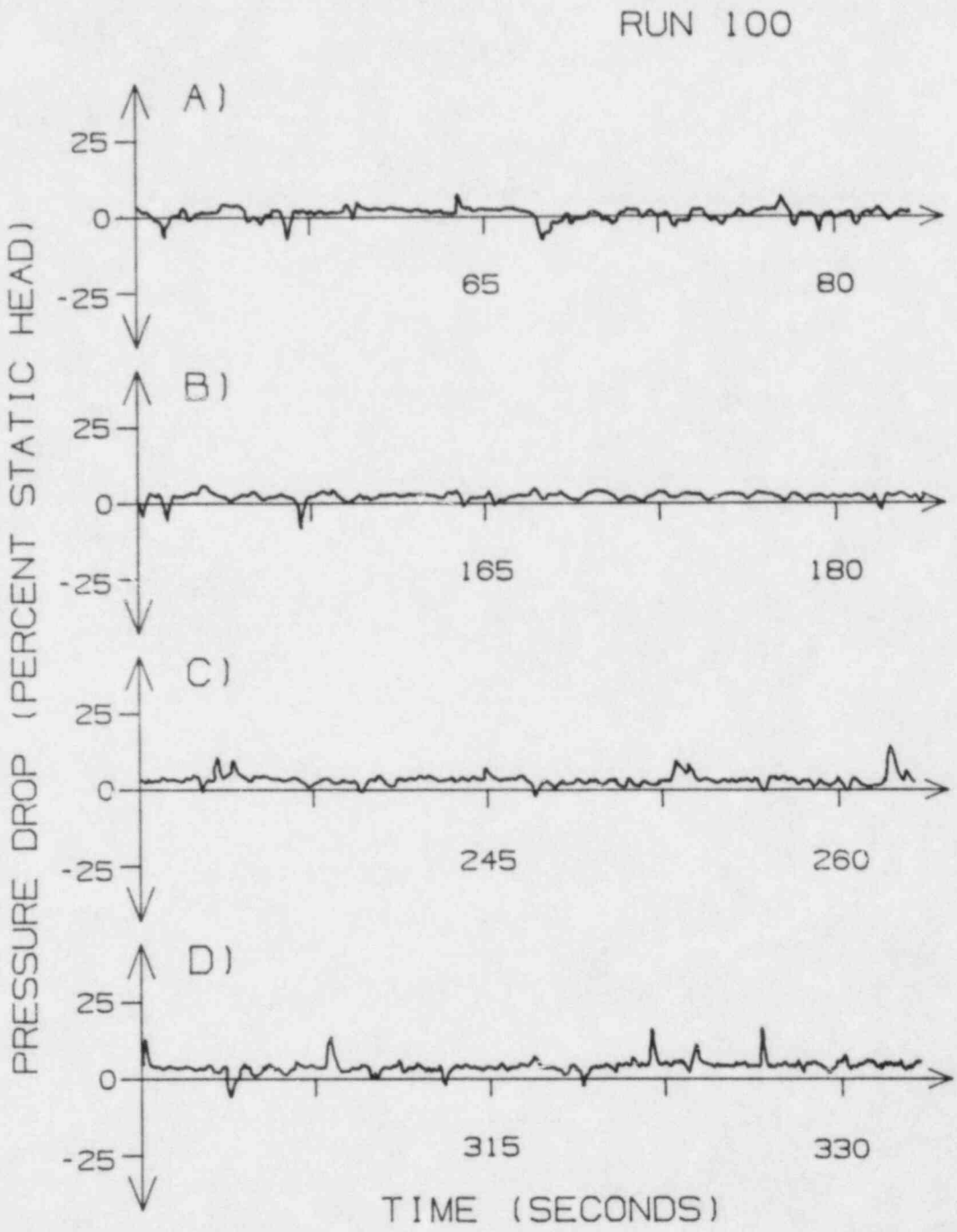

Figure 6-3. Pressure drop stripchart during four different time intervals for run 100

time compression of that plot. The nature of the phenomena responsible for the actual scatter could not be determined specifically, but several possibilities exist, including measurement noise, liquid droplet impact at the pressure taps, and the stochastic nature of two-phase flow.

In order to determine reasonable void fractions as a function of time, a first order least squares approximation was obtained for the raw differential pressure measurements and is represented by the line in figure 6-2. By subtracting the friction and acceleration pressure drops from the smoothed total pressure drop, the gravitational pressure drop as a function of time was determined, as shown in figure 6-4. Figure 6-5 shows the void fraction calculated from the gravitational pressure drop. Since measurement of void fraction by differential pressure drop is not very accurate, the significant finding of the void fraction calculations is the decrease in void fraction as the quench front approaches the measurement region. The actual void fraction measurements are accurate to only 0.03, but since the inaccuracy is due primarily to quality modeling errors and calibration errors, which would not change during an experiment, the trend indicated is in itself significant.

Figures 6-4 and 6-5 are based on the actual quality model mentioned in section 6.2. As concluded in the discussion, the vapor superheat is small in the region close to the quench front, and then increases at a rate corresponding to a nearly frozen-quality flow further downstream. The match actual probe quality

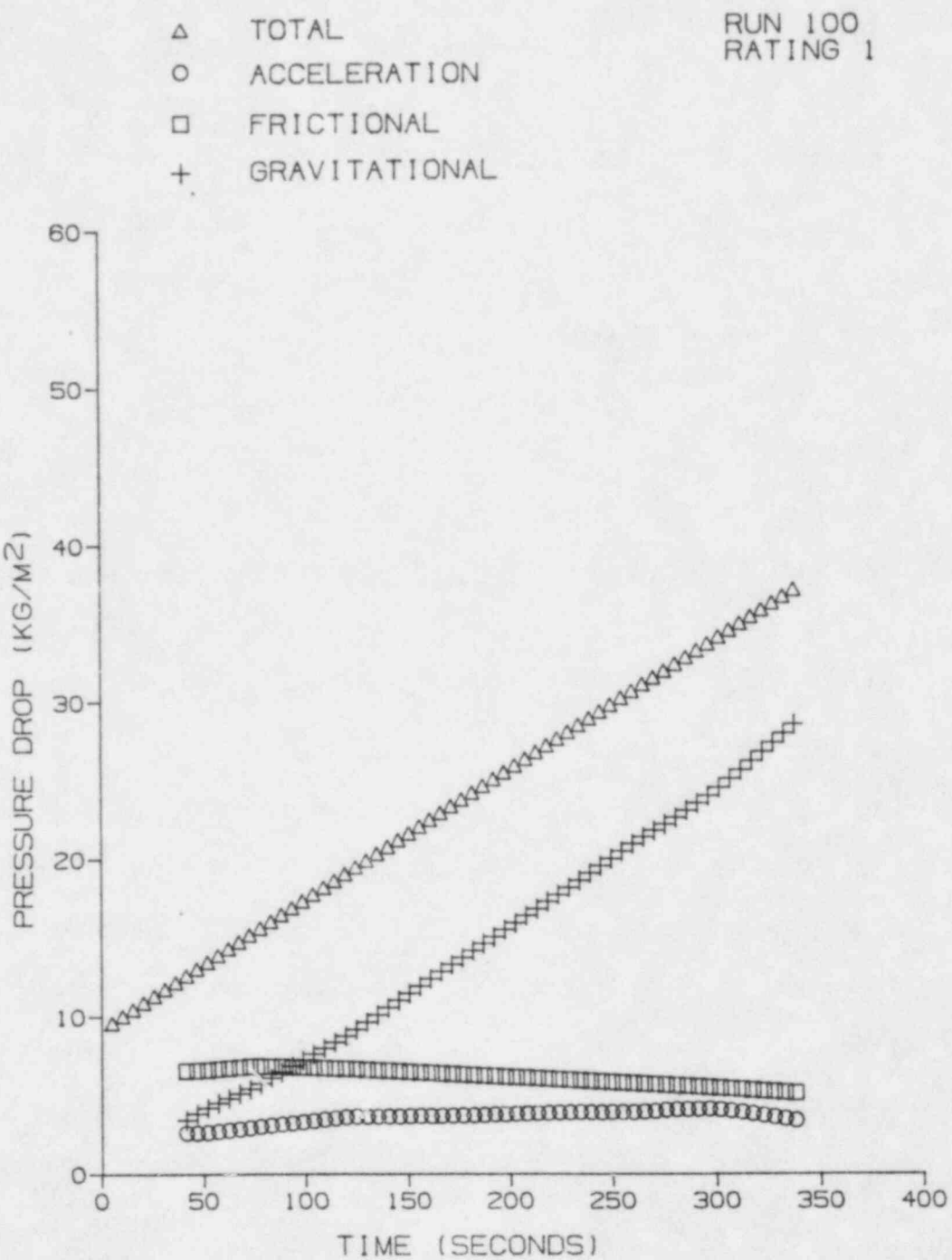

Figure 6-4. Pressure drop vs. time based on the actual quality model for run 100

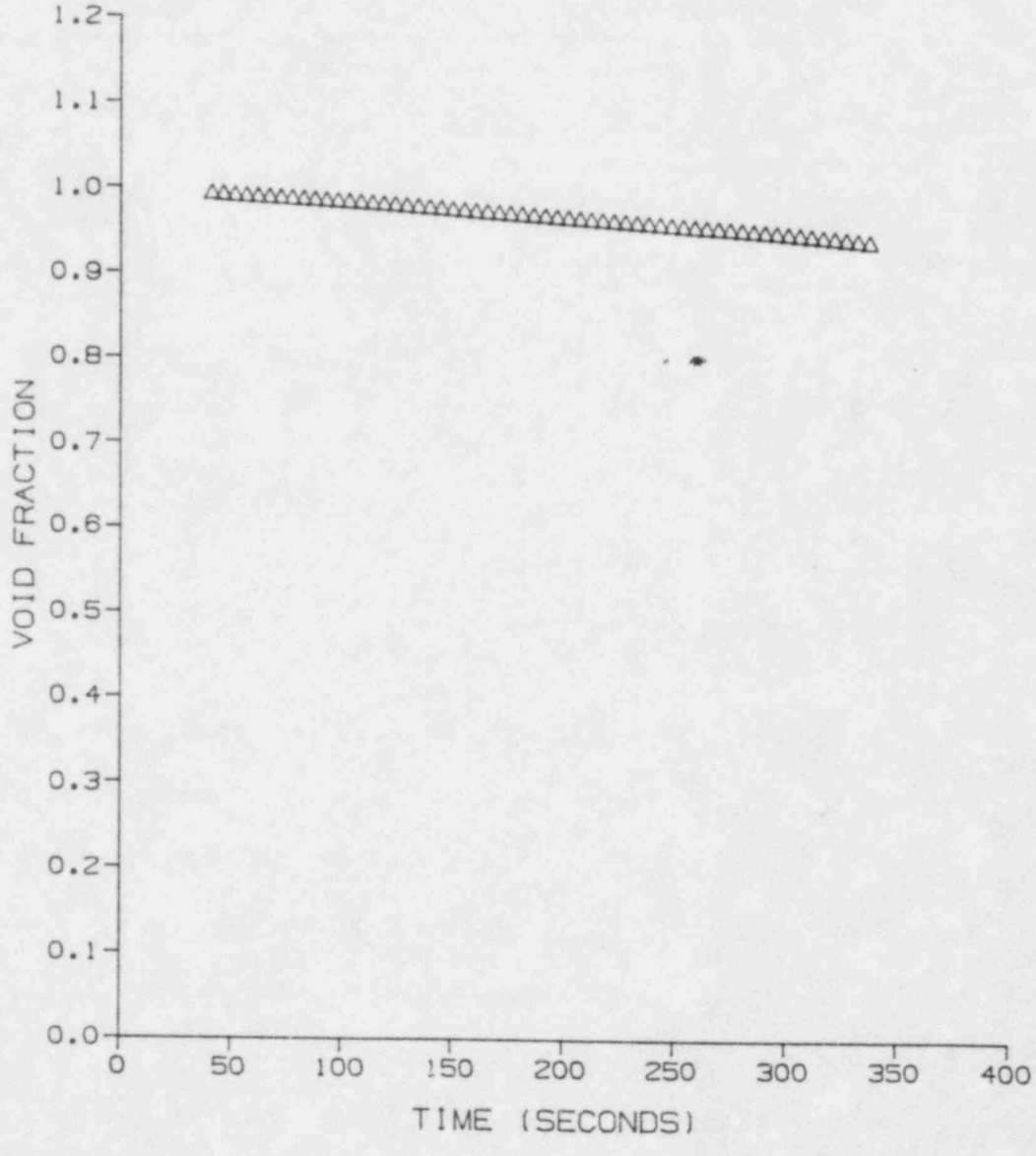

Figure 6-5. Void fraction vs. time based on the actual quality model for run 100

model fits this scenario the best, but as indicated in table 6-1, the other two models yield frictional and acceleration pressure drops of the same magnitude as the model used.

Table 6-1 Total pressure drop (dpt), based on least squares curve fit to the raw data, and the corresponding frictional and acceleration pressure drop for the three different quality models. The elapsed time between each line is 31.2 seconds. (differential pressure in kg/m^2)

Equilibrium				Frozen			Match Actual		
dp_t	dp_f	dp_a	void	dp_f	dp_a	void	dp_f	dp_a	void
10.4	4.2	1.0	0.991	7.7	2.5	1.004	6.6	2.6	0.999
11.7	4.3	1.1	0.989	7.8	2.8	1.002	6.8	2.9	0.997
13.4	4.4	1.3	0.986	7.7	3.2	1.000	6.8	3.4	0.994
15.3	4.5	1.3	0.982	7.6	3.4	0.995	6.6	3.6	0.990
17.7	4.5	1.4	0.976	7.2	3.5	0.990	6.4	3.7	0.985
20.4	4.5	1.4	0.971	7.1	3.6	0.984	6.2	3.8	0.979
23.4	4.5	1.4	0.964	6.9	3.7	0.977	6.0	3.9	0.972
26.8	4.5	1.4	0.957	6.7	3.7	0.969	5.8	3.9	0.964
30.5	4.5	1.5	0.949	6.4	4.0	0.961	5.6	4.1	0.956
34.5	4.5	1.5	0.940	6.0	4.1	0.952	5.3	3.7	0.946

The resulting uncertainties in void fraction due to model limitations were on the order of 0.01. As the quench front approaches the measurement region the total pressure drop becomes much larger than the frictional and acceleration pressure drops of all the models. Therefore, the selection of different quality models would not alter the trends demonstrated by these data.

The objectives of the void fraction measurement were 1) provide an approximate void fraction for each data point, and 2) show the change in void fraction with time for each run. Because of inaccurate zero settings, data acquisition limitations, induced

descending quench fronts, and rapid fluctuations in the pressure drop measurement, the quantity of pressure drop data obtained during some experiments was insufficient to support either objective. Many experiments were subject to only one or two of these limitations, thereby permitting the approximate void fraction to be calculated for many data points. While data shown here are typical of the high quality, low mass flux, slow quench front runs, the quantity and quality of raw data for many runs was not sufficient to support the second objective.

In order to help assess the implications of the void fraction results, a plot of theoretical void fractions was performed. The information shown in figure 6-6 is illustrative only and does not represent any data obtained in this investigation. When the experiment begins, the test section is flooded in argon and has a void fraction of 1. The line with the plus signs is based on the void fraction that would result if all the liquid mass flow, based on inlet quality and mass flow rate, remained uniformly distributed in the test section. This would be the minimum possible homogeneous void fraction as a function of time. Obviously the void fraction remains far above this line, which implies that most of the liquid entering the test section either evaporates or exits the test section outlet. The other series of curves is the void fraction based on the CHF quality, with no change in the quality downstream of CHF (adiabatic), and various slip ratios ranging from 1.0 to 60.0. This plot does not present any data, and is presented solely to illustrate what the slip ratio would be for a given void fraction. Since these curves are based on constant quality flow when the

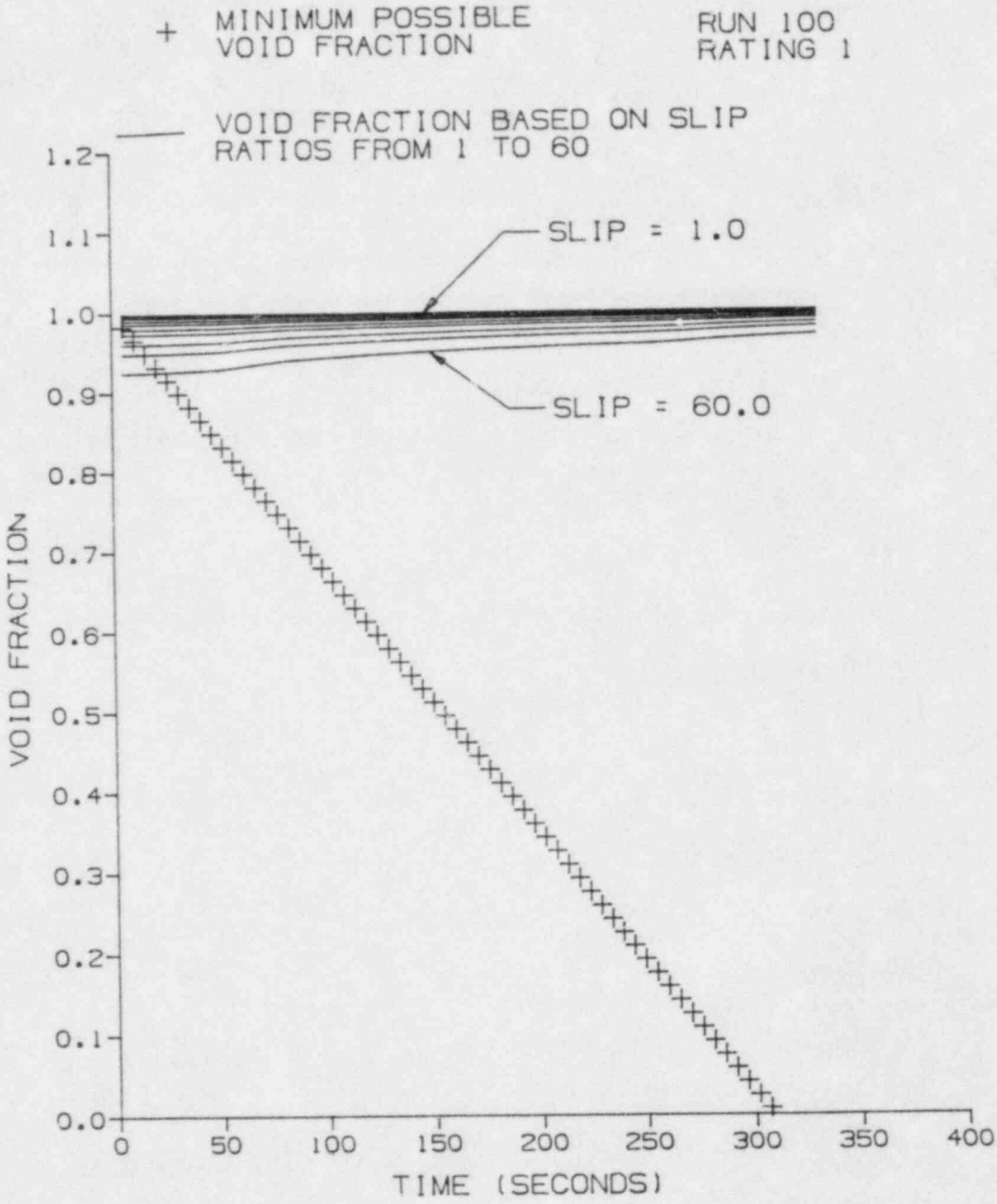

Figure 6-6. Theoretical void fractions vs. time for run 100

quality is actually increasing, the slip ratio corresponding to a void fraction would actually represent a minimum value since the addition of heat increases vapor volumetric flow and reduces liquid flow. With more vapor present and less liquid present, the slip ratio would have to be higher for the same void fraction. By comparing figures 6-5 and 6-6, the void fraction measurements obtained during this run indicates slip ratios greater than 50 in the region immediately downstream of the CHF location. This finding was consistently demonstrated by the void fraction data obtained during this investigation.

The results of the void fraction calculations presented in figure 6-5 are plotted in figure 6-7 as a function of the distance between the quench front and the middle of the 50 cm pressure drop measurement region. It is important to note that the void fraction is an average value for the 50 cm upstream of the vapor probe. When the quench front is 50 cm from the mid-point of the measurement region it is only 75 cm from the upper pressure tap and only 25 cm from the lower pressure tap.

While void fraction data were not available for all of the reported data points, the data that were obtained consistently displayed a trend towards decreasing void fraction as the quench front approached the measurement region. More significantly, the data indicated low slip ratios far from the quench front, and very high slip ratios (50 or more) in the 50 cm region immediately downstream of the quench front. The inference is that liquid pushed off the wall at the CHF point requires a significant axial distance to attain an established slip ratio with respect to the vapor. This

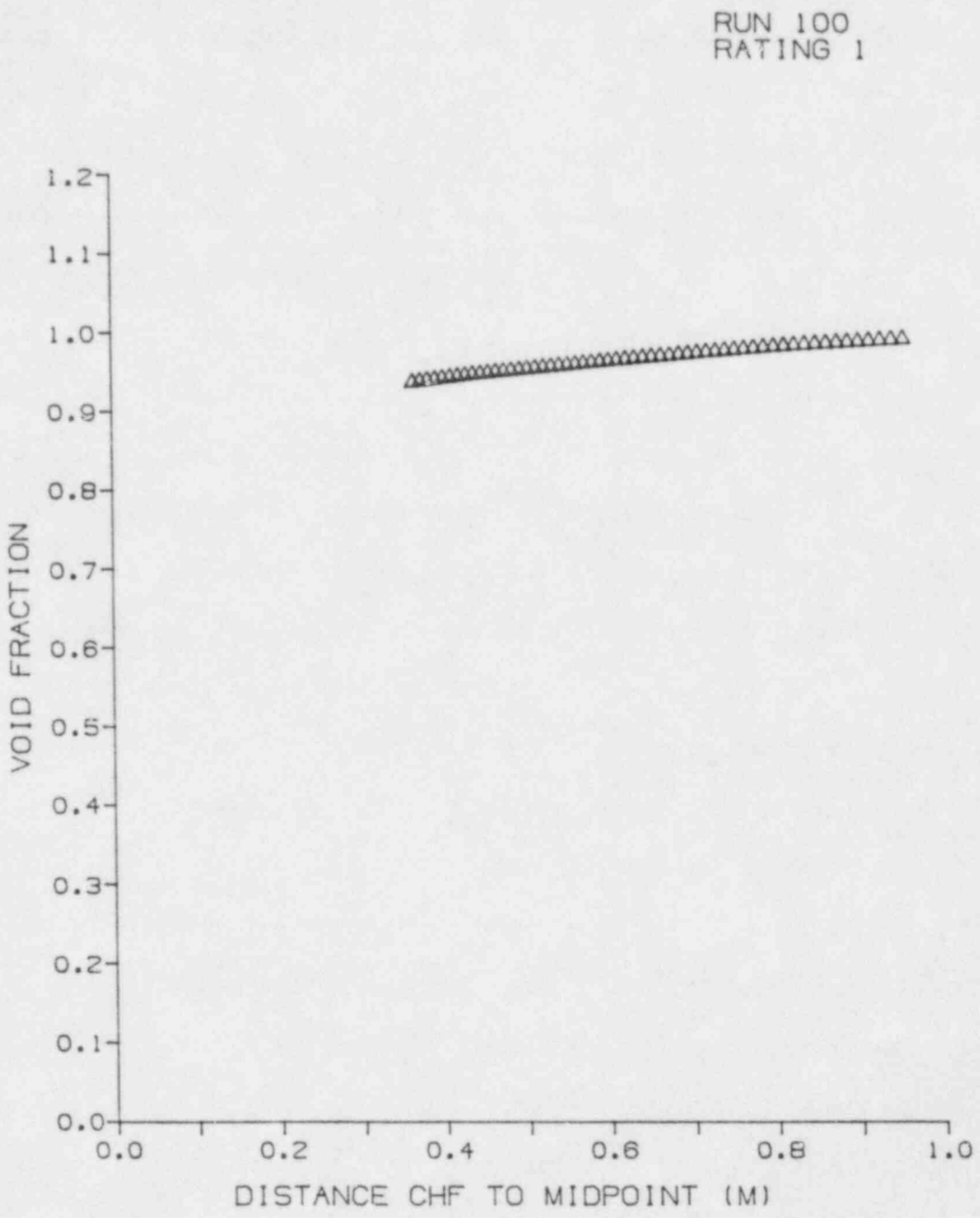

Figure 6-7. Void fraction vs. distance from CHF to midpoint of measurement region based on actual quality model for run 100

behavior could be significant to modeling of the non-equilibrium heat transfer behavior.

7. DISCUSSION

The results of this experimental program are significant in three areas: improvements in experimental technique for measuring vapor superheat in post-CHF flow, observations of the nature of convective dispersed flow film boiling, and definition of future experiments to assist in the refinement of non-equilibrium models for post-CHF heat transfer. The first area is discussed in Appendix B, and the second and third areas are discussed here.

7.1 Experimental Findings About Post-CHF Heat Transfer

The data obtained demonstrate previously observed trends for wall temperatures and wall heat fluxes in post-CHF flow. The vapor temperature measurements yielded unexpected trends for vapor superheats as a function of axial distance from the quench front. As demonstrated below, the results were found to be readily duplicated for different experiments performed at the same inlet conditions.

Data from two runs at similar inlet flow conditions are shown in figure 7-1. The instantaneous axial distribution of wall superheats and the measured vapor superheat are plotted for three different times (A,B,C) during the history of each run. At any one instant, the wall superheat rises rapidly immediately downstream from the CHF location and attains superheats in the order of 300 to 500 C in the convective film

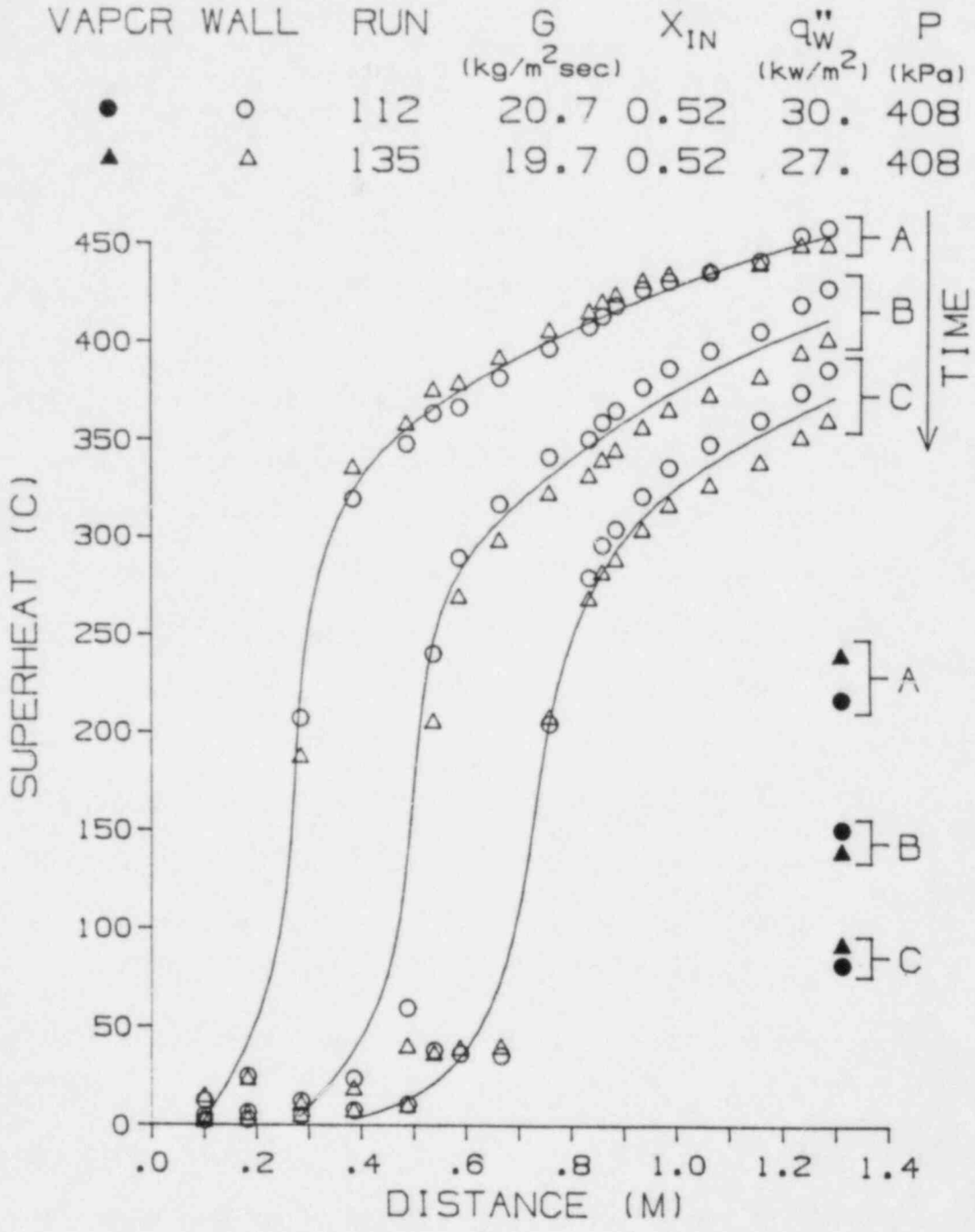

Figure 7-1. Temperature vs. time for two moving quench front experiments at similar inlet conditions

boiling region. With increasing time in each experiment, the CHF location propagates upward into the test section, as indicated by the progression of axial wall temperatures from times A to C. The corresponding vapor superheats detected by the vapor probe at a fixed axial location are indicated for each of the three time instants. Clearly, as the CHF quench front approached the location of the probe station, the measured vapor superheats decreased in magnitude. The two runs plotted in figure 7-1 also give a representative indication of the experimental duplicability in these tests. As listed in the legend, the test parameters (G, Xin, Q, P) were similar for the two runs. In the actual test sequence, these two runs were separated by a complete quench of the test section and a restart of the experiment. Duplicability of wall superheats in the film boiling regime was of the order of 5 percent (20 C out of 400 C), and the duplicability of vapor superheats was of the order of 10 percent (25 C out of 250 C).

An Eulerian view of the quench experiment can be obtained by plotting the wall superheat at a given axial position versus time, as illustrated in figure 7-2. The heated wall in the convective film boiling regime experienced a normal quench history marked by an initial period of relatively slow precursor cooling until local superheats decreased to the range of 250 to 350 C.

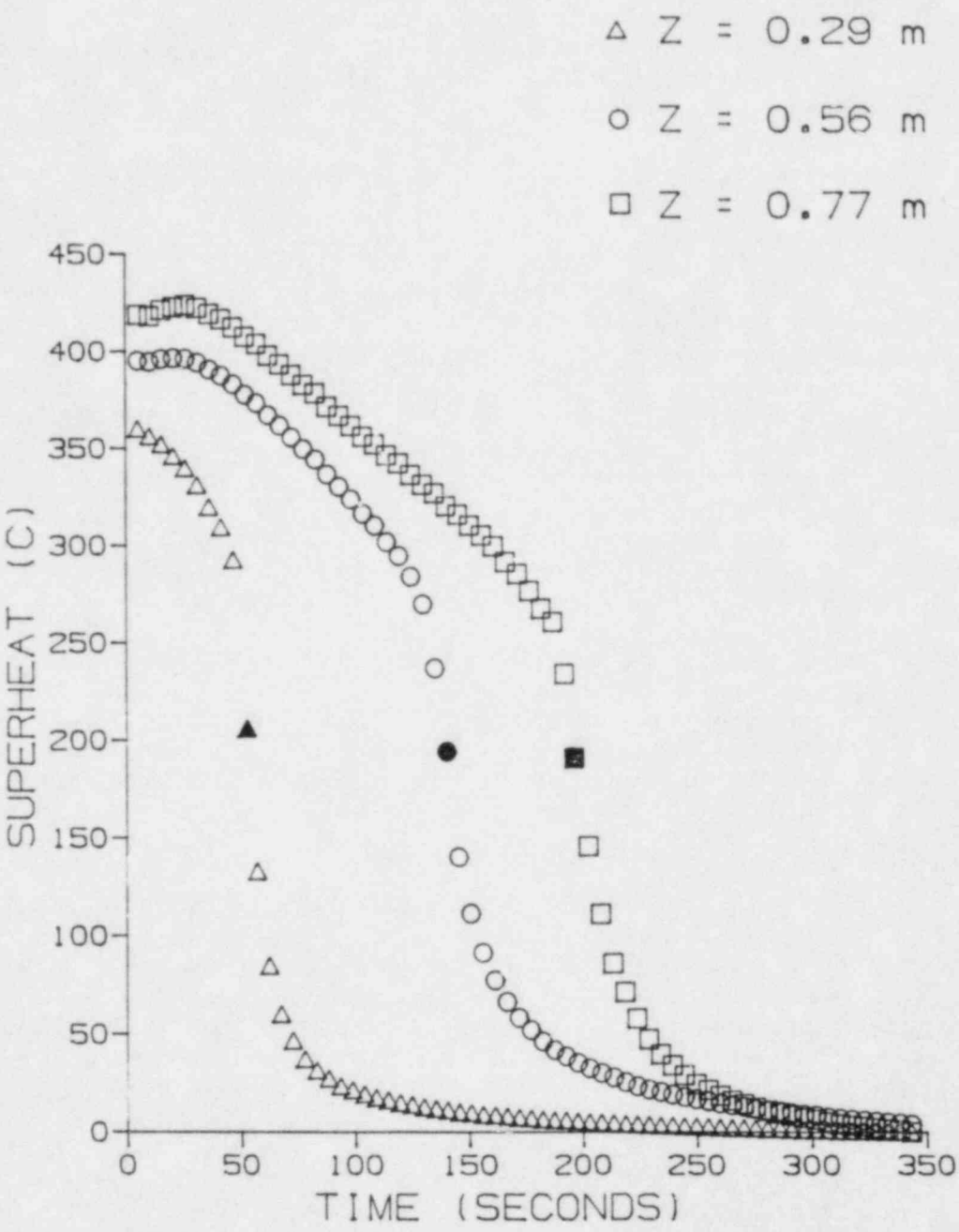

Figure 7-2. Temperature vs. time for run 135 at three axial locations

The precursor cooling stage was followed by a period of rapidly decreasing superheat temperatures indicating quenching of the local wall towards the fluid saturation temperature. In these experiments, the CHF quench front was defined as passing a particular thermocouple when that thermocouple indicates a maximum in the rate of temperature decrease. For each of the three axial positions illustrated in figure 7-2, the time of passage of the quench front is indicated by the dark symbol.

A cross plot of the time to quench at each thermocouple location then provides a clear indication of the propagation of the CHF location along the length of the test section. Results for two runs are shown in figure 7-3. The quench front velocity for each run is essentially constant as indicated by the linear lines through the data points. The slopes of these lines indicate that the quench front velocity for these two runs were in the range of 0.4 cm/sec.

In each run, the inlet hydraulic conditions including the inlet flow quality were held constant during the quench history. Since net heat flux into the fluid occurs along the length of the test section, the resulting equilibrium vapor quality at the CHF location (Z_{CHF}) increased with time as the quench front propagated up the test section. For the two runs illustrated in figure 7-3, the CHF qualities were calculated by heat balance

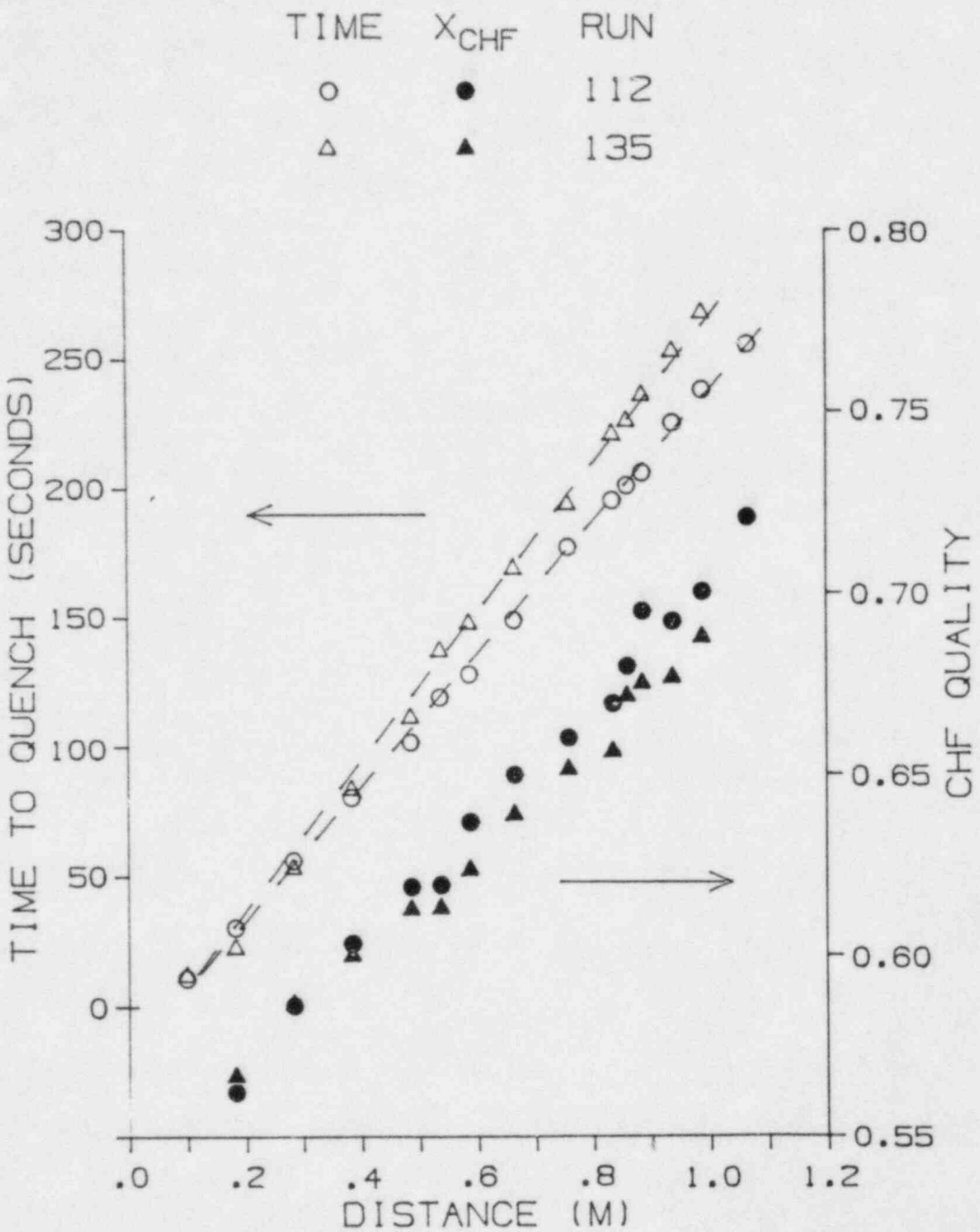

Figure 7-3. Time to quench and CHF quality vs. axial position for two moving quench front experiments at similar inlet conditions

and are indicated in the figure. As the CHF location propagated over a distance of 1 m, the local quality at the CHF location increased from 0.57 to 0.72. The change in flow quality at the initial and final CHF locations during any one run decreased with decreasing heat flux.

Heat transfer from the wall during convective film boiling is commonly understood to be proportional to the difference between wall superheat and vapor superheat. Figure 7-4 shows a plot of wall and vapor superheats in the vicinity of the vapor sampling probe during the quench history of two runs. Clearly, as the quench front approached the measurement station (with increasing time), there is a significant decrease in the wall superheat in spite of the essentially constant wall heat flux. However, there is a corresponding decrease in the local vapor superheat so that the difference between wall and vapor superheats remained relatively constant, indicating only a minor change in the effective wall heat transfer coefficient as plotted in figure 7-5. Also plotted on figure 7-4 are curves calculated for the vapor temperature if no further vaporization were to occur beyond the CHF location. Theoretically, this "frozen quality" vapor temperature must be an upper bound for the non-equilibrium vapor superheat. The experimentally measured vapor superheats at the probe station satisfied this thermodynamic

VAPOR	WALL	RUN	G (kg/m^2sec)	X_{IN}	q''_w (kw/m^2)	P (kPa)
●	○	112	20.7	0.52	30.	408
▲	△	135	19.7	0.52	27.	408

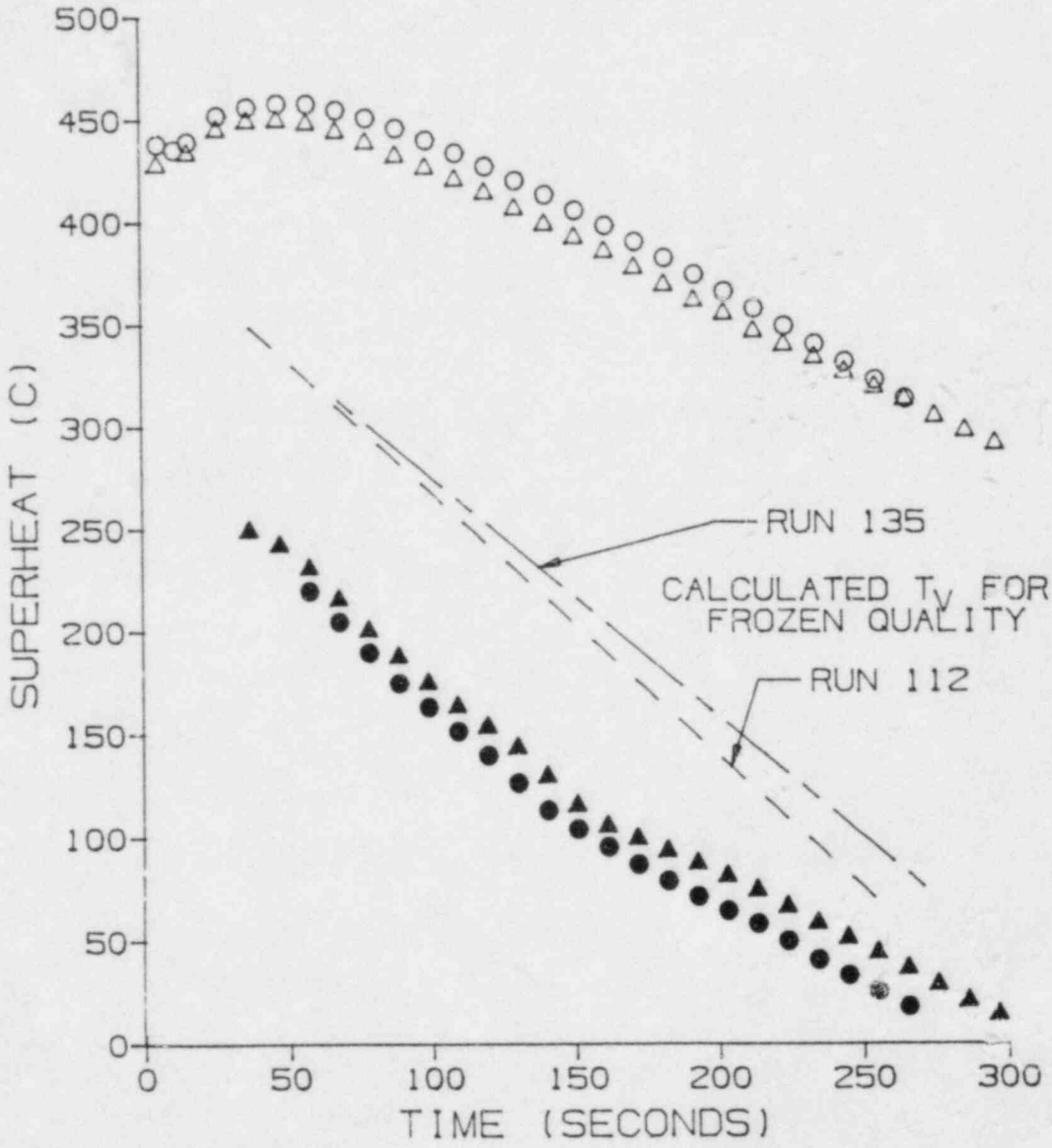

Figure 7-4. Temperature vs. time at Z=1.31 m for two moving quench front experiments at similar inlet conditions

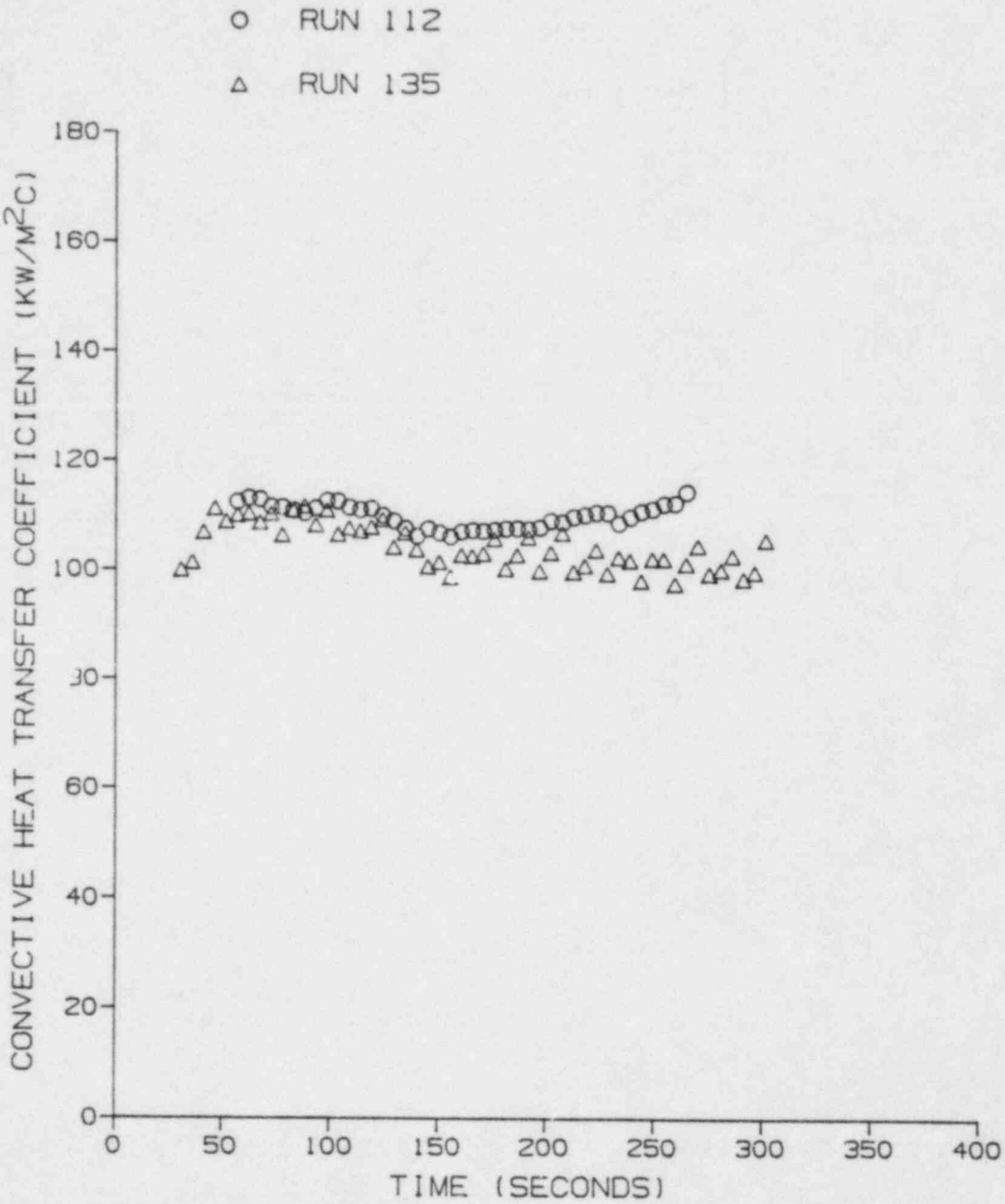

Figure 7-5. Convective heat transfer coefficient vs. time at the vapor probe for two runs at similar inlet conditions

limiting condition. Finally, the data shown in figure 7-4 are for the two runs with similar test parameters and therefore give an indication of the reproducibility of these experiments.

Combining the results shown in figure 7-4 with the information regarding instantaneous quench front location shown in figure 7-3, it is possible to transform the experimental results to obtain plots of wall superheats and vapor superheats as a function of distance (dZ) from the quench front. Figure 7-6 shows such data for the two sample runs, illustrating the fact that this technique of slowly propagating quench front with time varying CHF quality can be used to obtain measurements of non-equilibrium wall and vapor superheats at various axial distances from the CHF location with the use of just a single vapor probe. The data plotted in figure 7-6 show that the wall superheat evidently increased steeply immediately downstream of the CHF location and then leveled off to a slower and more constant rate of increase with increasing axial distance. In contrast, the data on vapor superheats indicate that there was a region (of approximately 0.3 m) downstream from the CHF location where the vapor superheat is fairly small (less than 50 C for these two runs). At greater axial distances, the vapor superheat then increased rapidly and at a rate approximately paralleling that for the wall superheat. Compared to the theoretical "frozen quality"

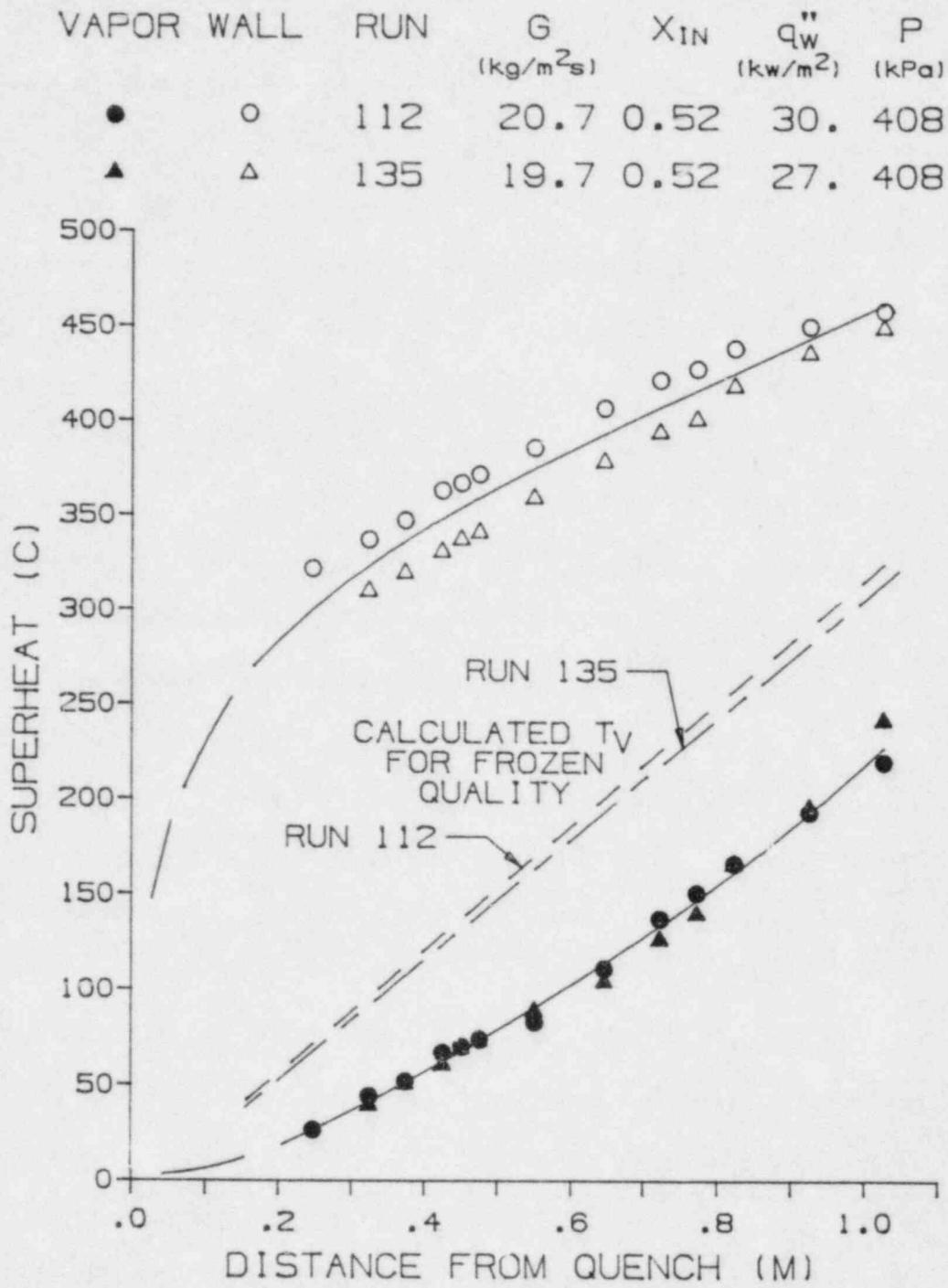

Figure 7-6. Wall and vapor temperatures at the vapor probe vs. distance between the probe and the quench front for two moving quench front experiments at similar inlet conditions

limit, the measured vapor superheats were consistently lower as required by thermodynamic considerations. The behavior illustrated in figure 7-6 for the two sample runs was found to be consistently displayed by all the data obtained in these tests.

The results illustrated in figure 7-6 are particularly significant in two respects. First, the fact that vapor superheats remained small for a significant distance (of the order of 0.3 m) downstream from the CHF location indicates that the vaporization process is relatively efficient in that region near to the CHF front. This implies the existence of a "transition" region immediately downstream from CHF where there is a higher volumetric concentration of liquid in the two-phase mixture than would be expected in established dispersed-film boiling convection. Void fraction measurements based on the differential pressure measured over the 50 cm before the vapor probe confirm the presence of more liquid immediately downstream of the quench front. Figure 7-7 shows the void fraction calculated from the differential pressure measurements plotted as a function of the distance between the quench front and the center of the 50 cm long measurement region. With an increased liquid presence immediately downstream of the quench front, both interfacial vapor-liquid heat transfer and liquid-wall heat transfer would be enhanced, leading to enhanced liquid vaporization. It

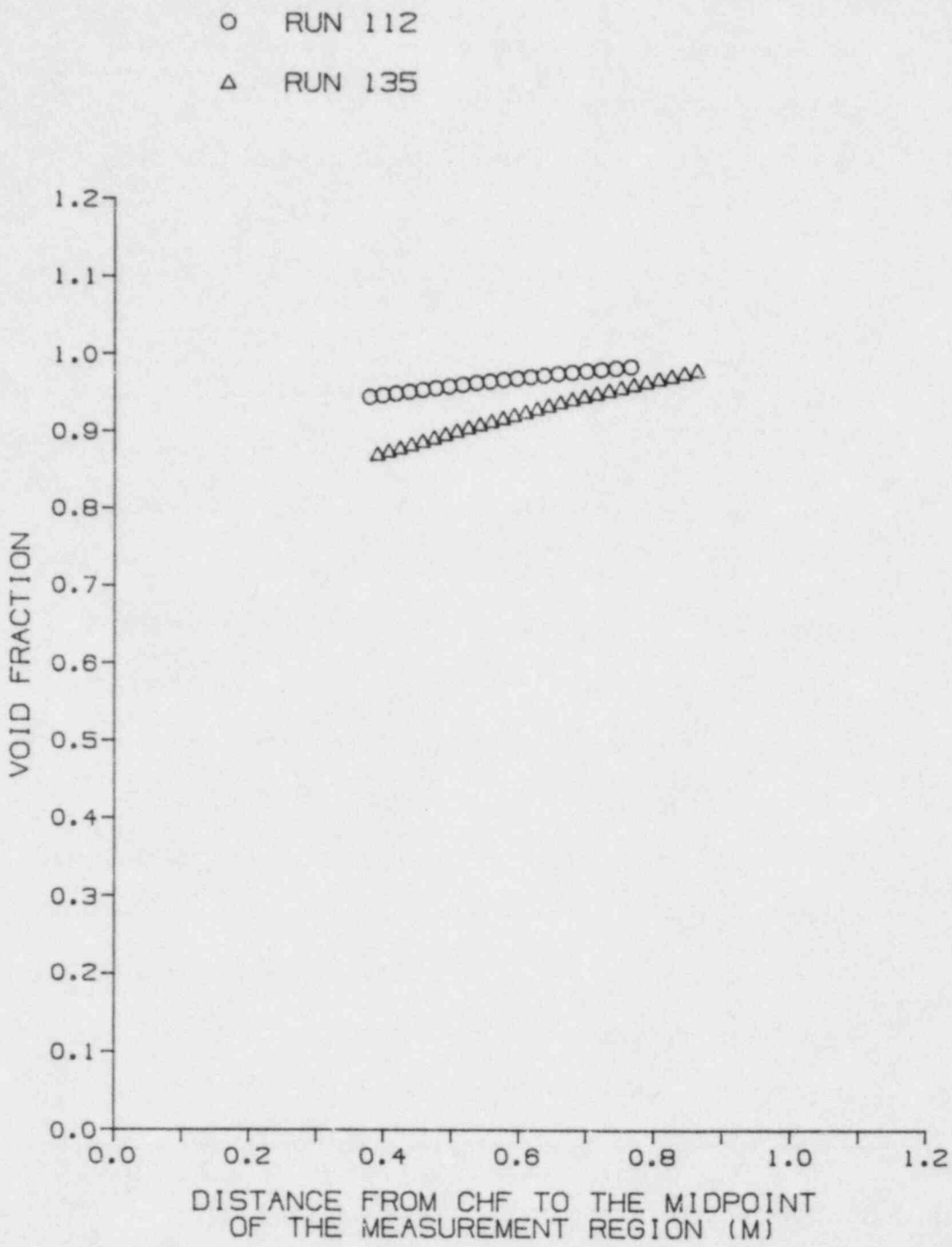

Figure 7-7. Void fraction vs. distance from CHF for two runs at similar inlet conditions

is hypothesized by the authors that this "transition" region corresponds to an engagement length where the liquid that sputters from the wall in the region of CHF becomes engaged with the higher velocity vapor. Secondly, the data in figure 7-6 strongly indicates that at greater distances downstream from the CHF location (dZ greater than 0.6 m for these tests) the rate of increase in vapor superheat with axial distance approaches the rate of increase calculated for the theoretical frozen quality limit. Though the absolute magnitude of the vapor superheat remains below the frozen quality limit, an equal rate of change (slope of the curve in figure 7-6) implies that the intensity of vaporization in this region becomes small, approaching zero. This is a somewhat unexpected finding. It had commonly been accepted that at greater axial distances where the absolute vapor superheat is high, the vapor to liquid heat transfer would be increased due to the greater driving force. These experimental results appear to indicate that in the established convective film boiling region, beyond the "transition region", the heat transfer between superheated vapor and entrained liquid drops is in fact relatively inefficient. These two observations have important implications for the phenomenological modeling of convective film boiling heat transfer and need to be confirmed by separate experiments.

Figure 7-8 shows similar transformed axial information results. These data are composites from four different runs at times selected to give approximately equal flow quality at the CHF point. This is in contrast to the data shown in figure 7-6 which correspond to results from single runs which had time varying flow qualities at the CHF point. The results plotted in figure 7-8 were obtained from a series of runs with varying inlet qualities which permitted us to obtain data at a moment during the quench history when the flow qualities at the CHF location were approximately equal. The results are seen to be similar to those displayed in figure 7-6, indicating that the significant findings regarding the nonequilibrium vaporization process as discussed above are pertinent to convective film boiling with fixed flow quality at the CHF locations, as well as to single film boiling cases with varying CHF qualities. Figures 7-9 and 7-10 further illustrate this finding by plotting the equilibrium and actual qualities for the eight data points presented in figure 7-8. The tendency towards an actual quality curve that is nearly constant at distances from the quench front greater than approximately 40 cm illustrates the lack of vapor generation far from the quench front. While this trend is demonstrated throughout all of the data obtained, only data points with the same CHF quality illustrate this phenomena as clearly as figures 7-9 and 7-10.

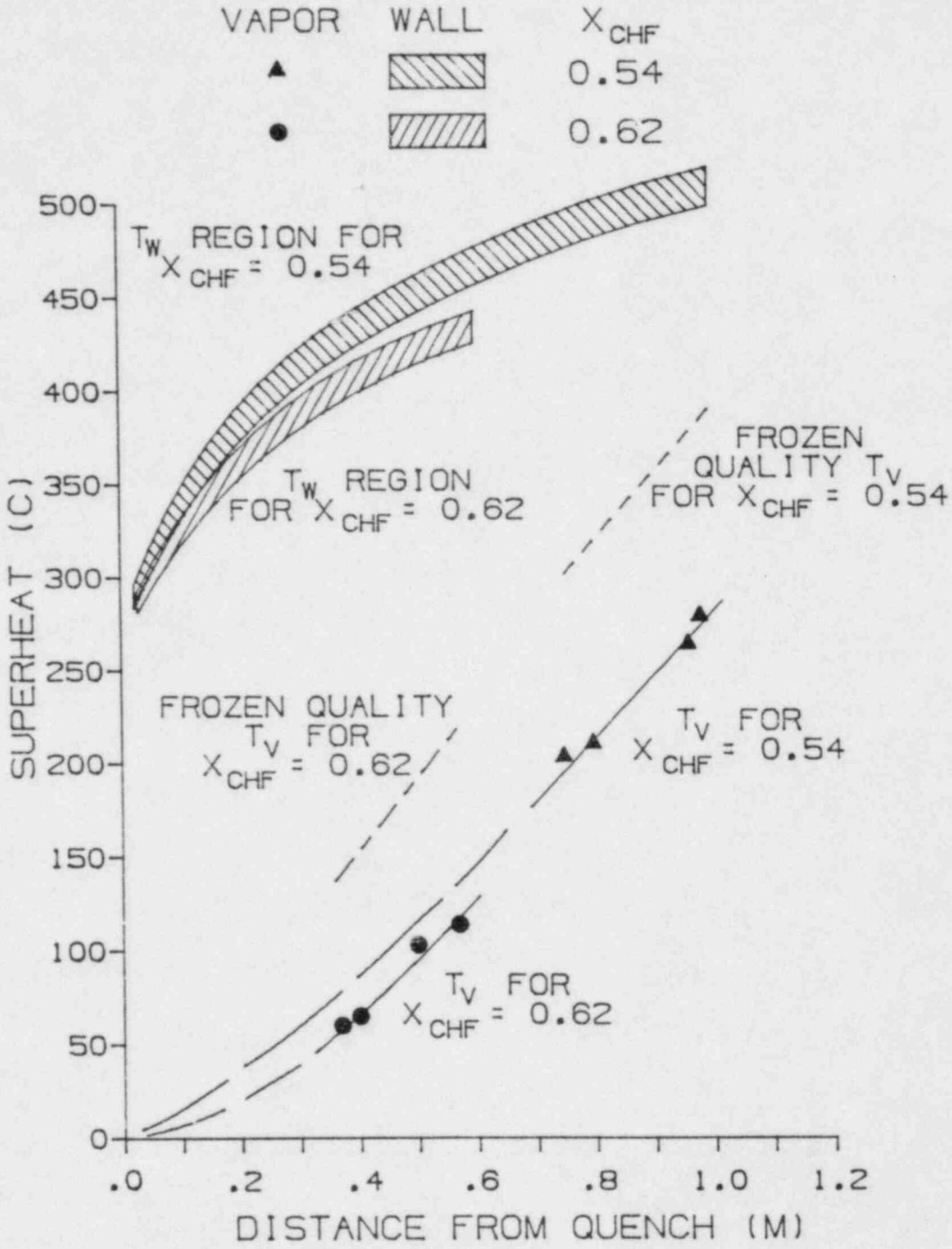

Figure 7-8. Temperature vs. distance for four different runs at the times when Xchf=0.54 and Xchf= 0.62

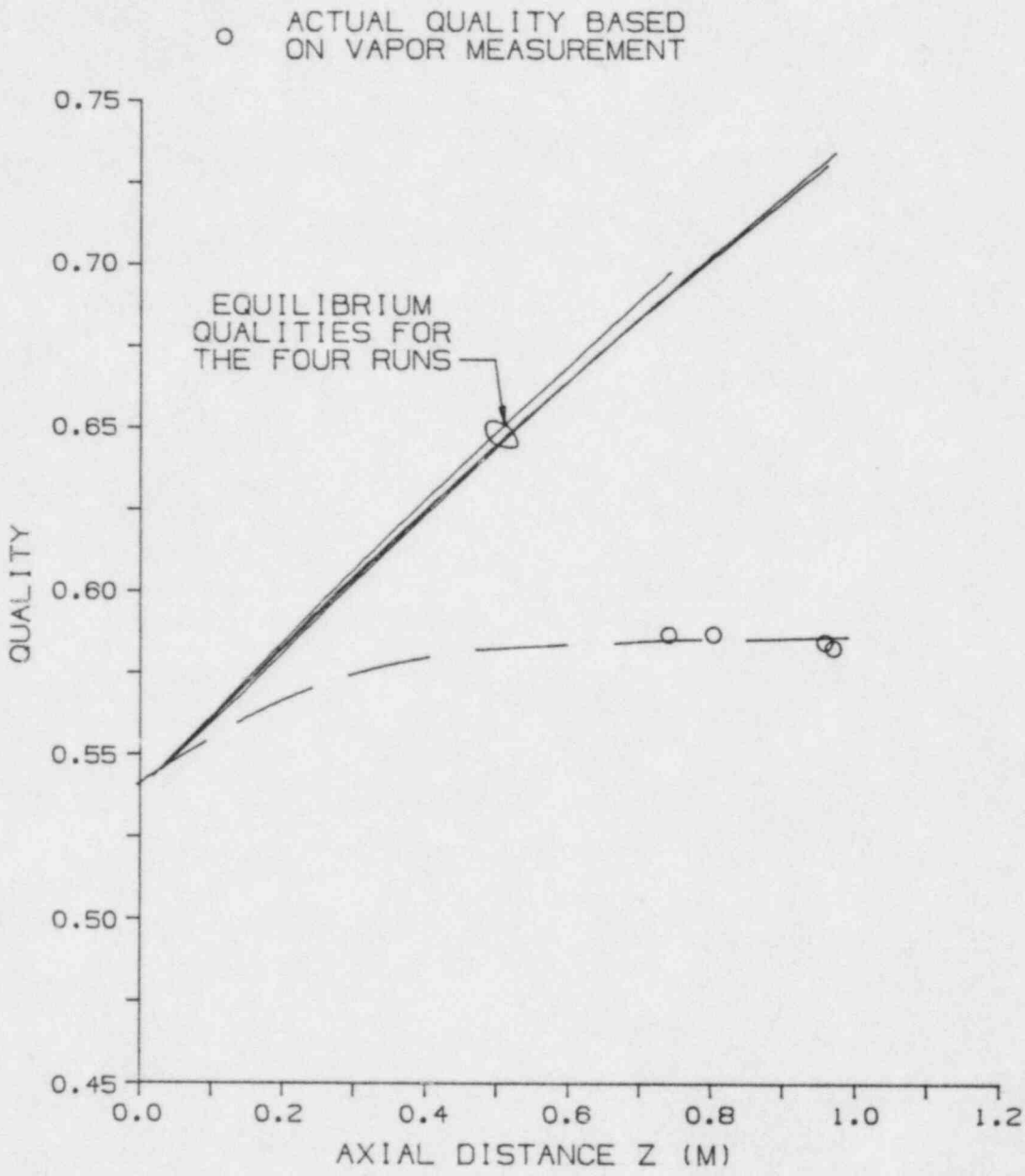

Figure 7-9. Equilibrium and actual qualities from four different runs at similar inlet conditions at the times when Xchf=0.54

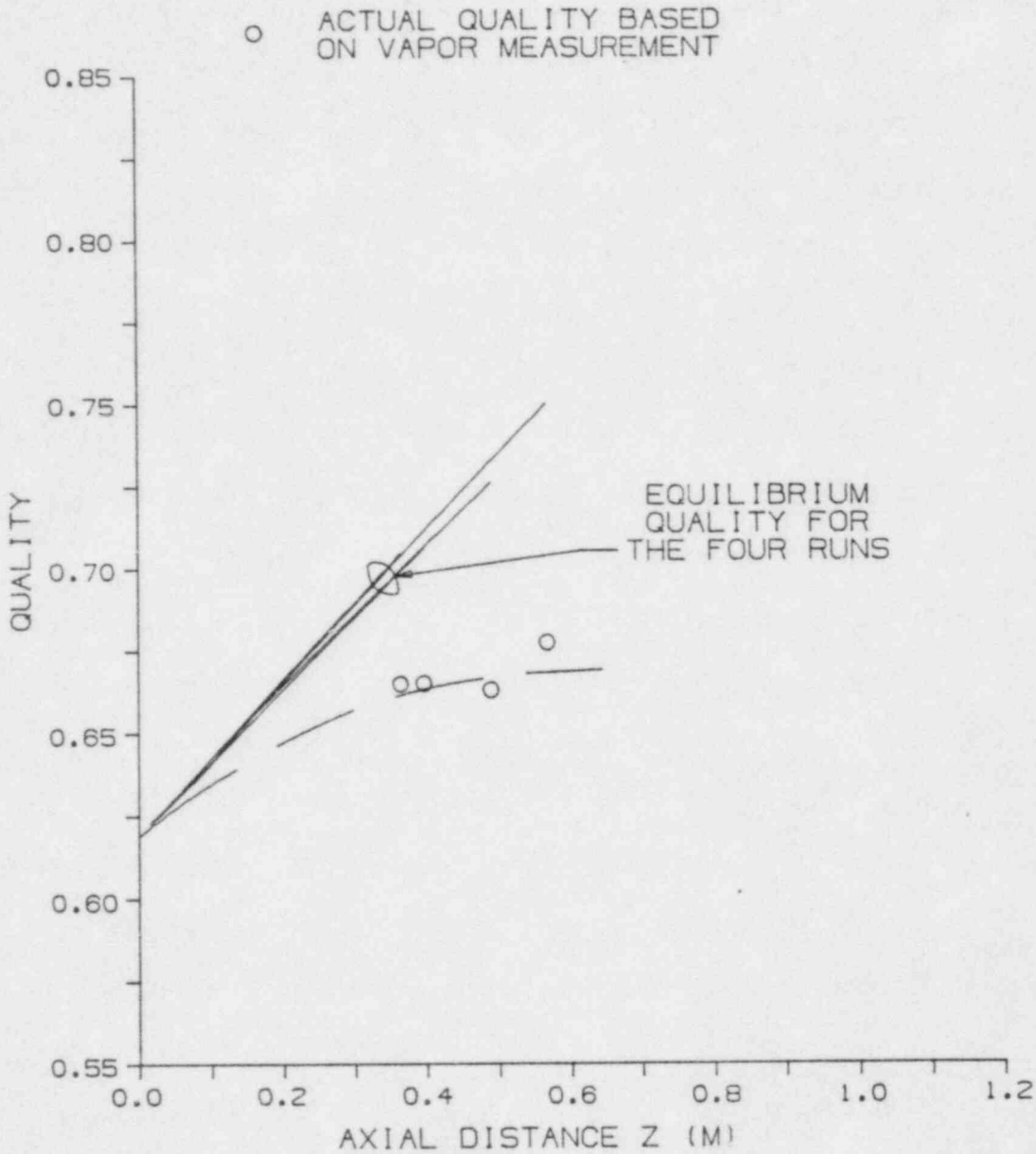

Figure 7-10. Equilibrium and actual qualities from four different runs at similar inlet conditions at the times when Xchf=0.62

An attempt was made to compare these experimental data with the few available measurements from previous studies. Because of the very limited data base, it was not possible to obtain a direct one-on-one comparison with matched parameters. Figure 7-11 shows a comparison of the data from two runs in this experiment with recently reported results from Idaho National Engineering Laboratory [7.1], at reasonably comparable conditions. The moving quench data of the present experiments (up to a dZ of 1.05 m) are compared to the fixed-quench front data from reference [7.1] for dZ of 1.35-1.95 m. Though the two separate tests did not overlap in the magnitude of the axial distance, extrapolation between the two sets of experimental data indicates very good agreement in both wall superheats and vapor superheats.

Figure 7-12 shows an attempt to compare the results with the data of reference [7.1], as well as the earlier published results of Nijhawan et al. [7.2]. It should be noted that due to the difficulty of matching all experimental parameters, the runs from various sources were only of approximate equivalency. Again, excellent agreement was obtained between the moving CHF measurements of the present study with the fixed CHF experiments from reference [7.1]. Nijhawan's data [7.2] bracketed these present results, as would be expected in view of the different range of flow qualities at the CHF point and the wall heat flux.

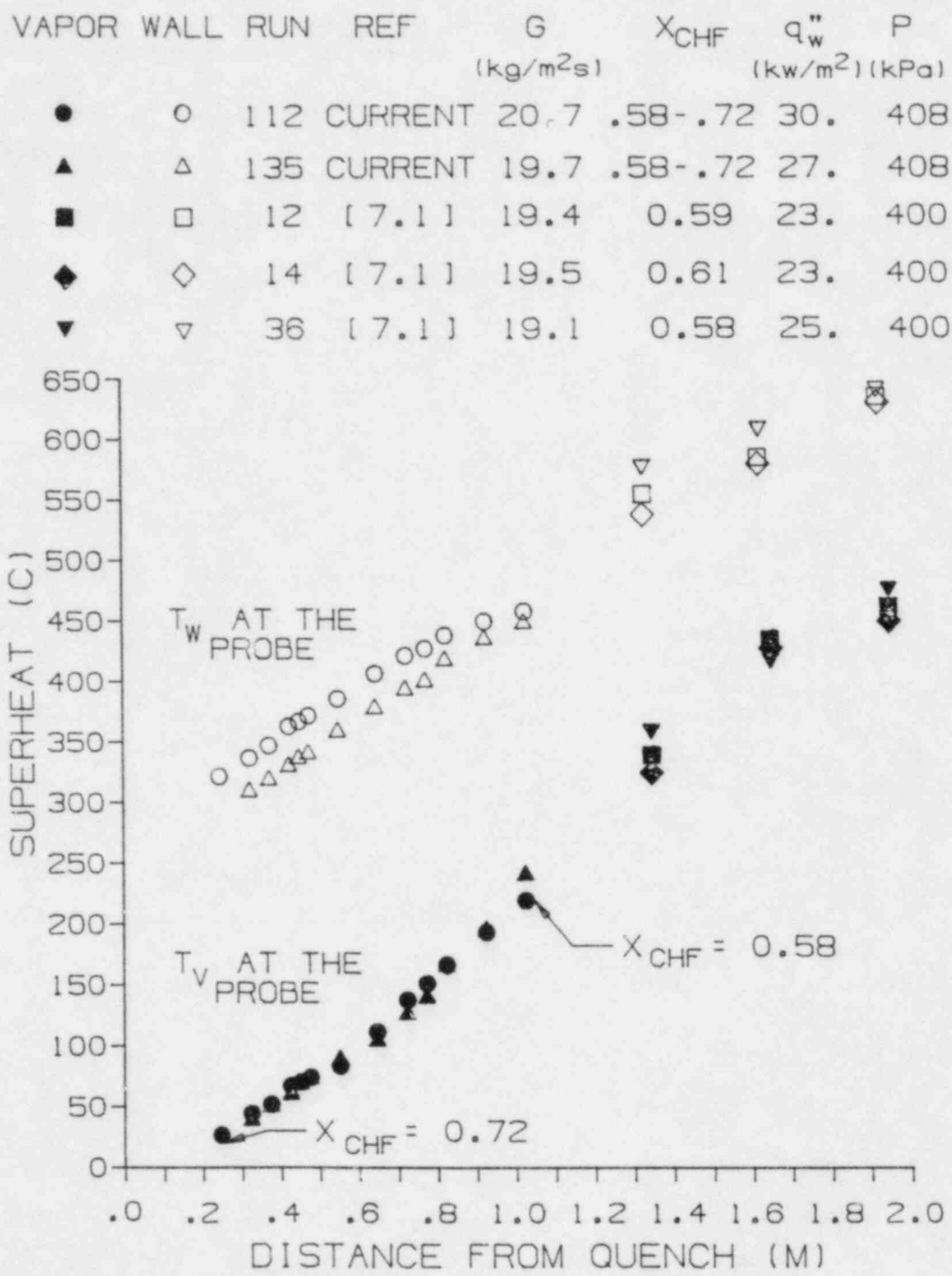

Figure 7-11. Temperatures at the vapor probe vs. distance between the quench front and the vapor probe for five comparable runs

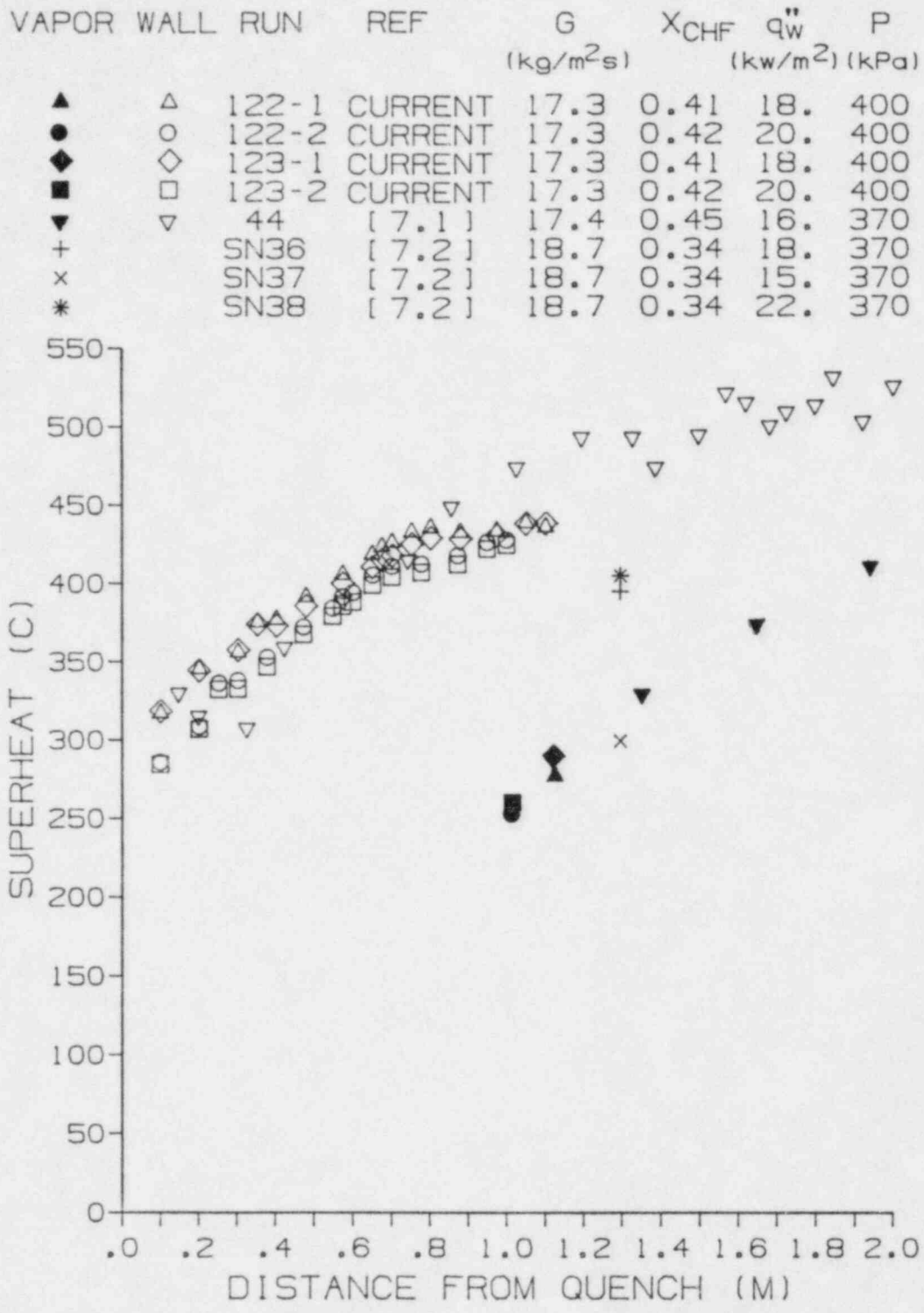

Figure 7-12. Wall temperature profile and vapor temperature downstream of the CHF location for six comparable runs

In general, the agreement between data from the present experiment with the limited published data (as shown in figures 7-11 and 7-12) indicate reasonable consistency and lends a degree of confidence to the experimental findings.

7.2 Suggestions for Future Research

The significant findings of this investigation suggest the need for future work in post-CHF, convective, dispersed flow film boiling. Improvements to the existing facility and a new test section would enable the acquisition of data over a wider range of inlet conditions. The concept of the "transition" region immediately downstream of the quench front needs to be verified by other experimental techniques. Improved void fraction measurements would shed considerable light on the magnitude of the localized decrease in void fraction. The void fractions indicated in this program imply slip ratios of 50 to 100 in the region immediately downstream of the quench front. With a vapor velocity on the order of 10 meters per second, the resulting average liquid velocity would be on the order of 10 cm per second. This has serious implications for the effects of spacers in nuclear reactor fuel bundles. In addition, the difference in effective heat transfer evident in the severely oscillatory runs suggests that the amplitude of the deviation from time averaged flow conditions may be a significant complication in modeling

the heat transfer in a nuclear reactor undergoing reflood after a loss of coolant accident.

Therefore it is recommended that experiments be performed to further quantify the axial variation of the void fraction in post-CHF flow, and examine in greater detail the nature of oscillating flow in post-CHF heat transfer. Improvements in the knowledge of void fraction would allow for significant refinements in the phenomenological models of the dispersed flow film boiling heat transfer process. Understanding the nature and consequences of oscillating post-CHF flow would assist in refining nuclear reactor heat transfer computer codes (TRAC, RELAP 5). Experiments designed to investigate the impact of flow obstructions on the post-CHF heat transfer process would also be valuable. This was one of the original goals of this investigation, but it became obvious during the program that a more complicated test section would be required. While experiments with flow obstructions would require a test section dedicated to that one task, knowledge of how a nuclear reactor fuel rod spacer interacts with post-CHF flow would be extremely valuable. Comparisons of the effect of spacers in the region close to the quench front where the localized void fraction is much lower than the homogeneous void fraction, and the far region where the vapor generation source function (Γ) is nearly zero could have

implications for nuclear reactor heat transfer codes. After encountering numerous experimental difficulties with probe induced wake effects and descending quench fronts, and with the discovery of a transition region immediately downstream of a quench front, it is felt that the spacer grid could provide significant enhancement of the heat transfer process at most flow qualities. Since fuel rod spacers are often spaced less than a half meter apart, it is probable that spacers would often reside within the "transition" region downstream of a quench front. The presence of the spacers in this region, characterized by its high slip ratios, might enhance liquid-wall contact and assist in further reduction of the void fraction in that region. At the same time, retention of liquid in this region would increase the local quality further downstream of the spacer, altering the heat transfer in that region. Superimpose on this an oscillating flow pattern and the possibilities are endless. Obviously there is a need for more work in this area.

SUMMARY

An experimental technique using slowly propagating CHF quench fronts was used to obtain measurements of nonequilibrium flow-film boiling conditions as a function of axial distance from the CHF location. Axial variation of wall superheats was consistent with previous findings indicating a rapid rise in the region close to the quench front, leveling off to a slower and fairly constant rate of rise further downstream. The new findings with respect to the vapor superheat indicated a "transition" region immediately downstream from CHF where the two-phase fluid remained close to the equilibrium thermodynamic state. It was hypothesized that the liquid requires a finite axial distance to engage the faster flowing vapor, and in this engagement region the volumetric presence of liquid is more significant than heretofore understood. This transition region is hypothesized to have relatively efficient vapor to liquid and wall to liquid heat transfer. At greater distances, the vapor superheat results indicate a relatively ineffective vapor to liquid heat transfer process. Thus, these experimental findings indicate a zone near the CHF front where the vaporization source intensity (Γ) is relatively high, followed by a far zone where the source intensity drops off to a relatively low magnitude (approaching zero). If these findings are confirmed by future experiments,

phenomenological modeling of the nonequilibrium heat transfer process in convective film boiling must account for these two regions of behavior.

NOMENCLATURE

A	flow area
C_L	liquid distribution parameters
C_p	specific heat
C_v	vapor distribution parameters
D	diameter
dp	pressure drop
f	friction factor
g	gravitational constant
G	mass flux
i	enthalpy
j_g^*	dimensionless vapor flux
j_g	volumetric vapor flux
P	pressure
P_H	heated perimeter
$\dot{q}$	internal heat generation
q''_{loss}	heat loss
q''_w	wall heat flux
T	temperature
t	time
V	velocity
X	quality
Z	axial distance

Greek

ρ	density
$\bar{\rho}$	two-phase homogeneous density

ε	surface roughness
α	void fraction
Γ	vapor source function
μ	viscosity

Subscripts

a	actual
acc	accelleration
b	boiler
CHF	critical heat flux
e	equilibrium
f	friction
fg	phase change
g	gravity
h	homogeneous
I	inconel
i	inner
ℓ	liquid
ls	saturated liquid
o	outer
s	saturation
t	total
v	vapor
w	wall

REFERENCES

Chapter 1

1.1 J.C. Chen, "Some Phenomenological Questions in Post-Critical-Heat Flux Heat Transfer," NATO Advanced Research Workshop on Two-Phase Flows and Heat Transfer, Spitzingsee, F.R. Germany, August-September, 1982.

1.2 D.C. Groeneveld, and J.C. Rousseau, "CHF and Post-CHF Heat Transfer: an Assessment of Prediction Methods and Recommendations for Reactor Safety Codes," NATO Advanced Research Workshop on Two-Phase Flows and Heat Transfer, Spitzingsee, F.R. Germany, August-September, 1982.

1.3 P. Saha, B.S. Shiralkar, and G.E. Dix, "A Post-Dryout Heat Transfer Model Based on Actual Vapor Generation Rate in Dispersed Droplet Regime," ASME Paper 77-HT-80.

1.4 S.W. Webb, J.C. Chen, and R.K. Sundaram, "Vapor Generation Rate in Nonequilibrium Convective Film Boiling," 7th International Heat Transfer Conference, Munich, 1982.

1.5 R.E. Mueller, "Film Boiling Heat Transfer Measurements in a Tubular Test Section," EURAEC-1971/GEAP-5423, 1967.

1.6 E.E. Polomik, "Transition Boiling Heat Transfer Program-Final Summary Report for Feb/63-Oct/67," GEAP-5563, 1967.

1.7 L.E. Hochreiter, "NRC/Westinghouse/EPRI FLECHT Low Flooding Rate Skew Axial Profile Results," presented at the 5th Water Reactor Safety Information Meeting, Washington, D.C., 1977.

1.8 M.J. Loftus, et al., "Non-Equilibrium Vapor Temperature Measurements in Rod Bundle and Steam Generator Two-Phase Flows," Proceedings OECD (NEA) CSNI Third Special Meeting on Trans. Two-Phase Flow, Pasedena, California, CSNI Report No. 61, 1981.

1.9 S. Nijhawan, J.C. Chen, R.K. Sundaram and E.J. London, "Measurements of Vapor Superheat in Post-Critical-Heat-Flux Boiling," Transactions ASME, Journal of Heat Transfer, Vol. 102, pp. 465-470, 1980.

1.10 S. Nijhawan, "Experimental Investigation of Thermal Non-Equilibrium in Post-Dryout Steam-Water Flow," Ph.D. Dissertation, Lehigh University, 1980.

1.11 R.C. Gottula, R.A. Nelson, J.C. Chen, S. Neti, and R.K. Sundaram, "Forced Convective Nonequilibrium Post-CHF Heat Transfer Experiments in a Vertical Tube," ASME-JSME Thermal Engineering Conference, Honolulu, March, 1983.

1.12 A. Annunziato, M. Cumo, and G. Palazzi, "Post Dry-Out Heat Transfer in Uncovered Core Accidents," ANS 2nd Nuclear Reactor Thermal-Hydraulics Conference, Santa Barbara, January, 1983.

Chapter 2

2.1 S. Nijhawan, J.C. Chen, R.K. Sundaram, and E.J. London, "Measurements of Vapor Superheat in Post-Critical-Heat-Flux Boiling," Transactions ASME, Journal of Heat Transfer, Vol. 102, pp. 465-470, 1980.

2.2 S. Nijhawan, "Experimental Investigation of Thermal Non-Equilibrium in Post-Dryout Steam-Water Flow," Ph.D. Dissertation, Lehigh University, 1980.

2.3 R.C. Gottula, R.A. Nelson, J.C. Chen, S. Neti, and R.K. Sundaram, "Forced Convective Nonequilibrium Post-CHF Heat Transfer Experiments in a Vertical Tube," ASME-JSME Thermal Engineering Conference, Honolulu, March, 1983.

2.4 E.M. Sparrow and R. Siegel, "Unsteady Turbulent Heat Transfer in Tubes," Transactions ASME, Journal of Heat Transfer, Vol. 82, pp. 170-180, 1960.

2.5 R. Siegel, "Heat Transfer for Laminar Flows in Ducts with Arbitrary Time Variations in Wall Temperature," Transactions ASME, Journal of Applied Mechanics, Vol. 27, pp. 241-249, 1960.

Chapter 3

3.1 S. Nijhawan, J.C. Chen, R.K. Sundaram, and E.J. London, "Measurements of Vapor Superheat in Post-Critical-Heat-Flux Boiling," Transactions ASME, Journal of Heat Transfer, Vol. 102, pp. 465-470, 1980.

3.2 D.C. Groeneveld and S.R.M. Gardiner, "A Method of Obtaining Flow Film Boiling Data for Subcooled Water," International Journal of Heat and Mass Transfer, Vol. 21, pp. 664-665, 1978.

3.3 M.K. Denham, D.F. Elliot and K.J. Shawyer, "Fundamental Studies of the Reflooding of an Inconel Tube in the Reflex Rig," United Kingdom Atomic Energy Authority Report Aeew-r 1353, 1980.

Chapter 6

6.1 D.R.H. Beattie and P.B. Whalley, "A Simple Two-Phase Frictional Pressure Drop Calculational Method," International Journal of Multiphase Flow, Vol. 8, pp. 83-87, 1982.

6.2 HTFS, Heat Transfer and Fluid Flow Service, AERE Harwell and NEL East Kibride, unpublished information, 1981.

6.3 C.J. Barcozy, "A Systematic Correlation for Two-Phase Pressure Drop," Chemical Engineering Prog. Symp., Ser. 62, pp. 232-249, 1966.

6.4 R.C. Martinelli, and D.B. Nelson, "Prediction of Pressure Drops During Forced Circulation Boiling of Water," Transactions of ASME, Vol. 70, pp. 695-702, 1948.

6.5 J.R.S. Thom, "Prediction of Pressure Drop During Forced Circulation of Water," International Journal of Heat and Mass Transfer, Vol. 7, pp. 709-724, 1964.

6.6 Y.Y. Hsu and R.W. Graham, Transport Processes in Boiling and Two-Phase Systems, Hemisphere Publishing Co., Washington, 1976.

6.7 G.B. Andeen, and P. Griffith, "Momentum Flux in Two-Phase Flow," Journal of Heat Transfer Trans. ASME, Vol. 90, pp. 211-222, 1968.

Chapter 7

7.1 R.C. Gottula, R.A. Nelson, J.C. Chen, S. Neti, and R.K. Sundaram, "Forced Convective Nonequilibrium Post-CHF Heat Transfer Experiments in a Vertical Tube," ASME-JSME Thermal Engineering Conference, Honolulu, March, 1983.

7.2 S. Nijhawan, "Experimental Investigation of Thermal Non-Equilibrium in Post-Dryout Steam-Water Flow," Ph.D. Dissertation, Lehigh University, 1980.

Appendix A

A.1 G.B. Wallis, One-Dimensional Two-Phase Flow, McGraw-Hill Book Co., New York, 1969.

Appendix B

B.1 S. Schaeffer, Masters Thesis to be Published, Lehigh University, 1984.

Appendix C

C.1 J.C. Chen, Technical Memorandum to the United States Nuclear Regulatory Commission, Lehigh University, 1982.

Appendix D

D.1 M.K. Denham, D.F. Elliot, and K.J. Shawyer, "Fundamental Studies of the Reflooding of an Inconel Tube in the Reflex Rig," United Kingdom Atomic Energy Authority Report Aeew-r 1353, 1980.

APPENDIX A: OBSERVATIONS FROM OSCILLATORY RUNS

All of the quantitative data reported in this report exhibited either a steady or slightly oscillatory flow pattern. In addition to these, about 25 percent of the experiments attempted during this investigation were observed to oscillate between two very different flow regimes. As noted in chapter 4, and illustrated by figure 4-5, these oscillatory runs all occurred at inlet flow qualities of less than 20 percent. During the rating process discussed in chapter 5, these oscillatory runs received a rating of 6 (16 for fixed-CHF experiments) if vapor probe measurements were obtained and a rating of 7 (or 17) if no vapor probe data were obtained. Data typical of these oscillatory experiments are illustrated in figures 5-13, 5-14, and 5-15. The operators noted during this run that the flow pattern visible in the sight glass at the boiler outlet alternated between single phase liquid flow and churn flow, even though the time averaged inlet quality was 4 percent. As indicated in figure 5-13, the wall temperatures oscillated 10 to 15 C during each 14 second cycle. For this run, with time average inlet conditions of G = 29.1 kg/m^2sec, Xin = 0.04, Pin = 245 pKa, and an electrical heat flux of 24 kw/m^2, the alternating storage and release of sensible heat by the test section resulted in the wall heat flux oscillating between 16 and 32 kw/m^2. The differential pressure recorded on the stripchart, as illustrated in

figure 5-15, appeared to indicate that one flow pattern may have been single phase vapor within the pressure drop measurement region. The extremely high vapor temperatures measured during this dry-out period occasionally approached to within 50 C of the highest test section wall temperature. None of the steady dispersed flow experiments in this investigation exhibited vapor temperatures this close to the wall temperature. Therefore the vapor probe and differential pressure measurements appear to indicate that during a portion of the oscillatory cycle, single phase vapor flow existed within the test section.

In addition to the time varying heat transfer characteristic of these runs, it should be noted that this run required 350 seconds to quench the entire test section, the same amount of time an experiment at the same mass flux, pressure, and average wall heat flux, but with a 53 percent inlet quality, took to quench the test section. Due to the oscillating runs' low quality, a quench region developed at the vapor probe and resulted in a descending quench front to assist the ascending quench front in quenching the test section. Therefore, for two runs with the same mass flux, the low quality oscillating run's ascending quench front was actually slower than the 53 percent run's ascending quench front.

Data are presented in figures A-1 and A-2 from an experiment at the same inlet conditions as the run illustrated in figures

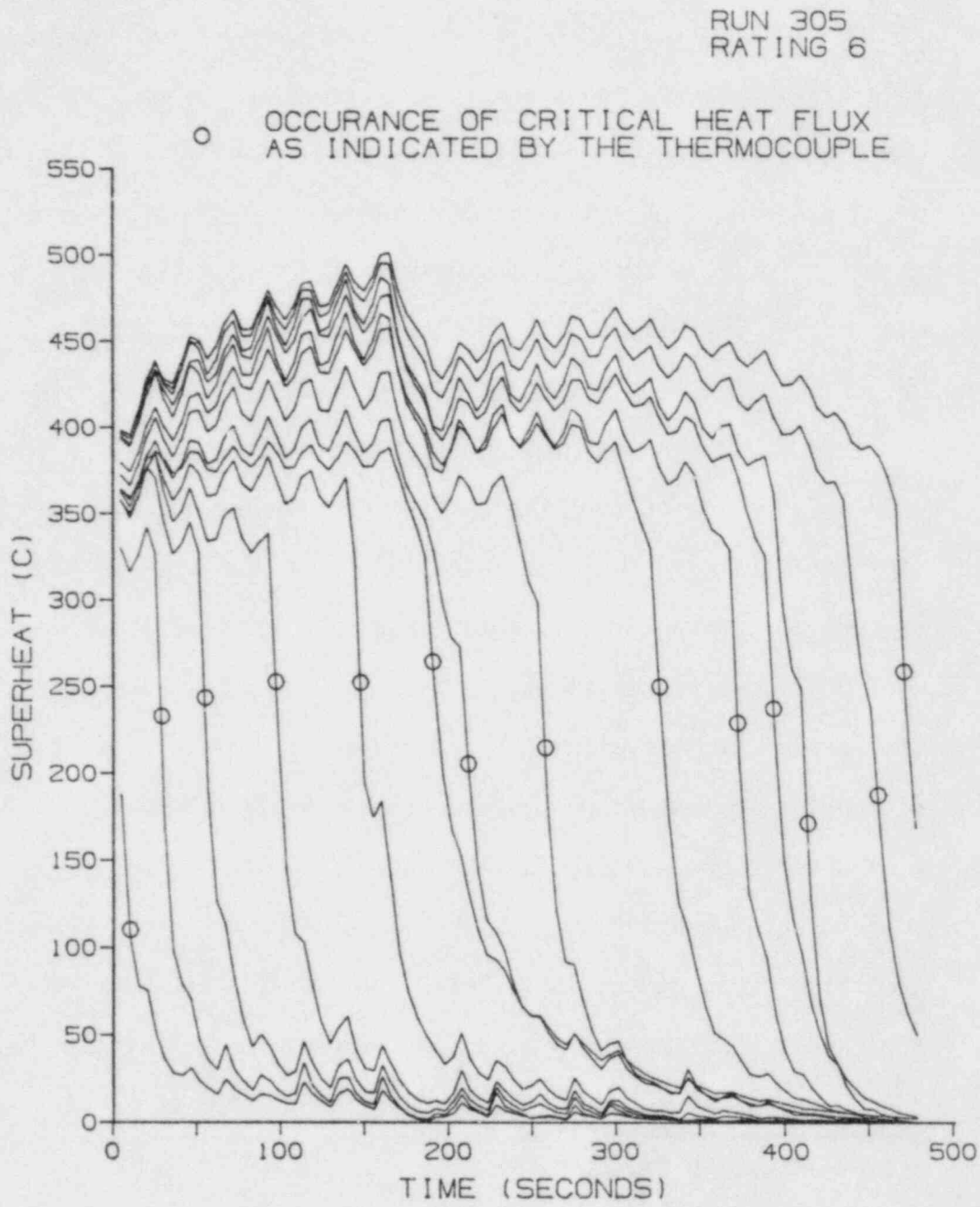

Figure A-1. Wall temperature vs. time for run 305

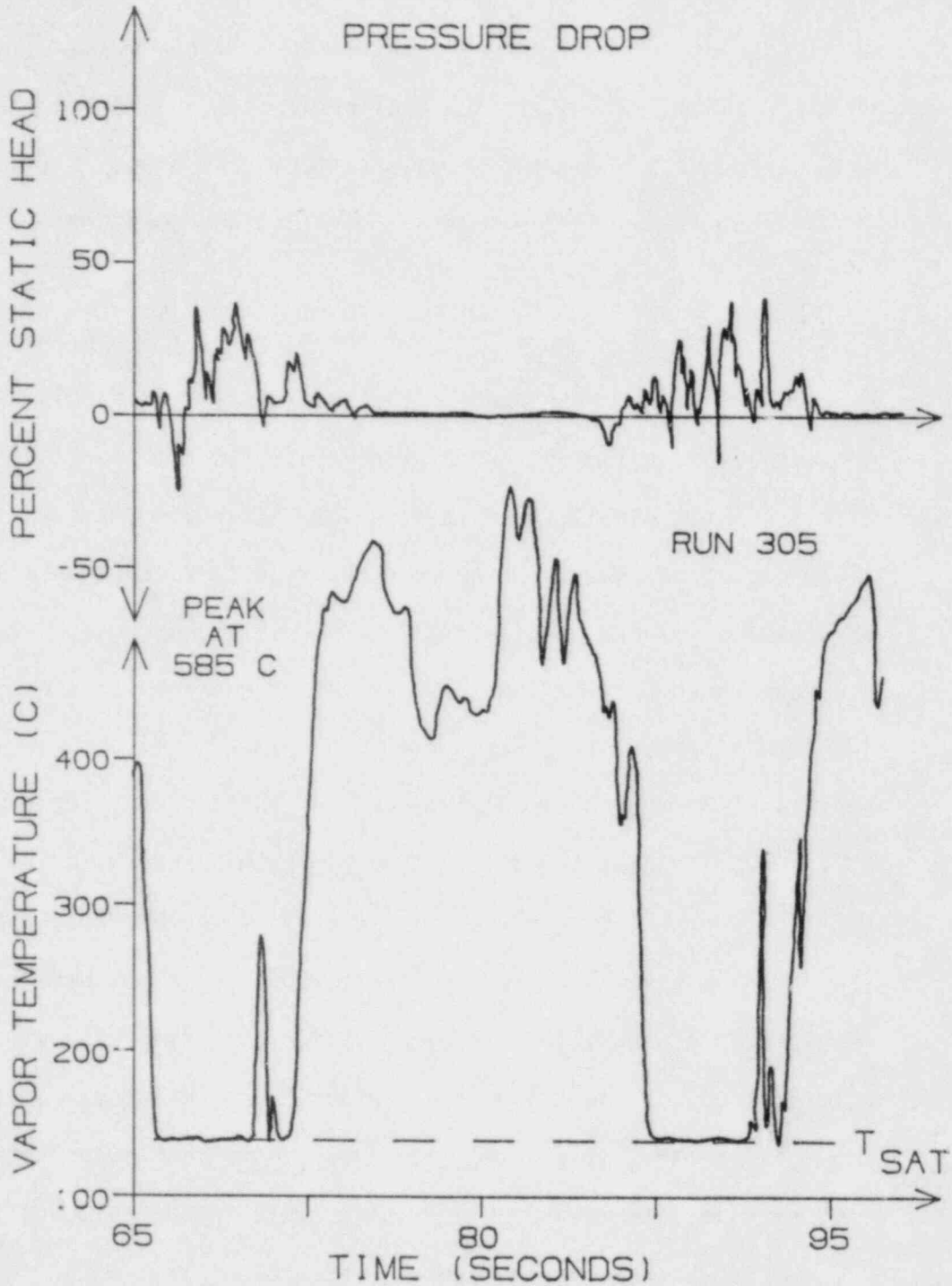

Figure A-2. Vapor probe and pressure drop stripchart for run 305

5-13, 5-14, and 5-15, but with an inlet pressure of 375 kPa. This run exhibits larger temperature oscillations over a period of 23 seconds. The larger oscillation in wall temperatures resulted in the wall heat flux oscillating between 15 and 40 kw/m^2. The steady decline in wall temperatures at approximately 170 seconds is due to the power supply shutting down when a wall temperature limit was exceeded.

These two runs are typical of the oscillatory experiments observed. Further quantitative observations are difficult to justify due to a lack of information about the time varying mass flux and inlet quality. In addition to the mode of oscillation discussed above, several runs were observed to exhibit a double oscillation. These runs alternated between steady churn flow and more rapid oscillations between bubbly and annular flow. The longer period was of the order of 1 minute, while the more rapid oscillations had a period of about 10 seconds. The cause of the oscillations is difficult to pin-point, and while it is possible that the two-phase loop assisted in the process, the low vapor velocities characteristic of these runs may have been unable to entrain all of the liquid all of the time. Ideally, cocurrent upward flow is desired during the experiment. This mode of operation allows the entrained liquid to flow out of the test section with the vapor. Problems with the operation of the loop could be expected if countercurrent flow existed, where liquid mass would tend to accumulate and the mass flow rate would oscillate.

To estimate the conditions in which cocurrent upward flow

would change to countercurrent flow, the flow reversal criteria given by Wallis [A.1] can be used. This criteria is:

$$j_g^* = 0.5$$

where

$$j_g^* = \frac{j_g \rho_g^{\frac{1}{2}}}{[gD(\rho_\ell - \rho_g)]^{\frac{1}{2}}}$$

and

$$j_g = \frac{Gx}{\rho_g}$$

Combining these equations gives the expression

$$Gx = 0.5\ [\rho_g gD(\rho_\ell - \rho_g)]^{\frac{1}{2}}$$

This flow reversal limit has been plotted in figure A-3 for the pressure range of 200 to 500 kPa. As is evident in figure A-3, most of the severely oscillatory runs were within, or close to, the flow reversal limit. Therefore it is not surprising that these runs oscillated, and that the source of the oscillation is not unique to post-CHF flow.

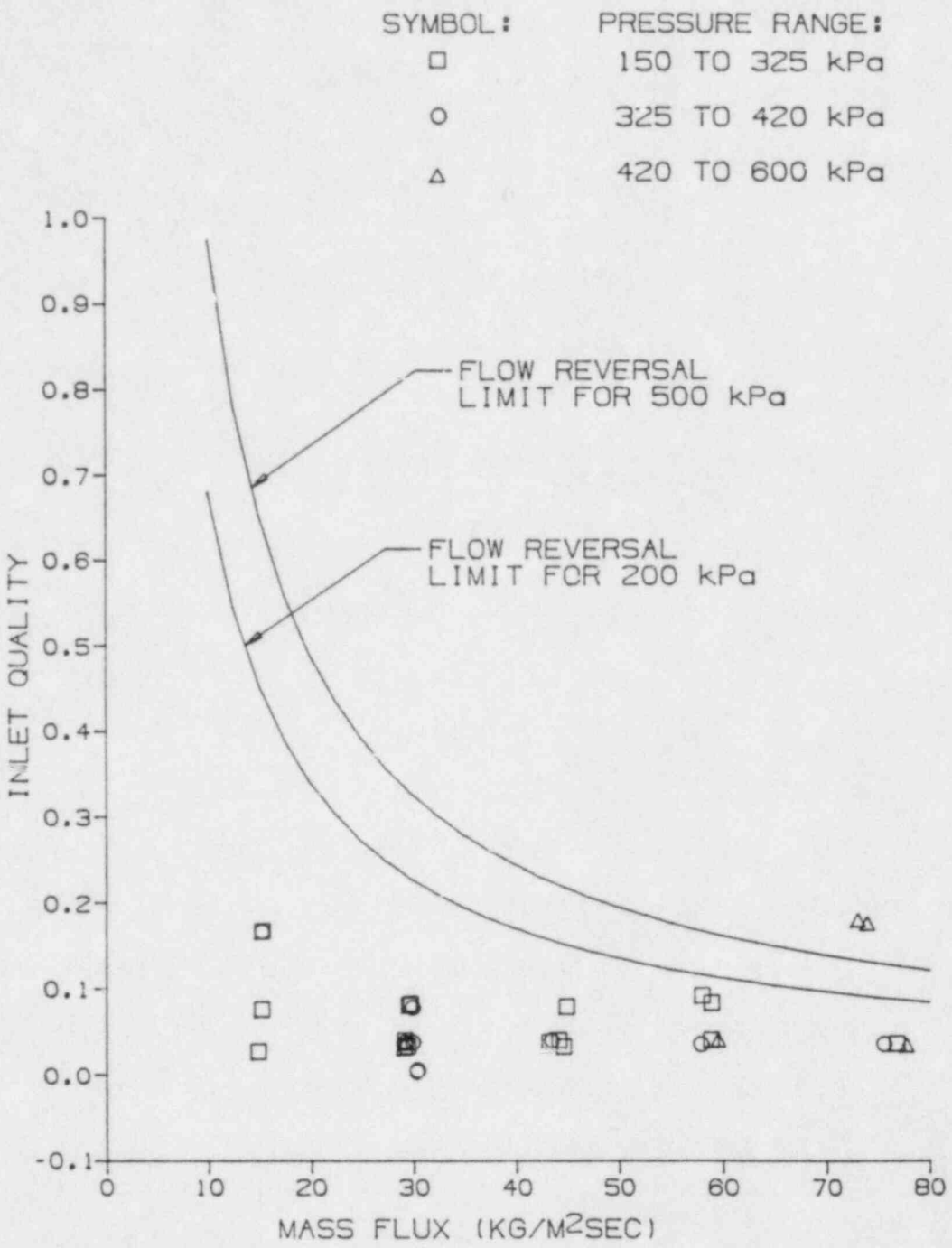

Figure A-3. Comparison of flow reversal limit with the mass flux and inlet quality of the severely oscillatory runs

APPENDIX B: DISCUSSION OF EXPERIMENTAL TECHNIQUE

The experimental program encountered difficulties with four different aspects of the experimental apparatus; (1) the design of the two-phase loop may have partially encouraged the oscillatory flows encountered at low qualities, (2) the hot patch technique was limited to a narrow range of operating conditions, (3) the vapor probe suffered from poor performance in the early phases of the program, and (4) the experiments often suffered from a top quench that limited the range of conditions where data were obtainable.

The primary cause of the severely oscillatory runs, discussed in Appendix A, was the low vapor velocity (at low flow qualities) being unable to entrain the liquid phase at a uniform rate. It is also possible that components of the two-phase loop may have contributed to the process. The primary purpose of the two-phase loop is to provide a steady flow with a uniform quality to the test section. An important feature of the loop is the single tube vertical upflow boiler. If the boiler wall temperatures are constant with time, then all of the electrical power input to the boiler is either lost to the surroundings, which occurs at a constant rate, or is input to the fluid. Since the fluid is near the saturation temperature when it enters the boiler, most of the energy is absorbed by

the fluid vaporization. As a result, if the inlet mass flow is constant, with a constant degree of sub-cooling, then the vapor generation rate inside the boiler is constant with time. Any variation in boiler exit quality would be the result of a change in liquid inventory within the boiler. Therefore the smaller the boiler volume, the less the flow quality will oscillate. In addition, the smaller the diameter, the greater the vapor velocity, and the more readily the liquid is entrained.

While the boiler used was of a small diameter, the hardware upstream of the boiler inlet was unable to supply a perfectly uniform inlet mass flux. Pressure oscillations at the boiler inlet resulted in mass flux oscillations between the preheater outlet and the boiler inlet. The severity of the oscillations could not be determined quantitatively, but operator observations suggest that while these flow oscillations did occur, they were not the primary cause of the oscillatory-flow-patterns observed in the sight glass. If the mass of subcooled liquid in the boiler began to vary, it is possible that the boiler wall temperatures and wall heat fluxes would oscillate, thereby varying the vapor generation rate in the boiler and the vapor mass flux at the boiler outlet. As is evident, the boiling process is very complicated. While correlations predict that all of the oscillatory runs encountered were within

the flow reversal limit, it is important that future experiments insure a constant mass flux at the boiler inlet, preferably with a positive displacement pump. Modifications to the preheater and flow control valve of the existing loop, with its centrifugal pump, would also result in more uniform flow.

The limited effectiveness of the hot patch in maintaining a fixed CHF-location was suspected to be the result of a bad braze joint between the Inconel tube of the test section and the hot patch copper block. Analysis of the heat transfer through thin layers of flux used in the brazing process predicted that typical critical heat fluxes would cause a temperature drop of several hundred degrees across 0.05 millimeters of flux. The thin sheet braze technique utilized in the braze joints is capable of leaving just such a film between the Inconel tube and copper hot patch if the braze does not flow adequately. Recent modifications to the existing test section by Schaeffer [B.1] confirmed that the braze joint was the problem. Future work with hot patches should utilize the braze casting technique of Schaeffer to insure proper operation of the hot patch.

Difficulties with vapor probe aspiration were resolved early in the experimental program. The separator concept was not recognized during previous experimental programs due to the use of extremely long and volumous tubes between the vapor

probes and the aspiration control valves. This large volume enabled vapor to condense in the tubes, thereby maintaining the volumetric flow necessary for proper probe operation. This also reduced the ability to adjust the vapor probes aspiration rate. Future vapor probes should use the separator concept to insure proper volumetric flow and provide for rapid response to adjustments of the aspiration flow control valves. In addition to the use of separators, the current program also features much smaller vapor probes. The small size makes fabrication more difficult, but comparisons with vapor probe traces from previous experiments indicates an improvement in performance. The extremely large volumetric flow of steam encountered when a plastic tube between the vapor probe and the control valve ruptured demonstrated that the small flow passages do not limit the aspiration rate.

The source of the vapor probe induced wake effect remains unknown. While data was obtained that graphically illustrates the wake effect, the range of conditions where it occurs is still not completely clear. Recent work showed that the probe was responsible in part, but that a bad braze joint in the top patch may also have been partly responsible [B.1]. Future experiments should attempt to resolve this probelm, which might also be due in part to the differential pressure measurement.

APPENDIX C: ESTIMATION OF MEASUREMENT UNCERTAINTIES

A. Measured Values

1. Mass Flux

Measurement error for the mass flux consists of two parts. Because of the poor orifice meter performance, mass flux was measured with a rotameter. Calibration error for the rotameter was +_1 percent of the indicated flow rate. Because of minor oscillations in the mass flow rate at the rotameter, an observational error of 0.4 kg/m^2sec must also be included. Therefore the total mass flux uncertainty was +_(0.4 kg/m^2sec + 0.01xG).

2. Boiler Inlet Temperature

The boiler inlet temperature was measured with a type J fluid thermocouple. An atmospheric boiling experiment demonstrated thermocouple accuracy within 0.3 degrees C. Estimated uncertainty for the data acquisition system was 0.2 C. Therefore, total uncertainty for boiler inlet was 0.5 C.

3. Test Section Pressure

The combination of calibration error for the pressure transducers and data acquisition system uncertainties resulted in a 3 kPa uncertainty for the inlet pressure.

4. Test Section Power

Test section voltage was measured directly by the precision voltmeter in the Ramp data acquisition system with an uncertainty

of 0.1 percent. The test section current was determined by measuring the voltage across a precision resistance located within the test section DC power supply. Total measurement error for the current was 0.5 percent, resulting in a test section power uncertainty of 0.6 percent.

5. Test Section Axial Position (Z)

Uncertainty of vapor probe position was approximately 0.3 cm due to thermal expansion of the test section. Uncertainty of wall thermocouple position was the sum of the expansion error, 0.3 cm, and an initial position error of 0.3 cm, for a total uncertainty of 0.6 cm.

6. Wall Temperature

Measurement error due to the data acquisition system was $\pm$1 C. Errors due to the thermal contact resistance between the thermocouple and the test section wall is approximately $\pm$2 C. Therefore total wall temperature measurement uncertainty is $\pm$3 C.

7. Vapor Temperature

The vapor temperature uncertainty includes two components:

a) Errors due to hardware inaccuracies, including stripchart uncertainties, of the order of $\pm$5 C.

b) Vapor probe interpretation error. This is dependent on the quality of the vapor probe response. As discussed in chapter 4,

the ratings of 1 to 5 specify vapor probe interpretation errors ranging from +_5 C to +_25 C. Therefore the total measurement and interpretation error for the vapor temperature ranges from +_10 C for class 1 runs to +_30 C for class 5 runs.

B. Calculated Values

8. Saturation Temperature

The saturation temperature is determined from the measured inlet pressure. Therefore the saturation temperature uncertainty was +_0.4 C for a +_3 kPa inlet pressure uncertainty.

9. Specific Enthalpy of Vaporization: i_{fg}

Based on measured inlet pressure i_{fg} uncertainty was therefore +_0.3 kj/kg.

10. Specific Heat of Liquid: $C_{p\ell}$

Based on measured inlet pressure $C_{p\ell}$ uncertainty was therefore +_0.0007 kj/kg.

11. Boiler Heat Losses

Boiler heat losses were typically 150 W. Estimated uncertainty for the boiler heat losses is +_10 W.

12. Boiler Power

Calibration experiments were run at a variety of power levels and power distributions for the AC power supply to determine

the boiler resistance. The experiments demonstrated uncertainties ranging from one percent at power levels under 3 kW to one-half percent at power levels greater than 5 kW.

13. Inlet Flow Quality

The following derivation of inlet quality uncertainty was derived by Chen [C-1] in a technical memorandum to the Nuclear Regulatory Commission:

$$X = \frac{\frac{1}{GA}(\dot{q}_b - q_{loss}) - C_{p\ell}(T_S - T_{IN})}{i_{fg}}$$

$$\delta X = \delta_{GA} \times \frac{\partial X}{\partial GA} + \delta\dot{q}_b \times \frac{\partial X}{\partial \dot{q}_b} + \partial q_{loss} \times \frac{\partial X}{\partial q_{loss}}$$

$$+ \delta T_s \times \frac{\partial X}{\partial T_s} + \delta T_{IN} \times \frac{\partial X}{\partial T_{IN}} + \delta C_{p\ell} \times \frac{\partial X}{\partial C_{p\ell}} + \delta i_{fg}\partial$$

$$= \delta_{GA} \times \frac{\dot{q}_b - q_{loss}}{i_{fg}(GA)^2} + \delta\dot{q}_b \times \frac{1}{i_{fg}GA} + \delta q_{loss} \times \frac{1}{i_{fg}GA}$$

$$+ \delta T_s \times \frac{C_{p\ell}}{i_{fg}} + \delta T_{IN} \times \frac{C_{p\ell}}{i_{fg}} + \partial C_{p\ell} \times \frac{(T_s - T_{IN})}{i_{fg}}$$

$$+ \delta i_{fg} \times \frac{\frac{1}{GA}(\dot{q}_b - q_{loss}) - C_{p\ell}(T_s - T_{IN})}{i_{fg}^2}$$

Sample cases at the four extreme cases are presented below.

Table C-1

Sample case	low G low X	high G low X	low G high X	high G high X
Parameter:				
X	0.04	0.04	0.70	0.40
G (kg/m^2sec)	14	70	14	70
δ_G	0.5	1.0	0.5	1.0
q_b(kw)	0.5	2.4	3.9	11.3
δ_{qb}(w)	5	25	40	55
Uncertainty:				
$\frac{\dot{q}_b - q_{loss}}{i_{fg}(GA)^2} \times \delta_{GA}$	0.0024	0.0016	0.028	0.0064
$\frac{1}{i_{fg}GA} \times \delta\dot{q}_b$	0.00095	0.0095	0.008	0.021
$\frac{1}{i_{fg}GA} \times \delta q_{loss}$	0.0019	0.0004	0.002	0.0004
$\frac{C_{P\ell}}{i_{fg}} \times \delta T_{IN}$	0.0011	0.001	0.001	0.001
TOTAL OF ALL OTHER TERMS	0.001	0.001	0.001	0.001
Total δX	0.008	0.013	0.04	0.03

14. CHF Location

The uncertainty for the CHF location is a combination of uncertainty for the thermocouple position and uncertainty for the exact location of the center of the "quench front". Total uncertainty is estimated to be 1 cm.

15. Test Section Wall Heat Flux

Total wall heat flux uncertainty was the sum of the electrical heat flux error (0.6%) and the heat loss uncertainty. Heat losses typically represented less than 10% of the total power input to the test section. Due to the time varying wall temperatures of a moving quench front experiment, the time varying heat losses are difficult to quantify exactly. As discussed in chapter 3, the heat loss error is estimated to be 25% worse case. Therefore the heat flux error due to heat loss errors was estimated to be 2.5%. Total wall heat flux uncertainty was estimated at 3 percent.

16. Change in Quality with Axial Distance

The change in equilibrium quality with axial distance is:

$$dX_e = \frac{q''_w \pi D_i dZ}{GA\, i_{fg}}$$

The uncertainty is:

$$\delta_{dX_e} = \delta q_w'' \times \frac{\pi D_i dZ}{GAi_{fg}} + \delta_{dZ} \times \frac{q_w'' \pi D_i}{GA\, i_{fg}}$$

$$+ \delta_{GA} \times \frac{q_w'' \pi D_i dZ}{(GA)^2 i_{fg}} + \delta i_{fg} \frac{q_w'' \pi D_i}{GA(i_{fg})^2}$$

· Typical Values:

$q_w'' = 3.0$ kw/m^2	$\delta q_w'' = 0.1$ kw/m^2
$dZ = 10$ cm	$\delta d_Z = 1.0$ cm
$G = 30$ kg/m^{2}sec	$\delta_G = 0.7$ kg/m^{2}sec
$i_{fg} = 2008$ kJ/kg	$\delta i_{fg} = 0.3$ kJ/kg

Typical uncertainty would be 0.0002 for a dX_e of 0.0013. Note that 0.00013 of the uncertainty is from the dZ uncertainty, which is not cumulative along the test section.

17. CHF Quality

The CHF quality uncertainty is the sum of the inlet quality error and the accumulated error from the change in equilibrium quality between the inlet and the quench front. Both errors were discussed previously, and can vary widely depending on the inlet conditions. The typical uncertainty range is from 0.01 to 0.04.

18. Equilibrium Quality at the Probe

Uncertainty of the equilibrium quality at the vapor probe is the sum of the inlet quality error and the accumulated error

from the change in equilibrium quality between the inlet and the vapor probe. Both errors were discussed previously, and can vary widely depending on the inlet conditions. The typical uncertainty range is from 0.01 to 0.04.

19. Actual Quality at the Probe

The actual quality suffers from the same uncertainty as the equilibrium quality, plus an uncertainty due to the vapor measurement. Depending on mass flowrate, the uncertainty resulting from vapor probe interpretation error may be as large as 0.02 for class 5 runs, resulting in an overall actual quality uncertainty ranging from 0.01 to 0.05.

20. Average Void Fraction

The average void fraction measured in the 50 cm region upstream of the vapor probe was subject to both experimental error in the differential pressure measurement, and in flow quality modeling errors as discussed in chapter 6. Total measurement uncertainty for all tabulated values reported as "average void fraction =" was estimated to be 0.03. Measurements that were based on small quantities of data suffered from a greater degree of uncertainty, and were tabulated as "average void fraction >". For these measurements the tabulated values were lowered to include the uncertainties, so that they represented a minimum void fraction measurement.

APPENDIX D: SAMPLE TABULATION

All 579 data points obtained from the 118 runs that produced data have been tabula ed in volume two of this report. Included here is a tabulation of the 15 data points obtained from run 100, of which sample plots were presented in chapter 5. The wall temperature, vapor temperature, and axial distance measurements were discussed in chapter 3. The mass flowrate, inlet quality, and test section pressure were easily determined during the preliminary data reduction phase.

Unlike the steady-state fixed CHF experiments, calculation of the wall heat flux for moving quench front experiments is a difficult task. The local wall heat flux is the sum of three components, electrical power input to the tubing, sensible heat stored or released by the tubing, and the time varying heat losses to the test section insulation:

$$q''_w = \frac{1}{P_H dZ} \left(\dot{q} - q''_{loss} - C_{p\rho} \frac{\pi}{4} (D_o^2 - D_i^2) dZ \frac{dT}{dt} \right) \qquad \text{(D-1)}$$

While power input and sensible heat are easy to calculate, the time varying heat losses must be estimated. As discussed in chapter 3, the results of an experiment conducted to quantify the effect permits the variation of heat loss with time to be approximated, but heat loss uncertainty still approaches 25

percent in some instances. The results of the wall heat flux calculation are illustrated in figure D-1, which plots the wall heat flux at two adjacent thermocouple locations versus time. The spikes represent the momentary increase in heat flux as the quench front passes the thermocouple.

For the data points obtained in this investigation, the axial variation of post-CHF wall heat flux was based primarily on the wall heat flux calculated at each of the thermocouples at the time reported. Unfortunately, the short length of tubing undergoing a quench at any instant in the experiment was often less than the thermocouple spacing. Figure D-1 illustrates the problem. When one of the thermocouples was undergoing the local quench, the other thermocouple had either been quenched previously, or was still in the post-CHF region. As a result, the axial variation in wall heat flux at the quench front could not be accurately described. Since each data point reported corresponded to the instant when a wall thermocouple was quenching, the thermocouples upstream and downstream of the CHF location were not typically in the quench region. Therefore, the wall heat flux data must be used carefully, since the wall heat flux at the quench front was based on the rate of temperature decrease observed at the thermocouple and does not represent the average wall heat flux between adjacent thermocouples. As

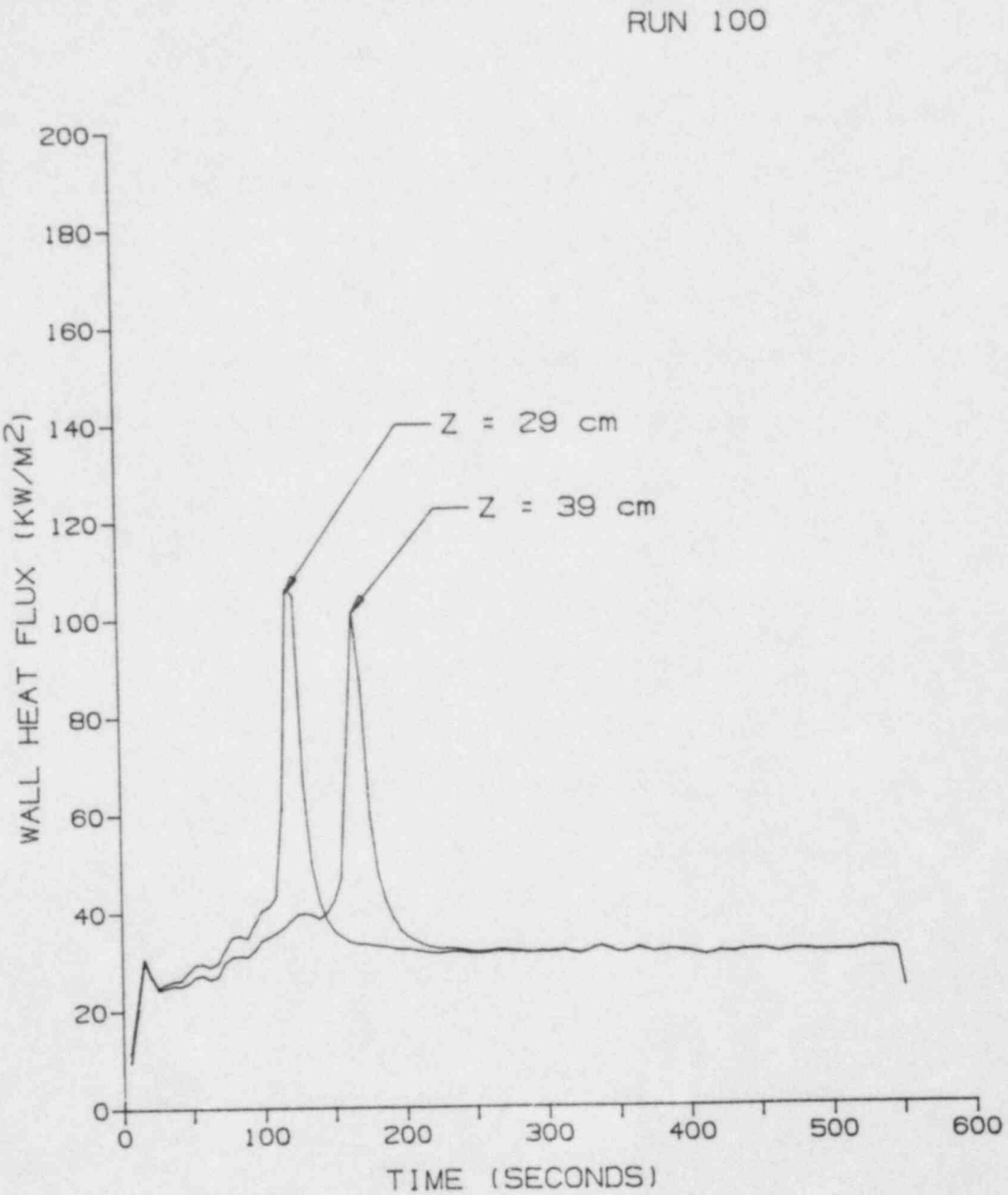

Figure D-1. Wall heat flux vs. time at two adjacent wall thermocouples for run 100

shown in figure D-2, the wall heat flux reported at the CHF location is only a peak value. The average wall heat flux in the quench region was calculated by performing an energy balance for the sensible heat of the test section tubing. By calculating the sensible heat released per unit length of test section during the quench process, and dividing it by the quench front velocity, the enthalpy input to the flow by the quench front can be accurately calculated.

The possibility of axial conduction in the tube wall was also investigated. As demonstrated in reference [D.1], the axial conduction term was negligible everywhere except directly at the quench front, where it had a minor effect. Since the heat addition to the flow at the quench front is based on an energy balance calculation, axial conduction corrections would not alter the net heat addition in the quench front region.

Determination of the average wall heat flux permits the flow equilibrium quality to be calculated as a function of axial distance. This is a simple energy balance calculation utilizing the technique outlined above for wall heat flux in the quench front region. Therefore the reader is cautioned not be use the wall heat flux reported at the CHF location as an average value. To properly arrive at the net heat addition to the fluid between the thermocouple upstream of the quench front,

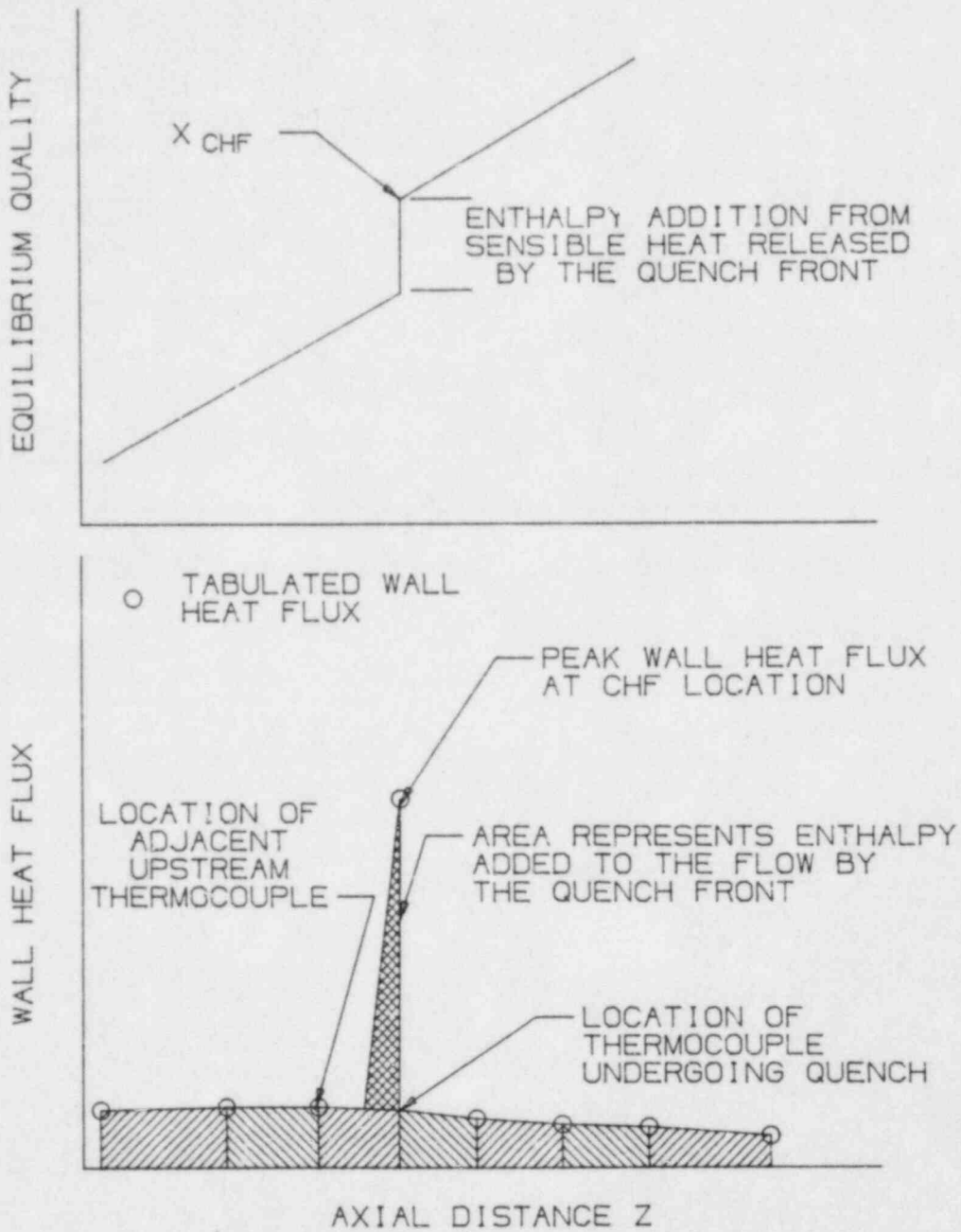

Figure D-2. Wall heat flux and flow equilibrium quality vs. axial distance for a typical data point

and the thermocouple at the quench front, the DXE (change in equilibrium quality) value should be used. The DXE value is the change in flow equilibrium quality between the previous thermocouple and the thermocouple corresponding to the tabulated DXE value. In addition, it should be noted that the energy input to the flow by the quench front has been included in calculating the "dryout" equilibrium quality (XCHF), since the dryout quality is defined as the flow equilibrium quality at the location where liquid-wall contact no longer occurs.

The tabulation of the 15 data points obtained from run 100 utilize similar nomenclature, except that subscripts are not available on the computer printout. Table D-1 presents the nomenclature cross reference necessary to properly interpret the tabulation.

Table D-1

Tabulation	Proper Nomenclature
XCHF	X_{CHF}
TW	T_w
TV	T_v
XA	X_a
XE	X_e
QW	q''_w
DXE	dX_e

The sample tabulation follows;

SERIAL NO: 100 RATING: 1

INLET PRESSURE = 378. kPa

INLET MASS FLUX = 14.8 kg/m2sec

INLET QUALITY = 0.62

SATURATION TEMPERATURE = 141.6 C

POINT: 1

AT TIME: 50.2 secs

AT Z= 10.0 cm XCHF= 0.64

AT Z= 131.3 cm TV= 428.C
XA= 0.69
XE= 0.89

FROM Z= 81.3 to Z= 131.3
AVERAGE VOID FRACTION= 0.99

Z (cm)	TW (C)	QW (w/cm2)	XE	DXE (%)
0.0	144.	0.00	0.62	
7.5	144.	0.00	0.62	-0.1
10.0	259.	9.59	0.64	1.6
18.3	456.	3.38	0.66	2.2
28.5	497.	2.93	0.68	2.6
38.6	512.	2.66	0.71	2.3
48.8	522.	2.51	0.73	2.2
53.9	525.	2.53	0.74	1.1
58.9	532.	2.53	0.75	1.0
66.6	550.	2.50	0.76	1.6
76.1	561.	2.43	0.78	1.9
83.7	573.	2.46	0.80	1.5
86.2	571.	2.39	0.80	0.5
88.8	577.	2.40	0.81	0.5
93.9	578.	2.31	0.82	1.0
98.9	577.	2.28	0.83	0.9
106.6	574.	2.19	0.84	1.4
116.1	572.	2.16	0.86	1.7
123.7	583.	2.04	0.87	1.3
128.8	591.	2.01	0.88	0.8
133.5	547.	2.16	0.89	0.8
138.3	571.	2.26	0.90	0.9
142.3	580.	2.16	0.91	0.7

POINT: 2

AT TIME: 81.4 secs

AT Z= 18.3 cm XCHF= 0.68

AT Z= 131.3 cm TV= 441.C
XA= 0.73
XE= 0.94

FROM Z= 81.3 to Z= 131.3
AVERAGE VOID FRACTION= 0.99

Z (cm)	TW (C)	QW (w/cm2)	XE	DXE (%)
0.0	144.	0.00	0.62	
7.5	144.	0.00	0.62	-0.1
10.0	161.	3.32	0.63	0.3
18.3	350.	15.13	0.68	4.9
28.5	493.	3.53	0.70	2.7
38.6	519.	3.12	0.73	2.8
48.8	537.	2.99	0.75	2.5
53.9	541.	2.83	0.77	1.2
58.9	548.	2.91	0.78	1.2
66.6	566.	2.89	0.80	1.8
76.1	579.	2.82	0.82	2.2
83.7	588.	2.90	0.84	1.8
86.2	590.	2.81	0.84	0.6
88.8	596.	2.83	0.85	0.6
93.9	600.	2.76	0.86	1.2
98.9	602.	2.62	0.87	1.1
106.6	603.	2.53	0.89	1.6
116.1	604.	2.46	0.91	1.9
123.7	618.	2.43	0.92	1.5
128.8	626.	2.42	0.93	1.0
133.5	579.	2.52	0.94	1.0
138.3	600.	2.57	0.95	1.0
142.3	610.	2.55	0.96	0.8

SERIAL NO: 100 RATING: 1

INLET PRESSURE = 378. kPa

INLET MASS FLUX = 14.8 kg/m2sec

INLET QUALITY = 0.62

SATURATION TEMPERATURE = 141.6 C

POINT: 3

AT TIME: 122.2 secs

AT Z= 28.5 cm XCHF= 0.70

AT Z= 131.3 cm TV= 419.C
XA= 0.77
XE= 0.97

FROM Z= 81.3 to Z= 131.3
AVERAGE VOID FRACTION= 0.98

Z (cm)	TW (C)	QW (w/cm2)	XE	DXE (%)
0.0	144.	0.00	0.62	
7.5	144.	0.00	0.62	-0.1
10.0	152.	3.23	0.63	0.7
18.3	162.	3.38	0.65	2.3
28.5	344.	14.27	0.70	5.6
38.6	495.	3.92	0.73	2.7
48.8	526.	3.44	0.76	3.1
53.9	538.	3.26	0.78	1.4
58.9	545.	3.23	0.79	1.3
66.6	564.	3.22	0.81	2.0
76.1	580.	3.16	0.83	2.5
83.7	587.	3.19	0.85	2.0
86.2	592.	3.16	0.86	0.7
88.8	597.	3.14	0.87	0.7
93.9	605.	3.11	0.88	1.3
98.9	610.	3.05	0.89	1.3
106.6	615.	3.02	0.91	1.9
116.1	619.	2.99	0.94	2.3
123.7	634.	2.97	0.95	1.9
128.8	642.	2.96	0.97	1.2
133.5	592.	2.94	0.98	1.1
138.3	611.	3.00	0.99	1.2
142.3	620.	3.01	1.00	1.0

POINT: 4

AT TIME: 167.4 secs

AT Z= 38.6 cm XCHF= 0.73

AT Z= 131.3 cm TV= 391.C
XA= 0.78
XE= 0.97

FROM Z= 81.3 to Z= 131.3
AVERAGE VOID FRACTION= 0.97

Z (cm)	TW (C)	QW (w/cm2)	XE	DXE (%)
0.0	144.	0.00	0.62	
7.5	144.	0.00	0.62	-0.1
10.0	148.	3.18	0.63	0.7
18.3	152.	3.21	0.65	2.2
28.5	164.	3.35	0.68	2.7
38.6	534.	11.26	0.73	5.3
48.8	496.	3.64	0.76	2.7
53.9	519.	3.33	0.77	1.4
58.9	527.	3.29	0.78	1.4
66.6	549.	3.20	0.80	2.1
76.1	568.	3.14	0.83	2.5
83.7	576.	3.14	0.85	1.9
86.2	581.	3.11	0.85	0.6
88.8	586.	3.11	0.86	0.7
93.9	597.	3.08	0.87	1.3
98.9	603.	3.09	0.89	1.3
106.6	610.	3.04	0.91	1.9
116.1	616.	3.03	0.93	2.4
123.7	632.	3.00	0.95	1.9
128.8	641.	2.97	0.96	1.2
133.5	594.	2.95	0.97	1.1
138.3	608.	3.00	0.98	1.2
142.3	616.	3.02	0.99	1.0

SERIAL NO: 100 RATING: 1

INLET PRESSURE = 378. kPa

INLET MASS FLUX = 14.8 kg/m2sec

INLET QUALITY = 0.62

SATURATION TEMPERATURE = 141.6 C

POINT: 5

AT TIME: 226.5 secs

AT Z= 48.8 cm XCHF= 0.75

AT Z= 131.3 cm TV= 359.C
XA= 0.80
XE= 0.98

FROM Z= 81.3 to Z= 131.3
AVERAGE VOID FRACTION= 0.96

Z (cm)	TW (C)	QW (w/cm2)	XE	DXE (%)
0.0	144.	0.00	0.62	
7.5	144.	0.00	0.62	-0.1
10.0	146.	3.11	0.63	0.6
18.3	147.	3.12	0.65	2.1
28.5	151.	3.13	0.67	2.6
38.6	159.	3.22	0.70	2.6
48.8	355.	13.55	0.75	5.0
53.9	479.	3.78	0.76	1.3
58.9	494.	3.71	0.78	1.5
66.6	523.	3.59	0.80	2.3
76.1	548.	3.43	0.83	2.7
83.7	557.	3.46	0.85	2.1
86.2	563.	3.35	0.86	0.7
88.8	568.	3.37	0.86	0.7
93.9	581.	3.28	0.88	1.4
98.9	588.	3.21	0.89	1.3
106.6	598.	3.16	0.91	2.0
116.1	605.	3.14	0.94	2.5
123.7	621.	3.17	0.96	2.0
128.8	631.	3.19	0.97	1.3
133.5	589.	3.15	0.98	1.2
138.3	598.	3.19	0.99	1.2
142.3	605.	3.16	1.00	1.0

POINT: 6

AT TIME: 263.1 secs

AT Z= 53.9 cm XCHF= 0.76

AT Z= 131.3 cm TV= 338.C
XA= 0.81
XE= 0.97

FROM Z= 81.3 to Z= 131.3
AVERAGE VOID FRACTION= 0.96

Z (cm)	TW (C)	QW (w/cm2)	XE	DXE (%)
0.0	144.	0.00	0.62	
7.5	144.	0.00	0.62	-0.1
10.0	145.	3.15	0.63	0.7
18.3	146.	3.17	0.65	2.1
28.5	148.	3.17	0.67	2.7
38.6	153.	3.19	0.70	2.6
48.8	177.	3.60	0.73	2.8
53.9	376.	8.74	0.76	2.9
58.9	456.	3.95	0.77	1.3
66.6	498.	3.65	0.79	2.4
76.1	530.	3.49	0.82	2.8
83.7	540.	3.42	0.84	2.2
86.2	548.	3.42	0.85	0.7
88.8	554.	3.37	0.86	0.7
93.9	567.	3.31	0.87	1.4
98.9	576.	3.25	0.89	1.3
106.6	586.	3.20	0.91	2.0
116.1	595.	3.16	0.93	2.5
123.7	611.	3.13	0.95	2.0
128.8	621.	3.12	0.96	1.3
133.5	580.	3.12	0.98	1.2
138.3	587.	3.17	0.99	1.2
142.3	595.	3.17	1.00	1.0

SERIAL NO: 100 RATING: 1

INLET PRESSURE = 378. kPa

INLET MASS FLUX = 14.8 kg/m2sec

INLET QUALITY = 0.62

SATURATION TEMPERATURE = 141.6 C

POINT: 7

AT TIME: 279.5 secs

AT Z= 58.9 cm XCHF= 0.78

AT Z= 131.3 cm TV= 330.C
XA= 0.83
XE= 0.98

FROM Z= 81.3 to Z= 131.3
AVERAGE VOID FRACTION= 0.95

Z (cm)	TW (C)	QW (w/cm2)	XE	DXE (%)
0.0	144.	0.00	0.62	
7.5	144.	0.00	0.62	-0.1
10.0	144.	3.15	0.63	0.7
18.3	145.	3.16	0.65	2.1
28.5	148.	3.17	0.67	2.7
38.6	151.	3.19	0.70	2.6
48.8	166.	3.35	0.73	2.7
53.9	265.	4.83	0.74	1.7
58.9	376.	10.87	0.78	3.1
66.6	481.	3.88	0.80	2.0
76.1	519.	3.63	0.83	2.9
83.7	530.	3.61	0.85	2.3
86.2	538.	3.55	0.86	0.7
88.8	545.	3.60	0.86	0.8
93.9	559.	3.45	0.88	1.5
98.9	569.	3.37	0.89	1.4
106.6	580.	3.32	0.91	2.1
116.1	589.	3.27	0.94	2.6
123.7	605.	3.28	0.96	2.0
128.8	615.	3.31	0.97	1.4
133.5	574.	3.27	0.98	1.3
138.3	580.	3.34	1.00	1.3
142.3	589.	3.27	1.01	1.1

POINT: 8

AT TIME: 314.6 secs

AT Z= 66.6 cm XCHF= 0.80

AT Z= 131.3 cm TV= 304.C
XA= 0.85
XE= 0.98

FROM Z= 81.3 to Z= 131.3
AVERAGE VOID FRACTION= 0.95

Z (cm)	TW (C)	QW (w/cm2)	XE	DXE (%)
0.0	144.	0.00	0.62	
7.5	144.	0.00	0.62	-0.1
10.0	144.	3.14	0.63	0.7
18.3	144.	3.17	0.65	2.1
28.5	146.	3.18	0.67	2.7
38.6	148.	3.17	0.70	2.6
48.8	156.	3.25	0.73	2.7
53.9	201.	3.55	0.74	1.4
58.9	199.	3.75	0.76	1.5
66.6	343.	12.89	0.80	4.1
76.1	485.	3.91	0.82	2.5
83.7	502.	3.74	0.85	2.4
86.2	514.	3.67	0.85	0.8
88.8	522.	3.65	0.86	0.8
93.9	538.	3.61	0.88	1.5
98.9	550.	3.53	0.89	1.5
106.6	563.	3.42	0.91	2.2
116.1	573.	3.37	0.94	2.6
123.7	589.	3.36	0.96	2.1
128.8	599.	3.35	0.98	1.4
133.5	558.	3.36	0.99	1.3
138.3	563.	3.43	1.00	1.3
142.3	574.	3.38	1.01	1.1

SERIAL NO: 100 RATING: 1

INLET PRESSURE = 378. kPa

INLET MASS FLUX = 14.8 kg/m2sec

INLET QUALITY = 0.62

SATURATION TEMPERATURE = 141.6 C

POINT: 9

AT TIME: 362.2 secs

AT Z= 76.1 cm XCHF= 0.82

AT Z= 131.3 cm TV= 266.C
XA= 0.87
XE= 0.98

VOID FRACTION DATA
NOT AVAILABLE

Z (cm)	TW (C)	QW (w/cm2)	XE	DXE (%)
0.0	144.	0.00	0.62	
7.5	144.	0.00	0.62	-0.1
10.0	143.	3.20	0.63	0.7
18.3	143.	3.20	0.65	2.2
28.5	144.	3.20	0.67	2.7
38.6	146.	3.22	0.70	2.6
48.8	150.	3.22	0.73	2.7
53.9	175.	3.36	0.74	1.4
58.9	168.	3.34	0.76	1.4
66.6	165.	3.39	0.78	2.1
76.1	343.	8.75	0.82	4.7
83.7	457.	3.87	0.84	2.0
86.2	475.	3.71	0.85	0.8
88.8	487.	3.69	0.86	0.8
93.9	507.	3.62	0.87	1.5
98.9	522.	3.54	0.89	1.5
106.6	538.	3.47	0.91	2.2
116.1	551.	3.39	0.94	2.7
123.7	567.	3.40	0.96	2.1
128.8	578.	3.38	0.97	1.4
133.5	539.	3.28	0.99	1.3
138.3	541.	3.41	1.00	1.3
142.3	553.	3.36	1.01	1.1

POINT: 10

AT TIME: 418.3 secs

AT Z= 83.7 cm XCHF= 0.84

AT Z= 131.3 cm TV= 239.C
XA= 0.89
XE= 0.98

VOID FRACTION DATA
NOT AVAILABLE

Z (cm)	TW (C)	QW (w/cm2)	XE	DXE (%)
0.0	144.	0.00	0.62	
7.5	144.	0.00	0.62	-0.1
10.0	143.	3.12	0.63	0.6
18.3	143.	3.11	0.65	2.1
28.5	144.	3.15	0.67	2.6
38.6	144.	3.12	0.70	2.6
48.8	146.	3.14	0.73	2.6
53.9	160.	3.20	0.74	1.3
58.9	155.	3.19	0.75	1.3
66.6	152.	3.21	0.77	2.0
76.1	163.	3.37	0.80	2.6
83.7	314.	12.01	0.84	3.9
86.2	424.	4.14	0.84	0.7
88.8	443.	3.96	0.85	0.9
93.9	473.	3.72	0.87	1.6
98.9	495.	3.61	0.88	1.5
106.6	515.	3.53	0.91	2.3
116.1	531.	3.44	0.93	2.7
123.7	549.	3.40	0.95	2.1
128.8	561.	3.37	0.97	1.4
133.5	523.	3.29	0.98	1.3
138.3	522.	3.36	0.99	1.3
142.3	537.	3.33	1.00	1.1

SERIAL NO: 100 RATING: 1

INLET PRESSURE = 378. kPa

INLET MASS FLUX = 14.8 kg/m2sec

INLET QUALITY = 0.62

SATURATION TEMPERATURE = 141.6 C

POINT: 11

AT TIME: 439.7 secs

AT Z= 86.2 cm XCHF= 0.84

AT Z= 131.3 cm TV= 226.C
XA= 0.90
XE= 0.98

VOID FRACTION DATA
NOT AVAILABLE

Z (cm)	TW (C)	GW (w/cm2)	XE	DXE (%)
0.0	144.	0.00	0.62	
7.5	144.	0.00	0.62	-0.1
10.0	143.	3.16	0.63	0.7
18.3	143.	3.16	0.65	2.1
28.5	143.	3.17	0.67	2.6
38.6	144.	3.17	0.70	2.6
48.8	145.	3.18	0.73	2.6
53.9	157.	3.24	0.74	1.3
58.9	151.	3.23	0.75	1.3
66.6	149.	3.21	0.77	2.0
76.1	158.	3.33	0.80	2.5
83.7	169.	4.03	0.82	2.3
86.2	321.	11.28	0.84	1.9
88.8	421.	4.46	0.85	0.7
93.9	458.	3.88	0.87	1.7
98.9	483.	3.74	0.88	1.6
106.6	505.	3.61	0.90	2.3
116.1	522.	3.55	0.93	2.8
123.7	541.	3.53	0.95	2.2
128.8	554.	3.54	0.97	1.5
133.5	518.	3.40	0.98	1.3
138.3	516.	3.38	1.00	1.3
142.3	531.	3.35	1.01	1.1

POINT: 12

AT TIME: 445.1 secs

AT Z= 88.8 cm XCHF= 0.86

AT Z= 131.3 cm TV= 222.C
XA= 0.91
XE= 0.98

VOID FRACTION DATA
NOT AVAILABLE

Z (cm)	TW (C)	GW (w/cm2)	XE	DXE (%)
0.0	144.	0.00	0.62	
7.5	144.	0.00	0.62	-0.1
10.0	143.	3.18	0.63	0.7
18.3	143.	3.18	0.65	2.2
28.5	143.	3.18	0.67	2.7
38.6	144.	3.19	0.70	2.6
48.8	145.	3.19	0.73	2.7
53.9	156.	3.23	0.74	1.3
58.9	151.	3.21	0.75	1.3
66.6	149.	3.22	0.77	2.0
76.1	156.	3.31	0.80	2.5
83.7	161.	3.70	0.82	2.2
86.2	252.	6.44	0.83	1.0
88.8	347.	13.30	0.86	2.5
93.9	451.	3.90	0.87	1.4
98.9	478.	3.74	0.89	1.6
106.6	501.	3.62	0.91	2.3
116.1	519.	3.49	0.94	2.8
123.7	538.	3.44	0.96	2.2
128.8	551.	3.33	0.97	1.4
133.5	515.	3.34	0.99	1.3
138.3	514.	3.39	1.00	1.3
142.3	529.	3.36	1.01	1.1

SERIAL NO: 100 RATING: 1

INLET PRESSURE = 378. kPa

INLET MASS FLUX = 14.8 kg/m2sec

INLET QUALITY = 0.62

SATURATION TEMPERATURE = 141.6 C

POINT: 13

AT TIME: 481.0 secs

AT Z= 93.9 cm XCHF= 0.87

AT Z= 131.3 cm TV= 193.C
XA= 0.92
XE= 0.97

VOID FRACTION DATA
NOT AVAILABLE

Z (cm)	TW (C)	QW (w/cm2)	XE	DXE (%)
0.0	144.	0.00	0.62	
7.5	144.	0.00	0.62	-0.1
10.0	142.	3.17	0.63	0.7
18.3	142.	3.16	0.65	2.1
28.5	143.	3.18	0.67	2.7
38.6	143.	3.17	0.70	2.6
48.8	144.	3.17	0.73	2.7
53.9	152.	3.20	0.74	1.3
58.9	147.	3.20	0.75	1.3
66.6	145.	3.19	0.77	2.0
76.1	149.	3.22	0.80	2.5
83.7	147.	3.20	0.82	2.0
86.2	159.	3.46	0.83	0.7
88.8	154.	3.42	0.83	0.7
93.9	313.	10.32	0.87	3.3
98.9	442.	3.87	0.88	1.3
106.6	476.	3.57	0.90	2.3
116.1	500.	3.45	0.93	2.7
123.7	522.	3.38	0.95	2.1
128.8	535.	3.38	0.96	1.4
133.5	497.	3.49	0.98	1.4
138.3	498.	3.33	0.99	1.3
142.3	516.	3.27	1.00	1.1

POINT: 14

AT TIME: 502.6 secs

AT Z= 98.9 cm XCHF= 0.88

AT Z= 131.3 cm TV= 182.C
XA= 0.93
XE= 0.97

VOID FRACTION DATA
NOT AVAILABLE

Z (cm)	TW (C)	QW (w/cm2)	XE	DXE (%)
0.0	144.	0.00	0.62	
7.5	144.	0.00	0.62	-0.1
10.0	142.	3.13	0.63	0.6
18.3	142.	3.14	0.65	2.1
28.5	142.	3.14	0.67	2.6
38.6	142.	3.15	0.70	2.6
48.8	143.	3.16	0.73	2.6
53.9	150.	3.18	0.74	1.3
58.9	145.	3.17	0.75	1.3
66.6	144.	3.17	0.77	2.0
76.1	146.	3.18	0.80	2.5
83.7	145.	3.18	0.82	2.0
86.2	150.	3.27	0.82	0.7
88.8	148.	3.24	0.83	0.7
93.9	180.	3.97	0.85	1.5
98.9	335.	10.69	0.88	3.3
106.6	455.	3.70	0.90	2.0
116.1	486.	3.48	0.93	2.8
123.7	509.	3.35	0.95	2.1
128.8	523.	3.31	0.96	1.4
133.5	482.	3.45	0.98	1.3
138.3	487.	3.35	0.99	1.3
142.3	506.	3.29	1.00	1.1

SERIAL NO: 100 RATING: 1

INLET PRESSURE = 378. kPa

INLET MASS FLUX = 14.8 kg/m2sec

INLET QUALITY = 0.62

SATURATION TEMPERATURE = 141.6 C

POINT: 15

AT TIME: 539.0 secs

AT Z= 106.6 cm XCHF= 0.91

AT Z= 131.3 cm TV= 170.C
XA= 0.95
XE= 0.98

VOID FRACTION DATA
NOT AVAILABLE

Z (cm)	TW (C)	QW (w/cm2)	XE	DXE (%)
0.0	144.	0.00	0.62	
7.5	144.	0.00	0.62	-0.1
10.0	142.	3.20	0.63	0.7
18.3	142.	3.20	0.65	2.2
28.5	142.	3.20	0.67	2.7
38.6	142.	3.20	0.70	2.6
48.8	142.	3.20	0.73	2.7
53.9	147.	3.23	0.74	1.3
58.9	142.	3.22	0.75	1.3
66.6	142.	3.20	0.77	2.0
76.1	143.	3.22	0.80	2.5
83.7	142.	3.21	0.82	2.0
86.2	143.	3.24	0.83	0.7
88.8	143.	3.23	0.83	0.7
93.9	151.	3.31	0.85	1.4
98.9	170.	3.67	0.86	1.4
106.6	338.	11.88	0.91	4.5
116.1	456.	3.85	0.93	2.5
123.7	487.	3.70	0.96	2.4
128.8	503.	3.59	0.97	1.5
133.5	456.	3.63	0.98	1.4
138.3	468.	3.50	1.00	1.4
142.3	491.	3.44	1.01	1.1

* U.S. GOVERNMENT PRINTING OFFICE: 1983-381-297:3237

NRC FORM 335 (7.77)

U.S. NUCLEAR REGULATORY COMMISSION

BIBLIOGRAPHIC DATA SHEET

1. REPORT NUMBER *(Assigned by DDC)*
NUREG/CR-3363, Vol. 1
TS-831-I

4. TITLE AND SUBTITLE *(Add Volume No., if appropriate)*
MEASUREMENTS OF AXIALLY VARYING NONEQUILIBRIUM IN POST-CRITICAL-HEAT-FLUX BOILING IN A VERTICAL TUBE (Main Report and Appendices A-D)

2. *(Leave blank)*

3. RECIPIENT'S ACCESSION NO.

7. AUTHOR(S)
David G. Evans, Stephen W. Webb and John C. Chen

5. DATE REPORT COMPLETED
MONTH May YEAR 1983

9. PERFORMING ORGANIZATION NAME AND MAILING ADDRESS *(Include Zip Code)*
Institute of Thermo-Fluid Engineering and Science
Lehigh University
Bethleham, Pennsylvania 18015

DATE REPORT ISSUED
MONTH June YEAR 1983

6. *(Leave blank)*

8. *(Leave blank)*

12. SPONSORING ORGANIZATION NAME AND MAILING ADDRESS *(Include Zip Code)*
Division of Accident Evaluation
Office of Nuclear Regulatory Research
U.S. Nuclear Regulatory Commission
Washington, D.C. 20555

10. PROJECT/TASK/WORK UNIT NO.

11. CONTRACT NO.
FIN No. B6794

13. TYPE OF REPORT
Topical Report

PERIOD COVERED *(Inclusive dates)*
May 1982 to May 1983

15. SUPPLEMENTARY NOTES

14. *(Leave blank)*

16. ABSTRACT *(200 words or less)*

To supplement the very limited steady-state data available, experiments have been run with quench fronts propagating slowly up into a tubular test section and measurements of wall heat flux, wall temperature, and nonequilibrium vapor temperature as functions of distance beyond the quench front were obtained. Since the time required for the quench front to propagate a few millimeters corresonded to many fluid residence-time, transient convective heat transfer theory indicates that the thermal data thus obtained are quasi-steady state. The significant experimental findings indicates a zone of two-phase fluid in thermodynamic equilibrium near the CHF location where the vaporization source intensity (Γ) is relatively high. This is followed by a far zone of rapidly developing non-thermodynamic equilibrium two-phase fluid where the source intensity drops off to a relatively low magnitude.

17. KEY WORDS AND DOCUMENT ANALYSIS

17a. DESCRIPTORS

Post-CHF
Convective Film Boiling
Quench Front Heat Transfer
Non-thermodynamic Equilibrium Heat Transfer

17b. IDENTIFIERS/OPEN-ENDED TERMS

18. AVAILABILITY STATEMENT
Unlimited

19. SECURITY CLASS *(This report)*
Unclassified

21. NO. OF PAGES

20. SECURITY CLASS *(This page)*
Unclassified

22. PRICE
$

NRC FORM 335 (7.77)

UNITED STATES
NUCLEAR REGULATORY COMMISSION
WASHINGTON, D.C. 20555

120555078877 1 1AN1R2
US NRC
ADM-DIV OF TIDC
POLICY & PUB MGT BR-PDR NUREG
W-501
WASHINGTON DC 20555